ÉTUDE DE NOUVEAUX POLYMÈRES THERMOSENSIBLES EN SOLUTION AQUEUSE ET DE LEUR CHANGEMENT DE SOLUBILITÉ INDUIT PAR LE PH

Par

Hu Zhang

Thèse présentée au Département de chimie en vue
de l'obtention du grade de docteur ès science (Ph.D.)

FACULTÉ DES SCIENCES
UNIVERSITÉ DE SHERBROOKE

Sherbrooke, Québec, Canada, avril 2016

avril 06, 2016

le jury a accepté la thèse de monsieur Hu Zhang
dans sa version finale

Membres du jury

Professeur Yue Zhao
Directeur de recherche
Département de chimie

Professeur Christian Pellerin
Évaluateur externe
Département de chimie
Université de Montréal

Professeur Serge Lacelle
Évaluateur interne
Département de chimie

Professeur Armand Soldera
Évaluateur interne
Département de chimie

Professeur Guillaume Bélanger
Président-rapporteur
Département de chimie

SOMMAIRE

Les polymères stimuli-répondants sont capables de changer leurs propriétés ou structures de façon importante en réagissant à un signal de stimulation. Parmi ceux-ci, des polymères sensibles à une variation de température ont fait l'objet de beaucoup de recherches et de développement, parce qu'un changement de température est un stimulus facile à appliquer, et que des fluctuations de température spontanées se produisent dans le milieu biologique. En plus, des polymères thermosensibles peuvent également répondre à d'autres stimuli tels que la lumière, le pH ou un champ magnétique. Ces polymères répondants à deux (ou plus) stimuli sont particulièrement intéressants pour des applications pratiques, notamment dans le domaine de biologie ou biomédical car des systèmes biologiques peuvent répondre sélectivement à de multiples changements dans les conditions environnantes plutôt qu'à un seul stimulus. La recherche menée dans cette thèse porte sur le développement de nouveaux polymères thermosensibles en solution aqueuse et l'étude de leur contrôle de solubilité à la fois par le changement de température et de pH.

Les polymères thermosensibles en solution aqueuse peuvent afficher soit une température de solution critique inférieure (LCST) ou une température de solution critique supérieure (UCST). Fondamentalement, les polymères à LCST sont solubles dans l'eau à T<LCST mais deviennent insolubles à T>LCST, tandis que les polymères à UCST présentent une thermosensibilité inversée, étant solubles à T>UCST et insolubles à T<UCST. Jusqu'à présent, la plupart des études ont été consacrées aux polymères à LCST, alors que les polymères à UCST sont beaucoup moins étudiés. La raison principale est que ces derniers ne sont pas aussi facilement accessibles que leurs homologues à LCST. Ces deux types de polymères thermosensibles ont été étudiés dans cette thèse. En plus de la conception, la synthèse et la caractérisation de nouveaux polymères, en particulier les systèmes UCST,

un objectif principal de la thèse est d'exploiter l'effet du pH sur LCST ou UCST afin de développer des polymères dont la solubilité dans l'eau peut être commutée, entre état soluble et état insoluble, par un changement de pH, et ce à une température de solution constante.

Dans le premier projet, dans le but d'accroître l'ampleur du changement de la température LCST déclenché par une variation de pH, un nouveau comonomère portant un groupe d'acide acrylique et un groupe d'acide benzoïque de pareils pKa dans sa structure a été conçu et synthétisé, à savoir, le 4-((2-carboxyallyle)oxy)benzoïque (CAB). Par rapport aux comonomères contenant un seul groupe d'acide, cette structure particulière rend le comonomère plus hydrophobe dans l'état protoné (pH <pKa) dû au groupe phényle et plus hydrophile dans l'état déprotoné (pH> pKa) en raison de la double charge. L'efficacité de cette conception a été démontrée à l'aide d'un copolymère du N-isopropylacrylamide (NIPAM) et du CAB en tant que comonomère, P(NIPAM-*co*-CAB). Les mesures expérimentales ont montré un grand changement réversible de LCST lors d'un changement de pH, confirmant ainsi l'utilisation d'un tel comonomère comme une stratégie utile pour améliorer l'efficacité et la sensibilité du pH pour le contrôle de la température critique des polymères à LCST.

Dans le second projet, nos études ont montré que le copolymère statistique de poly (acrylamide-*co*-acrylonitrile) (P(AAM-*co*-AN)) synthétisé en utilisant la polymérisation radicalaire contrôlée par transfert de chaîne réversible par addition-fragmentation (RAFT) peut afficher une UCST stable en solution aqueuse. Nous avons montré que ce polymère peut alors être utilisé comme agent de transfert de chaîne macromoléculaire (macro-CTA) pour croître un second polymère de choix pour la synthèse de copolymères blocs (BCP). Trois copolymères diblocs représentatifs ont été ainsi synthétisés avec le deuxième bloc étant soit le polystyrène hydrophobe (PS), le poly(diméthylacrylamide) (PDMA)

hydrophile ou le poly(méthacrylate de N, N-diméthylaminoéthyl) (PDMAEMA) qui possède une LCST. Les structures auto-assemblées des ces trois copolymères présentent une variété de comportements thermosensibles dictés par UCST du bloc P(AAM-*co*-AN), tels que la dispersion-agrégation réversible de micelles, la dissolution-formation de micelles, et l'inversion des noyau et couronne de micelles. Nos résultats démontrent, pour la première fois, que le P(AAM-*co*-AN) est un polymère à UCST robuste pouvant être introduit dans des architectures polymères contrôlées productibles par la synthèse RAFT, et ce de la même façon que l'utilisation des homologues à LCST largement étudiés comme le PNIPAM. Cette possibilité ouvre la porte à l'exploration de nouveaux polymères thermosensibles basée sur la thermosensibilité opposée à LCST.

Il est connu que même quelques groupes chargés dans des polymères à UCST peuvent grandement affecter la température de séparation de phase en raison d'un changement de l'enthalpie de solution très faible associé au processus. Cette propriété a été exploitée dans le troisième projet ayant pour but de développer des polymères dont la solubilité dans l'eau est contrôlable par le pH de façon ultrasensible. Pour rendre le polymère P(AAM-*co*-AN) sensible au pH, des unités comonomères de l'acide acrylique (AAC) ou de la 4-vinylpyridine (4VP) ont été introduites dans le P(AAM-*co*-AN) résultant en deux nouveaux polymères, à savoir le P(AAM-*co*-AN-*co*-AAC) et le P(AAM-*co*-AN-*co*-4VP). Nos résultats ont montré une forte augmentation ou diminution de la température UCST en conséquence d'un petit changement du pH. En particulier, un échantillon du P(AAM-*co*-AN-*co*-4VP) présente un déplacement UCST supérieur à 57 ^{o}C lors d'un changement de 0,25 unité de pH, et son passage de l'état soluble à l'état insoluble à la température ambiante peut être observé visuellement sur un changement du pH aussi peu que 0,05 unité. Pour illustrer les applications possibles, un copolymère de trois blocs de type ABA est synthétisé en utilisant cet échantillon comme macro-CTA pour polymériser la diméthylacrylamide soluble dans l'eau (DMA), ce qui donne lieu au

P(AAM-*co*-AN-*co*-4VP)-*b*-PDMA-*b*-P(AAM-*co*-AN-*co*-4VP). À 37 ^{o}C, la micelle de ce copolymère triblocs peut être stable de pH 7,00 jusqu'à 4,75, mais brusquement dissociée au pH 4,50, ce qui suggère la possibilité de libération de médicament déclenchée par un très léger changement de pH. Cette étude démontre le potentiel de développement des polymères à UCST ainsi que leurs assemblages qui peuvent subir un changement de solubilité dans l'eau contrôlé par le pH d'une manière ultrasensible et, par conséquent, offre de nouvelles possibilités pour les applications

ABSTRACT

Stimuli-responsive polymers that undergo dramatic chemical or physical changes in response to external stimuli have attracted a great deal of attention from both fundamental and applied points of view. Among them, polymers sensitive to change in temperature have been particularly the focus of much research and development effort, because temperature change is a stimulus that can readily be applied in a reversible and non-invasive manner and spontaneous temperature fluctuations occur in biological environment. Moreover, many thermosensitive polymers can also respond to other stimuli such as light, magnetic field and pH. Such dual- or multi-stimuli-responsive polymers are particularly interesting for practical applications, especially in the biological area since biological systems can selectively respond to multiple environmental changes rather than a single stimulus. The research conducted in this thesis deals with the development of novel thermoresponsive polymers in aqueous solution and the study of their solubility control by both temperature and pH change.

Thermoresponsive polymers in aqueous solution can display either a lower critical solution temperature (LCST) or upper critical solution temperature (UCST). Basically, for LCST polymers, they are soluble at temperatures below LCST but become insoluble above LCST, while UCST polymers exhibit a reversed thermosensitivity by being soluble in water at temperatures above UCST and insoluble below the phase separation temperature. Until now, most studies have been dedicated to LCST polymers, and UCST polymers have much less been investigated because they are not as easily accessible as their LCST counterparts. These two types of thermosensitive polymers have been studied in this thesis. In addition to the design, synthesis and characterization of novel polymers, especially UCST systems, a main objective of the thesis is to explore the effect of pH on LCST or UCST in order to develop polymers whose water solubility can be switched, between soluble and insoluble state, by a change in pH at a constant solution temperature.

In the first project, in order to increase the magnitude of pH-triggered LCST shift, a new comonomer bearing an acrylic acid and a benzoic acid group of similar pKa in the structure was designed and synthesized, namely, 4-((2-carboxyallyl)oxy)benzoic acid (CBA). With respect to comonomers containing a single acid group, this particular comonomer structure makes it more hydrophobic in the protonated state (pH < pKa) due to the phenyl group and more hydrophilic in the deprotonated state (pH > pKa) due to the double charge. The efficiency of this design has been demonstrated by using CBA as a comonomer to polymerize with *N*-isopropylacrylamide (NIPAM) to obtain a copolymer P(NIPAM-*co*-CBA). The cloud point measurements showed large and reversible shift of LCST upon pH change, confirming the comonomer design principle as a useful strategy for enhancing the efficiency and sensitivity of the pH-responsiveness of LCST polymers.

In the second project, our studies found that the random copolymer of poly(acrylamide-*co*-acrylonitrile) (P(AAm-*co*-AN)) synthesized using the reversible addition-fragmentation chain transfer polymerization (RAFT) method can display a sharp and stable UCST in aqueous solution. We showed that this polymer can then be utilized as macromolecular chain transfer agent (macro-CTA) to grow a second polymer of choice for block copolymer (BCP) synthesis. Three representative diblock copolymers were synthesized with the second block being either hydrophobic polystyrene (PS) or hydrophilic poly(dimethylacrylamide) (PDMA) or poly(N,N-dimethylaminoethyl methacrylate) (PDMAEMA) displaying a LCST. The three BCPs of different designs can all exhibit thermally induced changes as dictated by the UCST of the P(AAm-*co*-AN) block, in a reversible and robust way in both pure water and phosphate-buffered saline (PBS). Their self-assembled structures exhibit a variety of behaviors such as the reversible dispersion-aggregation of micelles, dissolution-formation of micelles, and reversal of micelle core and corona. Our obtained results point out that P(AAm-*co*-AN) is a robust UCST polymer that can be introduced into controlled polymer architectures producible by RAFT, much the same way as using the extensively studied LCST

counterparts like poly(N-isopropylacrylamide) (PNIPAM). This possibility makes the door wide open to exploring new thermosensitive polymers based on the thermosensitivity opposite to the LCST.

Even a few charged groups in UCST polymers may affect greatly the phase separation temperature due to a small solution enthalpy change associated with the process. This property has been exploited in the third project to develop ultrasensitive pH-induced solubility switch. To render the UCST polymer P(AAm-*co*-AN) sensitive to pH, either acrylic acid (AAc) or 4-vinyl pyridine (4VP) comonomer units were introduced into P(AAm-*co*-AN) resulting in P(AAm-*co*-AN-*co*-AAc) or P(AAm-*co*-AN-*co*-4VP). The results found a large increase or decrease of the cloud point over a small change of pH. In particular, one P(AAm-*co*-AN-*co*-4VP) sample could exhibit a 57 ^{o}C cloud point shift over 0.25 pH unit, and its transition from soluble to insoluble state at room temperature can be visually observed over a pH change as little as 0.05 unit. To demonstrate possible applications, an ABA-type triblock copolymer was synthesized using this sample as macro-CTA to polymerize water-soluble dimethylacrylamide (DMA), giving rise to P(AAm-*co*-AN-*co*-4VP)-*b*-PDMA-*b*-P(AAm-*co*-AN-*co*-4VP). At 37 ^{o}C, the micelle of this triblock copolymer could be stable from pH 7.00 down to 4.75, but abruptly disassembled at 4.50, implying the possibility of drug release triggered by a slight pH change. This study demonstrates the potential of developing UCST polymers and their assemblies that can undergo ultrasensitive pH-controlled water solubility switch and thus offer new possibilities for applications.

ACKNOWLEDGEMENT

First I would like to express my special appreciation and thanks to my thesis supervisor Prof. Yue Zhao for offering me the opportunity to study in his group at the Université de Sherbrooke, for the constant guidance and encouragement during my pursuit of my Ph.D, and for always being so patient and supportive whenever I was facing a dilemma. I am eternally grateful to what he has taught me these years in Canada. I really learned a lot from Prof. Zhao, not limited to the scientific aspects.

I would like to thank two members on my doctoral committee, who are also in the jury of my thesis, Prof. Guillaume Bélanger and Prof. Serge Lacelle, as well as all the professors and staff working in the Department of Chemistry for their kind help during my Ph.D study in the Université de Sherbrooke. I also would like to thank Prof. Christian Pellerin (Université de Montréal) and Prof. Armand Soldera for serving in the jury of my thesis.

I also thank a number of persons for their help or assistance in one of the projects: Prof. Yves Dory and Mr. Thomas Marmin (synthesis of the new double-acid monomer), Prof. Armand Soldera and Mr. Étienne Cuierrier (DFT calculations), Mrs. Xia Tong (AFM), Dr. Shengwei Guo (some cloud point measurements) and Mr. Wizheng Fan (some GPC measurements).

I acknowledge the following people, my colleagues and dearest friends, who made my four years' stay in Sherbrooke full of joys and memories: Mrs. Xia Tong, Prof. Dongchen He, Prof. Li Wang, Dr. Dehui Han, Dr. Bin Yan, Dr. Hongji Zhang, Mr. Shangyi Fu, Dr. Shengwei Guo, Dr. Donghua Li, Dr. Bo He, Dr. Qiang Yan, Dr. Surjith Kumar, Dr. Feng Shi, Mr. Jean-François Wehrung, Dr. Olivier Boissière, Mr. Damien Habault, Dr. Juan Xuan, Mr. Guo Li, Mr. Weizheng Fan, Mr. Xili Lu, Mr. Jun Xiang, Mrs. Hui Xiao, Mr. Feijie Ge, Dr. Xin Zhao, Dr. Bin Yu, Ms. Amélie Auge, Mr. Farhad Farnia, Dr. Hojjat

Seyedjamali, Ms. Ailing Xie, Ms. Hongwei Niu, Mr. Lei Hu, Mr. Peng Luo, Dr. Di Gao, *etc*.

I would like to give my thanks and respect to the Chinese Scholar Council (CSC) for awarding me a scholarship to support my living and study in Canada. I also would like to thank all the members of the Service d'éducation du Consulat Général de la République Populaire de Chine à Montréal, especially Ms. Suli Yan for all their kind helps.

I express my deep thanks to my family for their great care and encouragement during my study in Canada, especially my parents, my wife Xiaoqing and my little daughter Sophia. Without your encouragement and accompany, none of this would have been possible.

Finally, I would like to acknowledge the following organizations for their financial support: Natural Sciences and Engineering Research Council of Canada (NSERC), Le Fonds de recherche du Québec: Nature et technologies (FQRNT) and the Université de Sherbrooke.

TABLE OF CONTENT

SOMMAIRE i

ABSTRACT v

ACKNOWLEDGEMENT viii

TABLE OF CONTENT x

LIST OF ABBREVIATIONS xii

LIST OF SCHEMES xiv

LIST OF FIGURES xv

LIST OF TABLES xxiii

INTRODUCTION 1

1. Basic Principles of Thermoresponsive Polymers in Aqueous Solution 2
2. Characterization of the Phase Transition 7
3. Polymers with LCST-type Thermoresponsiveness in Water 9
4. Polymers with UCST-type Thermoresponsiveness in Water 16
5. Thermo-pH Responsive Polymer 28
6. Objective of the Thesis 32

Chapter 1 A New Comonomer Design for Enhancing PH-Triggered LCST Shift of Thermosensitive Polymers 34

1.1 Introduction 34
1.2. Results and Discussion 36
1.2.1 The Comonomer Design 36
1.2.2 pH-induced LCST Shift 40
1.3 Experimental Section 46
1.3.1 Materials 46
1.3.2 Synthesis of the Comonomer CBA 47
1.3.3 Synthesis of the Random Copolymer P(NIPAM-*co*-CBA) 49
1.3.4 Characterizations 51
1.4 Conclusions 52
1.5 Statement of Contribution 53

Chapter 2 Uncharged UCST Block Copolymers and Their Diverse Thermoresponsive Micelles in Physiological Medium 54

2.1. Introduction 54
2.2. Experimental Section 55

2.2.1. Synthesis of P(AAm-*co*-AN) and its Diblock Copolymers 55
2.2.2. Characterizations..... 58
2.3. Results and Discussion..... 59
2.3.1. RAFT Synthesis, Characterization, and UCST Behavior 59
2.3.2. Diversiform UCST-Dictated Thermosensitivity of P(AAm-*co*-AN)-Based Block Copolymer Micelles..... 67
2.4. Conclusions..... 79
2.5. Statement of Contribution..... 80
Chapter 3 Ultrasensitive pH-induced Water Solubility Switch of UCST Polymers.....81
3.1. Introduction..... 81
3.2. Experimental Section 83
3.2.1. Materials 83
3.2.2. Synthesis of UCST Random Copolymers and Triblock Copolymer..... 83
3.2.3. Characterization methods..... 89
3.2.4. Determination of copolymer compositions..... 91
3.2.5. Determination of critical micelle concentration of P6 triblock copolymer..... 92
3.2.6. Preparation of Pyrene-loaded Micellar Solution..... 93
3.2.7. Preparation of Nile Red-Loaded Micelles..... 93
3.3. Results and Discussion..... 94
3.3.1. Water Solubility Switch Due to pH-Induced UCST Shift..... 94
3.3.2. Ultra-pH-sensitive Block Copolymer Micelle 102
3.4. Conclusions..... 107
3.5. Statement of Contribution..... 108
CONCLUSIONS AND PERSPECTIVES.....109
BIBLIOGRAPHY.....118

LIST OF ABBREVIATIONS

4VP: 4-vinyl pyridine

β-CD: *β*-cyclodextrins

ΔG_{mix}: Gibb's free energy of mixing

ΔH_{mix}: enthalpy of mixing

ΔS_{mix}: entropy of mixing

AAc: acrylic acid (AAc)

AAm: acrylamide

AFM: Atomic-force microscopy

AIBN: azobisisobutyronitrile

AN: acrylonitrile

AuNPs: gold nanoparticles

BA: benzoic acid

BCPs: block copolymers

CBA: 4-((2-carboxyallyl)oxy)benzoic acid.

d_6-DMSO: deuterated dimethyl sulfoxide

DFT: Density Functional Theory

DMA: dimethylacrylamide

DMAEMA: dimethylaminoethyl methacrylate

DMSO: dimethyl sulfoxide

DSC: differential scanning calorimetry

LCST: lower critical solution temperature

MAA: methacrylic acid (MAA)

Macro-CTA: macromolecular chain transfer agent

NIPAM: N-isopropylacrylamide

NMR: nuclear magnetic resonance

P (NIPAM-*co*-CBA): Poly(N-isopropylacrylamide-*co*-4-((2-carboxyallyl)oxy)benzoic acid)

P(AAm-*co*-AN): Poly(acrylamide-*co*-acrylonitrile)

P(AAm-*co*-AN-*co*-4VP): Poly(acrylamide-*co*-acrylonitrile-*co*-4-vinyl pyridine)

P(AAm-*co*-AN-*co*-4VP)-*b*-PDMA-*b*-P(AAm-*co*-AN-*co*-4VP): Poly(acrylamide-*co*-acrylonitrile-*co*-4-vinyl pyridine)-*b*-poly(dimethylacrylamide)-*b*-poly(acrylamide-*co*-acrylonitrile-co-4-vinyl pyridine)

P(AAm-*co*-AN-*co*-AAc): Poly(acrylamide-co-acrylonitrile-co-acrylic acid)

PAcrNPP: poly(N-acryloyl-N'-propylpiperazine)

PBS: Phosphate-buffered saline

PDEAEMA: poly(N,N'-diethylaminoethyl methacrylate)

PDEAM: poly(N,N-diethylacrylamide)

PDMA: Poly(dimethylacrylamide)

PDMAEMA: Poly(dimethylaminoethyl methacrylate)

PDMAPS: poly-[3-dimethyl(methacryloyloxyethyl) ammonium propane sulfonate]

PEPyM: poly(N-ethylpyrrolidine methacrylate

PMAAm: polymethacrylamide

PMEO2MA: poly(2-(2-methoxyethoxy)ethyl methacrylate)

PNAAAm: poly(N-aryloylasparagineamide)

PNAGA: poly(N-acryloylglycinamdie)

PNAGAAm: poly(N-acryloylglutamineamide)

PNAGA-co-BA: poly(Nacryloylglycinamide-co-butyl acrylate)

PNAGA-*co*-NAcAAm: poly(Nacryloylglycinamide-co-N-acetylacrylamide)

PNAGA-*co*-St: poly(N-acryloylglycinamide-co-styrene)

PNCPAM: poly(N-cyclopropylacrylamide)

PNIPAM: Poly(N-isopropylacrylamide)

PNMAAAm: poly(methacruloylasparagineamide)

PNNPAM: poly(N-n-propylacrylamide)

POEGMA: poly(oligo(ethylene glycol) methacrylate)s

PolySBMA: poly(sulfobetaine methacrylate)

PS: polystyrene

PSPP: poly(3-[N-(3-methacrylamidopropyl)-N,N-dimethyl]ammoniopropanesulfonate

PU: poly(allylurea)

RAFT: reversible addition fragmentation chain transfer

ST: styrene

T: absolute temperature

UCST: upper critical solution temperature

LIST OF SCHEMES

CHAPTER 1

Scheme 1. Synthesis of the comonomer 4-((2-carboxyallyl)oxy)benzoic acid (CBA) and its copolymerization with *N*-isopropylacrylamide yielding P(NIPAM-*co*-CBA).....38

LIST OF FIGURES

INTRODUCTION

Figure 1. Schematic representation of the polymer phase diagrams for polymers exhibiting (a) LCST behavior; (b) UCST behavior [17].....2

Figure 2. Schematic illustration of the clouding of a polymer solution by the coil-to-globule transition. The aggregation of the globules causes the solution to appear opaque [19]. 6

Figure 3. Phase transition of the polymer solution is characterized by solution transmittance changes as a function of temperature. 8

Figure 4. Chemical structures of selected representative LCST thermoresponsive homopolymers.....10

Figure 5. Illustration of temperature induced PNIPAM phase transition [30]. 11

Figure 6. Relationship between the number of oligo(ethylene glycol) units (m) and the cloud point. Data of methyl and ethyl ethers are plotted with ○ and △, respectively. The cloud points of 0.2 wt % polymer in water were measured at a heating rate of 0.3 °C min^{-1}. m=2.5 when polymers with equal composition of the two monomers (m=2 and m=3) (random copolymer) [41]. 14

Figure 7. Plots of transmittance as a function of temperature measured for aqueous solutions (3 $mg.mL^{-1}$) of either (A) a copolymer P(MEO_2MA-*co*-OEGMA) containing 5 mol % of OEGMA per chain (DP ≈ 100; Mw/Mn = 1.34), and (B) a homopolymer PNIPAM (DP ≈ 100; Mw/Mn = 1.12): solid lines, heating cycles; doted lines, cooling cycles [42]. 15

Figure 8. The UCST of zwitterionic polymers relies on intra- and intermolecular coulomb interaction: a) intragroup, b) intrachain, c) interchain [18]. 18

Figure 9. Synthetic route to hydrophobically modified zwitterionic copolymers and tunable UCST in aqueous solution under different conditions [63]. 19

Figure 10. Chemical structure of PNIPAM-*b*-PSPP block copolymers and schematic illustration of the temperature-dependent association states [68].....21
Figure 11. Chemical structures of the diblock copolymers tethered to gold nanoparticles (AuNPs) and schematic of both LCST and UCST thermal phase transitions on AuNP surface [79]. 22
Figure 12. Pathways of unintentional introduction of ionic species into UCST polymers such as PNAGA [91].....24
Figure 13. The cloud point of P(AAm-co-AN) in water or PBS buffer can be tuned by adjusting the comonomer ratio [93].....27
Figure 14. Schematic illustration of the strategies for controlling the delivery of drugs (circles) using thermoresponsive nanocarrier, A: diffusion-controlled release; B: drug release due to gel volume contraction. [107] 28
Figure 15. Schematic representation of thermosensitive nanocarrier working as a targeted drug delivery system with controlled drug release [108].....29
Chapter 1
Figure 16. Schematic illustration of nanogels encapsulating and releasing the drugs [119].32
Figure 17. Schematic illustration of pH-induced LCST shifts upon protonation and deprotonation of acid comonomer units. Enhanced LCST shift means larger gap between the low and high LCST at the same acid comonomer content.....37
Figure 18. Plots of transmittance vs. temperature for the solutions of different P(NIPAM-*co*-CBA) samples obtained at: a) pH 4.5, b) pH 5.0, c) pH 5.5 and d) pH 6.0.42
Figure 19. Plots of transmittance vs. temperature obtained at different pH values for the solutions of two P(NIPAM-*co*-CBA) samples: a) P1 and b) P2. 44
Figure 20. a) Plots of cloud point vs. pH for the solutions of different (NIPAM-*co*-CBA) samples. b) Transmittance change as a function of pH for the solution of P5 measured at 37 ^{o}C.....46
Finally, it should be mentioned that the present study focuses on only pH-induced LCST

shift. Reversely, since the polymer undergoes a phase transition between hydrated and dehydrated state, the dielectric constant of the local environment surrounding the acid groups may change, resulting in change in the actual pKa. In other words, the pH responsiveness of the polymer may be affected by the changing thermosensitivity. 46
Figure 21. The ^{1}H NMR spectrum of synthesized CBA monomer in d_6-DMSO. 49
Figure 22. The ^{1}H NMR spectra of synthesized copolymers (P1-P5) in d_6-DMSO. 50
Chapter 2
Figure 23. Left: Infrared spectrum of the sample P1 in Table 4 showing the characteristic absorption band of CN in acrylonitrile (AN) and that of CO in acrylamide (AAm). Right: Calibration curve obtained by plotting the integral ratio of the CO absorption band to the CN band vs. known content of AAm in mixtures of PAAM and PAN homopolymers (93).59
Figure 24. 1H NMR spectra in d_6-DMSO at 70 ^{o}C for the P(AAm-*co*-AN) macro-CTA (a) and the three diblock copolymers: P(AAm-*co*-AN)-*b*-PS (b), P(AAm-*co*-AN)-*b*-PDMA (b) and P(AAm-*co*-AN)-*b*-PDMAEMA (c). 62
Figure 25. SEC traces at 35 ^{o}C with polymers dissolved in DMF/DMSO (50:50): (a) three P(AAm-*co*-AN) samples, and (b) three diblock copolymers and the used macro-CTA....64
Figure 26. AFM phase image (tapping mode) of P(AAm-*co*-AN)-*b*-PDMAEMA thin film (image size: 1μm x 1μm). The film was prepared by spin-coating the block copolymer DMSO solution onto a mica substrate, followed by annealing in a vacuum oven at 145 ^{o}C for 4 days. The thickness of the film is about 70 nm, the surface roughness about 0.22 nm and the average sizes for the bright domains (harder P(AAm-*co*-AN)) and the dark domains (soft PPDMAEMA) are about 18 nm and 16 nm, respectively. 64
Figure 27. Transmittance change vs. temperature for a representative P(AAm-*co*-AN) (P3 in Table 4) both in pure water and in PBS (5 mg/mL). The difference in UCST is slight as compared to poly(N-acryloyl glycinamide) (89,91). 66
Figure 28. Plots of solution transmittance vs. temperature showing the UCST behavior in PBS solution (polymer concentration at 5 mg/mL; heating and cooling rate at 1 ^{o}C/min;

solid and dotted lines for cooling and heating scan, respectively): (a) P(AAm-*co*-AN) samples of different molecular weights and compositions; and (b) the same P(AAm-*co*-AN) sample (P1) subjected to ten consecutive heating and cooling cycles. ...66
Figure 29. Top: Variable-temperature ^{1}H-NMR spectra of P(AAm-*co*-AN) (P3 in Table 4) in D_2O recorded from 13 ^{o}C to 40 ^{o}C with an interval of 3 ^{o}C. Down: Change in the integral of the resonance peaks from 0.5 to 3 ppm as a function of temperature, indicating the UCST-determined water solubility. ...67
Figure 30. Left side: chemical structures of three diblock copolymers composed of the same UCST P(AAm-*co*-AN) block and a block of hydrophobic PS (a), hydrophilic PDMA (b) and LCST PDMAEMA (c). Right side: schematic illustration of the expected diverse thermoresponsive behaviors of their micelles. ...68
Figure 31. Characterization results for P(AAm-*co*-AN)-*b*-PS. (a) Transmittance change of the BCP micellar solution at two polymer concentrations upon a cooling-heating cycle (1 ^{o}C/min). (b) Change in the hydrodynamic diameter, D_H, on cooling of a micellar solution (0.5 mg/mL). (c) Reversible change in the size distribution of the micellar aggregates in water (0.5 mg/mL) upon temperature shift between 50 ^{o}C (>UCST) and 30 ^{o}C (<UCST).71
Figure 32. Characterization results for P(AAm-*co*-AN)-*b*-PDMA. (a) Transmittance change of the BCP micellar solution at two polymer concentrations upon a cooling-heating cycle (1 ^{o}C/min). (b) Change in the hydrodynamic diameter, D_H, on cooling of the micellar solution (1 mg/mL). (c) Reversible change in the size distribution of the solution (1 mg/mL) in PBS or in water upon temperature shift between 40 ^{o}C (>UCST) and 10 ^{o}C (<UCST). (d) Variable-temperature ^{1}H NMR spectra in D_2O. 72
Figure 33. Top: Variable-temperature ^{1}H-NMR spectra of P(AAm-*co*-AN)-*b*-PDMA (P7 in Table 4) in D_2O recorded from 7 ^{o}C to 31 ^{o}C with an interval of 3 ^{o}C. Down: Change in the integral of the resonance peaks from 1 to 1.8 ppm as a function of temperature, showing the UCST behavior of the P(AAm-*co*-AN) block in the diblock copolymer. 73
Figure 34. Characterization results for P(AAm-*co*-AN)-*b*-PDMAEMA. (a) Transmittance

change of the BCP micellar solution (polymer concentration: 5 mg/mL) upon a cooling-heating cycle (1 ^{o}C/min). (b) Change in the hydrodynamic diameter, DH, on cooling of the micellar solution (0.8 mg/mL). (c) Reversible change in the size distribution of the micellar aggregates in PBS or in water (0.8 mg/mL) upon temperature shift between 10 ^{o}C (UCST>T<LCST), 40 ^{o}C (LCST>T>UCST) and 70 ^{o}C (UCST<T>LCST). (d) Variable-temperature ^{1}H-NMR spectra in a D_2O solution.....76

Figure 35. Top: Variable-temperature ^{1}H-NMR spectra of P(AAm-*co*-AN)-*b*-PDMAEMA (P8 in Table 4) in D_2O recorded from 7 ^{o}C to 70 ^{o}C with an interval of 3 ^{o}C. Down: Change in the integral of the resonance peak of PDMAEMA (3.8-4.1 ppm) as well as that of P(AAm-*co*-AN) (1.3-2.0 ppm) as a function of temperature, showing the LCST behavior of the PDMAEMA block and the UCST of the P(AAm-*co*-AN) block in the diblock copolymer.....77

Figure 36. AFM images of the thermosensitive micellar aggregates of the three UCST diblock copolymers: (a) P(AAm-*co*-AN)-*b*-PS, showing that micelles formed at T>UCST of the P(AAm-*co*-AN) block (image at 50 ^{o}C) aggregate at T<UCST (20 ^{o}C); (b) P(AAm-*co*-AN)-*b*-PDMA, showing that micelles formed at T<UCST of the P(AAm-*co*-AN) block (image at 10 ^{o}C) dissolve at T>UCST (50 ^{o}C); and (c) P(AAm-*co*-AN)-*b*-PDMAEMA, showing that micelles formed at T>LCST of the PDMAEMA block (micelle core) and T>UCST of the P(AAm-*co*-AN) block (micelle corona) (image at 70 ^{o}C) can reverse the micelle core and corona at T<LCST and T<UCST (10 ^{o}C), with micelles dissolved at temperatures between LCST and UCST of the two blocks (35 ^{o}C).....79

Chapter 3

Figure 37. Chemical structures of the UCST random and block copolymers synthesized using RAFT polymerization. 84

Figure 38. The ^{1}H NMR spectrum of P1 (in d_6-DMSO). 86

Figure 39. The ^{1}H NMR spectra of P2 and P3 (in d_6-DMSO).....87

Figure 40. The ^{1}H NMR spectra of P4 and P5 (in d_6-DMSO).....88
Figure 42. Size exclusion chromatography (SEC) traces of the various polymers (P1-P6) dissolved in DMSO. All the polymers show a unimodal distribution. The sample P6 (triblock copolymer) was synthesized using P5 as macromolecular chain transfer agent, and its SEC trace shows shorter retention time, indicating chain growth. 90
Figure 43. Emission spectra of pyrene dissolved in aqueous solution of P6 at varying concentrations; inset: variation of **I1**/**I3** in pyrene emission spectra as a function of polymer concentration. The critical micelle concentration, determined as the intersection of the two lines, is about 1.0×10^{-3} mg.mL^{-1}. 93
Triblock copolymer micelles (1 mg.mL^{-1}) loaded with the pyrene dye (1×10^{-6} M) were prepared using the same method as that described above for the determination of CMC.93
Figure 44. Plots of solution transmittance vs. temperature for P(AAm-*co*-AN) (sample **P1**) in PBS solution at different pH values (polymer concentration: 5 mg/mL; heating and cooling rate: 1 ^{o}C/min; solid and dotted lines: cooling and heating runs respectively).....96
Figure 45. Plots of solution transmittance vs. temperature for P(AAm-*co*-AN-*co*-AAc) in PBS solution at different pH values (polymer concentration: 5 mg/mL; heating and cooling rate: 1 ^{o}C/min): a) sample **P2**, and b) sample **P3**. 96
Figure 46. Plots of solution transmittance vs. temperature for P(AAm-*co*-AN-*co*-4VP) in PBS solution at different pH values (polymer concentration: 5 mg/mL; heating and cooling rate: 1 ^{o}C/min): a) sample **P4**, and b) sample **P5**. 97
Figure 47. Change in cloud point as a function of solution pH for all random copolymers (samples 1-5). The seemingly vertical line for sample **P5** corresponds to a slope of 228 ^{o}C per unit pH. 98
Figure 48. Photographs of the **P5** solution at room temperature with various pH from 4.50 to 4.75, showing the transition of the polymer from soluble to insoluble state over pH increase from pH 4.60 to 4.65.....100
Figure 49. (a) Plots of solution transmittance vs. temperature for the **P5** solutions

(polymer concentration: 5 mg/mL; heating and cooling rate: 1 ^{o}C/min; solid and dotted lines: cooling and heating runs respectively) and (b) Plots of the UCST change as a function of ionic strength (data was calculated from this Fig.a) at pH 4.75 and pH 4.50 in PBS with additional 350 mM NaCl added, in water with 75 mM $CaCl_2$ and in water with 150 mM $CaCl_2$. In this Fig.a, the two vertical red dotted lines indicate the cloud point positions of **P5** in PBS solution (from Figure 46b); and these transmittance curves were normalized to 100% for clarity. 101

Figure 50. Plots of solution transmittance vs. temperature for the triblock copolymer P(AAm-*co*-AN-*co*-4VP)-*b*-PDMA-*b*-P(AAm-*co*-AN-*co*-4VP) in PBS solution at different pH values (polymer concentration: 5 mg/mL; heating and cooling rate: 1 ^{o}C/min).....103

Figure 51. DLS results of the triblock copolymer P(AAm-*co*-AN-*co*-4VP)-*b*-PDMA-*b*-P(AAm-*co*-AN-*co*-4VP) in PBS solution: a) size distribution at different pH values, and b) plot of hydrodynamic diameter (D_H) vs. solution pH.....103

Figure 52. a) Fluorescence emission spectra of Nile Red-loaded micellar solution of P(AAm-*co*-AN-*co*-4VP)-*b*-PDMA-*b*-P(AAm-*co*-AN-*co*-4VP) recorded at various pH (λ_{ex}=540 nm); b) plot of normalized fluorescence intensity vs. solution pH; c) and d) TEM images obtained by casting the solution at pH 4.75 and 4.50 respectively. 105

Figure 53. a) Fluorescence emission spectra of pyrene-loaded micellar solution of P(AAm-*co*-AN-*co*-4VP)-*b*-PDMA-*b*-P(AAm-*co*-AN-*co*-4VP) recorded at various pH ; b) variation of **I1**/**I3** in pyrene emission spectra as a function of solution pH.....106

CONCLUSIONS AND PERSPECTIVES

Figure 54. The scheme showing the rapid and selective separation of specific protein from the mixture by employing UCST polymer. 112

Figure 55. Upper: schematic Illustration of NIR-light-triggered UCST gel to sol process due to heating by encapsulated AuNRs. Lower: chemical structure of the UCST polymer

forming the hydrogel.....114
Figure 56. (a): Setup used to detect protein diffusing from the hydrogel into the aqueous solution after 785 nm laser irradiation. (b) Plots of the fluorescence emission intensity vs NIR irradiation time, showing a temporal control of the protein release by turning the NIR laser on and off.....115
Figure 57. upper: the structure of light responsive UCST polymers; down: light triggered release of drugs from light responsive UCST polymers formed micelle.....117

LIST OF TABLES

CHAPTER 1

Table 1. Hydration Energies, ESP surfaces and logP values from DFT Calculation (units in kJ/mol for hydration energies and ESP surfaces) 40

Table 2. Characteristics of Synthesized P(NIPAM-*co*-CBA) Random Copolymers 41

Table 3. Cloud Points (^{o}C) of Various Copolymer Solutions.....44

CHAPTER 2

Table 4. Summary of the Characterization of the UCST Random and Block Copolymers57

CHAPTER 3

Table 5. Characteristics of synthesized copolymers 85

Table 6: Cloud points (^{o}C) of various copolymer solutions obtained on cooling as well as on heating (in parentheses). 98

INTRODUCTION

All polymers can react more or less to changes of environmental conditions (stimuli), such as temperature, pH, light, ion concentration, electric or magnetic field and mechanical force, *etc*. In most cases, the properties of the polymers change gradually with these stimuli. However, some polymers can undergo dramatic transformations in their macroscopic properties as a consequence of minor external stimuli, which are called stimuli-responsive polymers (smart polymers). They are of special interest due to their good stimuli-responsiveness, easy processing and excellent mechanical properties. Therefore, a great deal of attention has been paid to this research area over many years (1-10). Based on the types of stimuli, stimuli-responsive polymers can be classified into three major categories: physical-(temperature, light, ultrasound and electric/magnetic field, *etc.),* chemical-(pH, carbon dioxide, light, ionic strength and reduction/oxidization, *etc.)* and biochemical- (enzyme, antigen and bio-signals, *etc.)* responsive polymers. Among different types of smart polymers, thermosensitive polymers have attracted particular attention because temperature is a stimulus that can be applied externally and reversibly in a non-invasive manner in contrast to, for instance, chemical additives. Furthermore, spontaneous temperature fluctuations also occur in nature during day and night cycles as well as in inflamed tissues in the context of biomedical and nanotechnology applications (11-17).

In the Introduction, we concentrate primarily our attention to the relevant literatures on temperature responsive polymers in aqueous media because most of the research projects presented in this thesis deal with thermoresponsive behaviours. A brief summary of the basic principles and characterizations of the thermoresponsive polymers is firstly given. The following sections present the two types of thermoresponsive polymers in aqueous solution, including those displaying either a lower critical solution temperature (LCST) or an upper critical solution temperature (UCST). Thermoresponsive polymers that can react

to other stimuli, like pH, will be discussed in the next section. In those sections, polymer properties, representative examples as well as their applications in the literature will also be discussed. The Introduction will be closed with a statement of the objectives of the thesis work.

1. Basic Principles of Thermoresponsive Polymers in Aqueous Solution

In general, polymers become more soluble in organic solvents upon heating. However, for polymers in aqueous solution with partial miscibility, two types of phase separation behaviours exist (6,18). If polymers exhibit good solubility (miscible) below a specific temperature and phase separation (or precipitation) above this temperature, this temperature is termed "lower critical solution temperature" and this system is considered as having the LCST phase behavior. In contrast to LCST, polymers characterized with UCST phase behaviour are well dissolved in water at high temperature and undergo phase separation below a certain temperature. Strictly speaking, the LCST and UCST are the lowest and highest temperature, respectively, at which two phases may be observed, which correspond to a certain polymer concentration. In practice, the terms of LCST and UCST are utilised irrespective of the polymer concentration for the sake of simplicity.

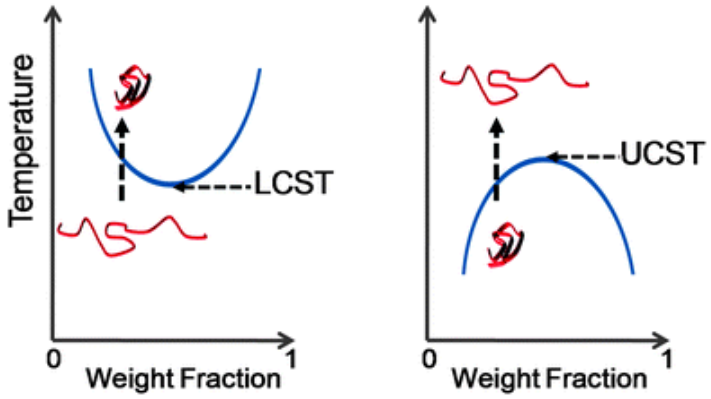

Figure 1. Schematic representation of the polymer phase diagrams for polymers exhibiting (a) LCST behavior; (b) UCST behavior [17].

Physical chemists usually use binary phase diagrams of phase separation temperature as a function of the polymer concentration to schematically depict these two types of polymer phase transitions as shown in Figure 1 (17). These curves represent the equilibrium concentration of the polymer in the two phases in the phase-separated state. The LCST and UCST are defined as the minimum and maximum temperature of these curves, respectively, of the phase diagrams. As mentioned above, the LCST and UCST are only at a distinct critical concentration. At any other concentrations the temperature where phase separation occurs is only the "phase transition temperature". Only one phase exists for all compositions above the UCST and below the LCST. Indeed, the phase transition temperature of some polymers like PNIPAM is almost independent of the concentration or molecular weight. Then the transition temperature at any given concentration is almost identical to the LCST. However, it is important to stress that the phase transition temperature of many polymers is concentration dependent. The detail of the differences will be discussed later in the Introduction.

From the thermodynamic point of view, thermoresponsive polymers present a fine balance between hydrophobic, hydrophilic and H-bond-mediated interactions in their structures. Around the critical or phase separation temperature, a small temperature change will make the polymer chains to collapse or to expand in response to the new adjustment of these interactions between the polymeric chains and the aqueous media.

One can use the Gibbs free energy to generally understand the dissolving or mixing process of a polymer in a given solvent (19).

$$\Delta G_{mix} = \Delta H_{mix} - T \Delta S_{mix}$$

where ΔG_{mix}, ΔH_{mix} and ΔS_{mix} are the changes in free energy, enthalpy and entropy, respectively, and T is the absolute temperature. The enthalpic effect, ΔH_{mix}, is due to the balance between intra- and intermolecular forces and due to solvation, e.g. hydrogen

bonding and hydrophobic interaction. The entropic effect, ΔS_{mix}, is related to the dissolution process itself and due to the ordered state of water molecules in the vicinity of the polymer.

In the case of a LCST phase transition, the Gibbs free energy becomes negative with decreasing the temperature. That means the changes of enthalpy and entropy of mixing both have to be negative.

For LCST: $\boldsymbol{\Delta H_{mix} < 0, \Delta S_{mix} < 0}$

Although the term $-T\Delta S_{mix}$ is positive, it is small at low temperature and ΔH_{mix} is a large negative value. Therefore, ΔG_{mix} is negative, meaning that the mixing is favored. In other words, the polymer is soluble at low temperature. With increasing the temperature, the positive value of positive term $-T\Delta Smix$ increases. At the same time, the negative value of ΔH_{mix} become smaller and smaller, resulting a positive ΔG_{mix}. The phase separation will occur with this positive ΔG_{mix} at high temperature.

In the case of a UCST phase transition, the Gibbs free energy becomes negative with increasing the temperature. That is to say, the changes of enthalpy and entropy of mixing both have to be positive.

For UCST: $\boldsymbol{\Delta H_{mix} > 0, \Delta S_{mix} > 0}$

The term $-T\Delta S_{mix}$ is always negative, but it is small at low temperature and ΔH_{mix} is a large positive value. Thus, ΔG_{mix} is positive, meaning that the mixing is unfavored. The negative value of the term $-T\Delta S_{mix}$ will become larger and larger with increasing the temperature while the positive value ΔH_{mix} become smaller, leading to a negative ΔG_{mix} at high temperature. This value change of ΔG_{mix} can explain why the polymer is insolube at low temperature and become soluble at high temperature in solution.

If the polymer is soluble at all temperatures, then

$$\Delta H_{mix} < 0, \Delta S_{mix} > 0$$

The final case is that

$$\Delta H_{mix} > 0, \Delta S_{mix} < 0$$

which means the polymer is insoluble at all temperature.

The key understanding of the equation for LCST polymer is that it requires negative entropy of mixing; the system become more "ordered" upon mixing. Actually, polymer that exhibits a LCST-type behavior in aqueous solution has extensive hydrogen bonding interactions with the surrounding water molecules at low temperature and restricted intra- and intermolecular hydrogen bonding between polymer molecules. In this state, the coiled structure is favoured as this allows for the maximum interaction between the polymer and water molecules, which make the polymer easier to dissolve in aqueous solution (Figure 2) (19). Thus, water loses entropy when it is associated to the polymer chains due to the formed directed (oriented) hydrogen bonding. Upon heating, the hydrogen-bonding with water weakens, while the intra- and intermolecular hydrogen bonding/hydrophobic interactions of the polymer become dominant, resulting in liberation of the well-organized water molecules into the bulk and the tendency of less contact between water and hydrophobic surfaces. These interaction changes will induce the polymer structure from coiled state to a denser globule state. Further aggregation of the globules causes the solution to appear opaque. That is to say, the enthalpic hydrogen bonding interaction ΔH_{mix} will decrease, but more importantly the entropy term ($-T\Delta S_{mix}$) will become dominant leading to a positive Gibbs free energy of mixing, thus leading to phase separation.

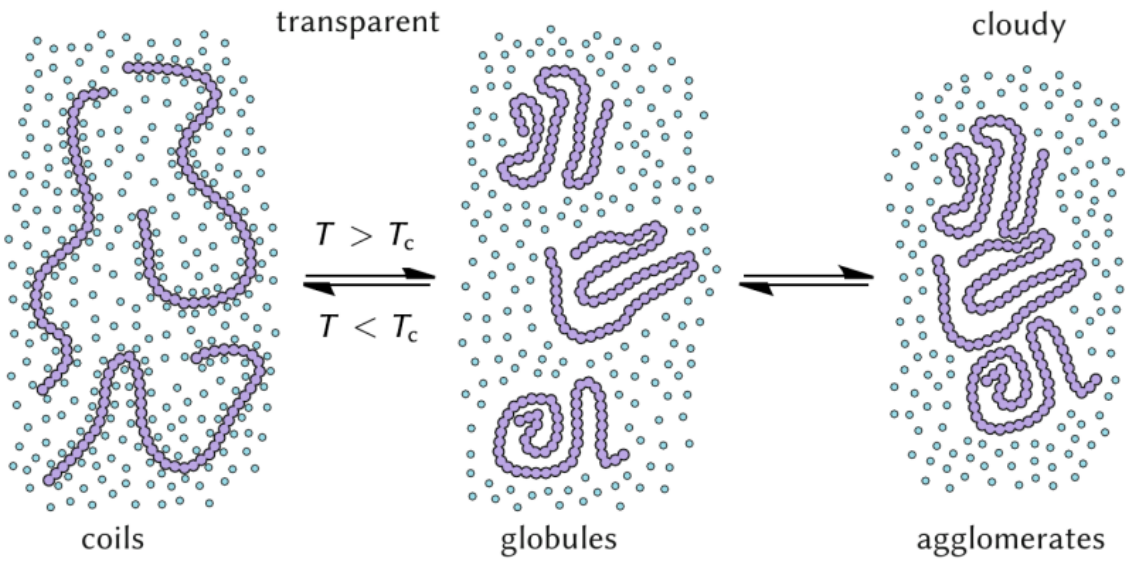

Figure 2. Schematic illustration of the clouding of a polymer solution by the coil-to-globule transition. The aggregation of the globules causes the solution to appear opaque [19].

In general, the LCST strongly depends on the polymer structure. It can be stated that better hydrated polymers have a higher LCST than less hydrated polymers. As such, increasing the molecular weight of a polymer, which decreases its hydration due to enhanced polymer–polymer interactions, will lead to a lower LCST. Furthermore, introducing hydrophobic end-groups or more hydrophobic (co)monomers will also decrease the LCST.

For UCST polymers, the polymer chains have strong supramolecular associative interactions strength between themselves. When this interaction is broken upon polymer dissolution, the loss in enthalpy energy is larger than the gain upon dissolution, leading a positive enthalpic component ΔH_{mix}, so is the entropic component ΔS_{mix} because the polymer dissolves in the aqueous solution. At low temperature the ΔH_{mix} exceeds the $T{\cdot}\Delta S_{mix}$ term, thus ΔG_{mix} is positive and the polymer is insoluble. With increasing the temperature, the supramolecular associative interaction between polymer chains

decreases, the $T \cdot \Delta S_{mix}$ term overweighs ΔH_{mix}, thus ΔG_{mix} becomes negative and the polymer dissolves spontaneously. Generally it can be said that UCST polymers exhibit stronger polymer-polymer interactions than LCST polymers.

The phase transition temperature of UCST polymers are directly correlated to the strength of the intermolecular interactions, thus incorporating hydrophobic end-groups or hydrophobic (co)monomers will increase the transition temperature because it will increase the hydrophobic environment for associative hydrogen bonding interactions. This hydrophobic environment enhances the hydrogen bonding strength leading to a higher UCST transition temperature (18). This effect is opposite to LCST polymer, which would decrease LCST transition.

2. Characterization of the Phase Transition

There are several methods which can be used to characterize the phase transition of thermoresponsive polymer solutions, such as differential scanning calorimetry (DSC), light scattering, turbidity measurement, *etc.* (20-23). Among these methods, measuring the cloud point using a turbidity meter (such as UV-Vis Spectroscopy) is the easiest and most common way to follow phase separation at a certain polymer concentration, that is, monitoring the solution transmittance changes of the polymer solution at 500–700 nm as a function of temperature (Figure 3). The high transmittance means that the polymer is soluble and solution is transparent. In contrast, the polymer is insoluble and solution appears cloudy which result in low transmittance. The "cloud point" is the temperature at which the solution has this change in transmittance. The definition of the cloud point varies in the literature. Generally, some people take the temperature at the transmittance drops from 100% to 90%; others define the temperature at 50% or inflection point of the transmittance curve. In this thesis, we take the inflection point as the "cloud point".

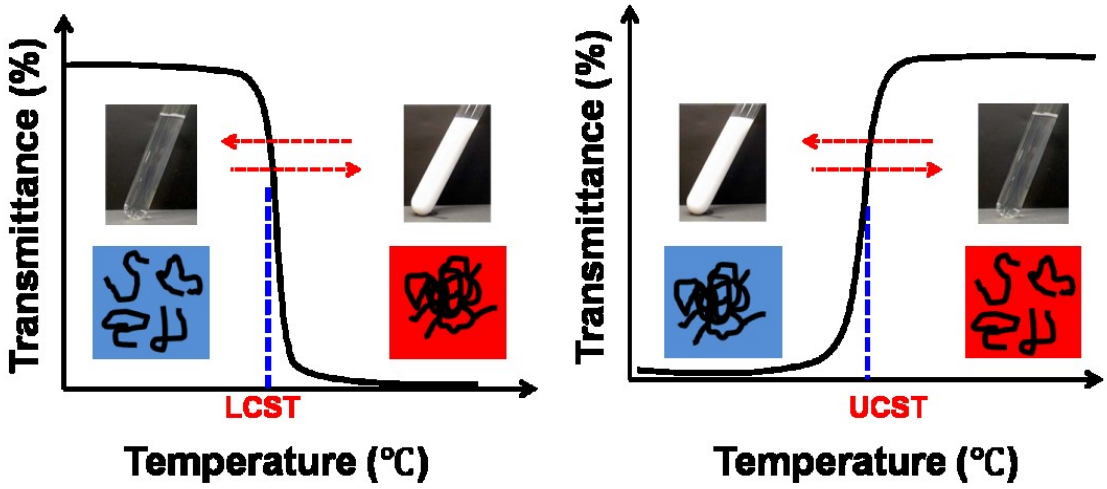

Figure 3. Phase transition of the polymer solution is characterized by solution transmittance changes as a function of temperature.

The cloud points of a given polymer solution can also be different on heating and cooling due to kinetic hindrance and aging in the collapsed state even with the same heating–cooling rates (like a typically used 1 ℃/min). The difference between the cloud point upon cooling and heating is noted as hysteresis. It was found that the hysteresis could be caused by the formation of some additional hydrogen bonds in the collapsed state (at temperatures above LCST) (24, 25). Thus, the cloud point determined from the turbidity measurement is dependent on many parameters. To this regard, when reporting the cloud point of thermoresponsive polymers in publication, it is important to emphasize the polymer concentration, the way the cloud point is determined (definition, on heating or cooling), as well as the heating and/or cooling rate.

As stated above, the phase transition temperature is not exactly the same as LCST or UCST. The LCST–UCST is found only at the maximum/minimum of the phase diagrams (Fig.1) at a distinct critical polymer concentration. The phase-separation temperature describes the phase boundary of the system in equilibrium and is concentration dependent. The cloud point upon cooling (heating) denotes the temperature where the solution

becomes turbid or clears at a fixed cooling (heating) rate. At this ceratin rate, the system may not be in equlilibrium. Thus, the cloud points upon cooling and heating measured by a turbidity meter also do not coincide with the phase transition temperature because of this potential kinetic effect. However, people often term the “LCST/UCST” instead of the determined cloud point in their statement for the purpose of simplicity. This will also be used in this thesis.

3. Polymers with LCST-type Thermoresponsiveness in Water

Numerous polymers are known to display LCST in aqueous solution and they have been summarized in many reviews (11,26,27). Generally, all LCST polymers which show phase transition between 0°C and 100°C have hydrophilic and hydrophobic groups with a subtle balance among them in their structure. Otherwise, the phase transition temperature will go out of the temperature range from 0°C to 100°C. The most common hydrophilic moieties are amides and ethers while hydrophobic moieties are short aliphatic groups. The most important types of LCST polymers will be selectively addressed in this section (Figure 4).

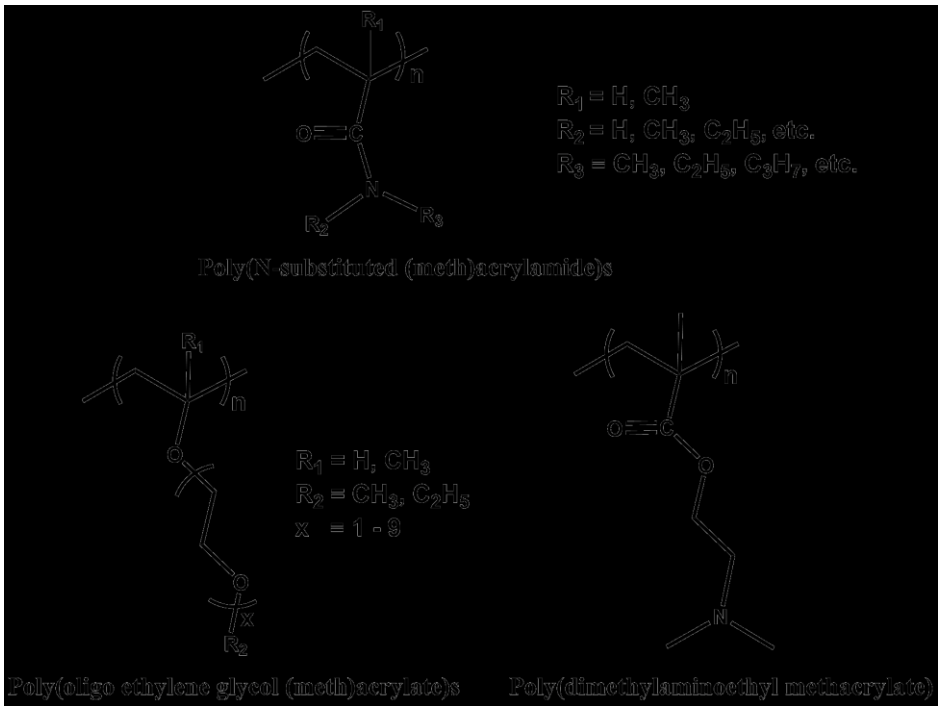

Figure 4. Chemical structures of selected representative LCST thermoresponsive homopolymers

3.1. Poly (*N*-substituted (meth)acrylamide)s

Poly(*N*-alkyl (meth)acrylamide)s bearing the amide functionality are perhaps the most common family of LCST thermoresponsive polymers (Fig. 4). Among them, a prominent example is PNIPAM (R_1,R_2=H, R_3=isopropyl), which was the first reported and the most studied, not only among this family but over all of thermoresponsive polymers (28–30). The first reason for the popularity of PNIPAM is that it shows the LCST between room and body temperature in water (LCST around 32°), making it very interesting for biomedical applications. Furthermore, the phase transition temperature of PNIPAM is relatively insensitive to slight changes of polymer concentration, polymer chain length and solution pH. In fact, small variations of these conditions only affect the LCST of PNIPAM by a few degrees (31). Thus, PNIPAM has always been considered to be the gold standard of thermoresponsive polymers.

The hydrophilic groups of PNIPAM are the repeating amides along the chain while the isopropyl groups are hydrophobic. As already mentioned, at low temperature, PNIPAM chains exist in the random-coil state with high flexibility due to the extensive hydrogen bonding between water molecules and the side amide groups. Upon increase of the temperature above LCST, the polymer inter-chain interaction (H-bonds between amide groups and hydrophobic attraction between the isopropyl groups) become dominate while thermal energy breaks the hydrogen bonding between water molecules and amide groups, which leads to the transition of polymer chains from coil state to globular conformation and finally induces the macroscopically phase separation of the polymer from water. This phase transition process is schematically illustrated in Figure 5 (30).

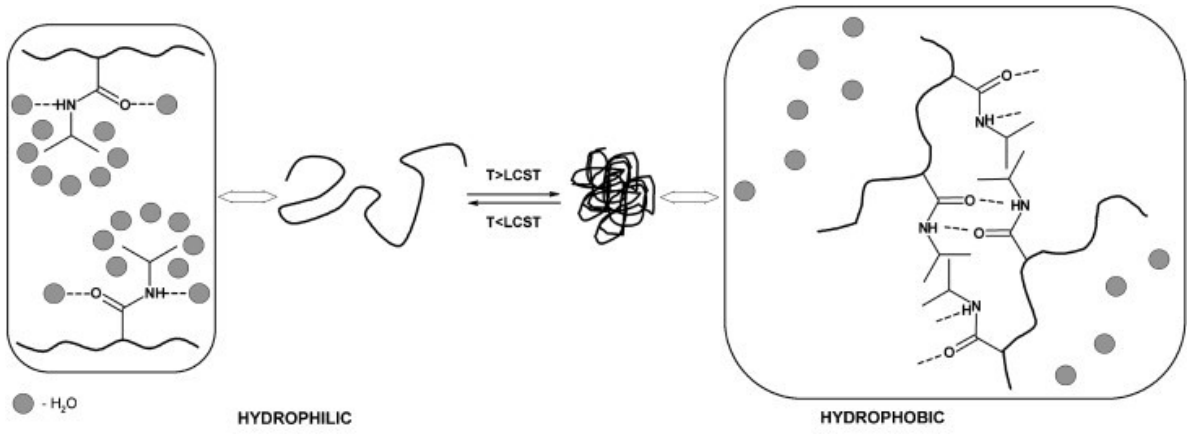

Figure 5. Illustration of temperature induced PNIPAM phase transition [30].

Poly(*N*-*n*-propylacrylamide) (PNNPAM) (R_3=propyl) and poly(*N*-cyclopropylacrylamide) (PNCPAM) (R_3=cyclopropyl) are the analogies of PNIPAM with the same group of R_1 and R_2 (R_1,R_2=H) but different R_3 (Fig. 4). They also show the LCST behaviour in water in the temperature range of 0 to 100 °C. However, although the structures of these poly(N-propylacrylamide)s are similar, their phase transition behaviours, such as the sharpness of the temperature responsiveness and the dependencies of transition temperatures on the polymer concentration, are different. The studies of the volume phase

transitions of these polymers gels show that PNNPAM and PNIPAM exhibit a discontinuous volume phase transitions around 26 and 36 °C, respectively, while PNCPAM undergoes a continuous volume change at 40-50 °C. Their phase transitions in aqueous solutions were also investigated by IR spectroscopy, static and dynamic light scattering. The result revealed that the difference of their phase transition behavior is due to the differences in the modes of the hydrophobic hydration of propyl group. Details of the differences were discussed in the literature (32–35).

Poly(N,N-diethylacrylamide) (PDEAM) (Fig. 4, R_1=H, R_2, R_3=C_2H_5) is another reported thermoresponsive polymer of similar structure and LCST (33 °C) as PNIPAM (36), leading to the comparison between them. PNIPAM has a secondary amide side group which is able to act as both hydrogen bond donor and acceptor thus can form intra- or inter chain hydrogen bonds (37). By contrast, PDEAM bears a tertiary amide side group and thus only act as hydrogen bond acceptor, making it unable to form hydrogen bonds between polymer chains and ultimately exhibit different phase behaviours (38). Firstly, PNIPAM shows the hysteresis of its phase transition due to the formed intra- or inter chain hydrogen bonds, while PDEAM does not exhibit hysteresis due to the absence of any formed hydrogen bonds by themselves, in the collapsed state at temperatures higher than the phase transition temperature (24,25). Secondly, with a similar monomer/cross-linker ratio, the swelling ratio of PNIPAM gel below LCST is much higher than that of PDEAM gel. The PDEAM gel also shows a broader phase transition temperature interval and a more pronounced dependency of the swelling ratio on the crosslinker content and slower reswelling kinetics (39).

3.2. Poly (oligo ethylene glycol (meth) acrylate)s

Despite the interesting properties of poly(N-alkyl (meth)acrylamide)s, especially PNIPAM, and the resulting extensive investigations in biomedical research (40),

scientists have been searching for alternative LCST polymers with further improved properties with regard to suppressing the occurrence of hysteresis and, most importantly, eliminating of the toxicity of *N*-isopropylacrylamide monomer. Poly(oligo ethylene glycol (meth)acrylate)s (Fig. 4) possessing oligo ethylene glycol side chains were found to be an interesting class of alternatives (41–44). As shown in Figure 6, their phase transition temperature can be tuned by variation of the number of ethylene glycol repeat units and the oligo ethylene glycol chain-end functionality, resulting in hydrophilicity change with similar chemical nature (41). For instance, poly(2-(2-methoxyethoxy)ethyl methacrylate) ($PMEO_2MA$) (2 ethylene oxide units) and $PMEO_3MA$ (3 ethylene oxide units) have transition temperatures around 26 and 52 °C, respectively. Poly(oligo(ethylene glycol) methacrylate)s (POEGMA) with even longer side chains can exhibit much higher LCSTs in water (typically 60-90 °C with 4–9 ethylene oxide units) (43). The transition temperature values of polymers with ethyl chain end were around 22–26 °C, lower than those of the corresponding polymers with methyl chain ends.

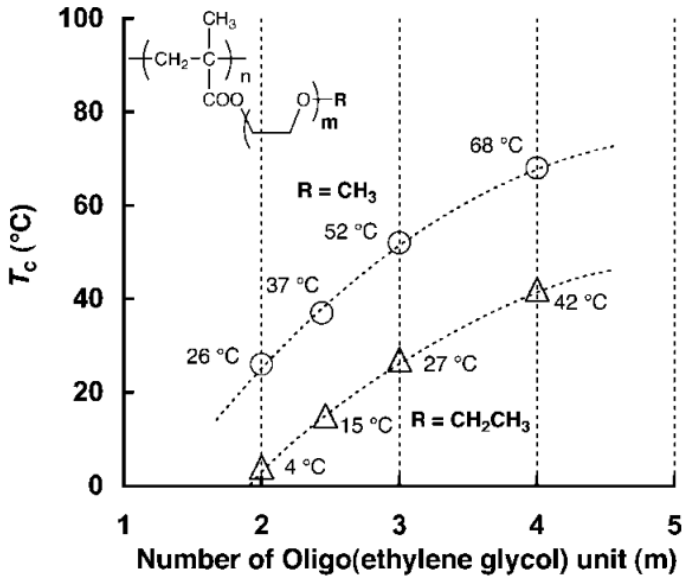

Figure 6. Relationship between the number of oligo(ethylene glycol) units (m) and the cloud point. Data of methyl and ethyl ethers are plotted with ○ and ∆ , respectively. The cloud points of 0.2 wt % polymer in water were measured at a heating rate of 0.3 °C min^{-1}. m=2.5 when polymers with equal composition of the two monomers (m=2 and m=3) (random copolymer) [41].

Since the LCSTs and solubility of the polymers are related to the balance of polymers' hydrophobicity and hydrophilicity, the transition temperature of the random copolymer P(MEO_2MA-*co*-PEGMA) copolymers can be fine-tuned between 26 and 90 °C by varying the ratio of the two monomers MEO_2MA and OEGMA (44,45). For example, copolymers with 5, 8, or 10% of OEGMA units in the initial comonomer feed show the cloud points of 32, 37, or 39 °C respectively. A detailed comparison of LCST behavior of such P(MEO_2MA-*co*-OEGMA) copolymers with PNIPAM was made by Lutz et al. (42). They found that both polymers have a similar thermoresponsive behavior with regard to salt, molecular weight and concentration dependence of the cloud point. However, P(MEO_2MA-*co*-OEGMA) copolymers exhibit a much more uniform thermal profile with heating and cooling cycles (no significant hysteresis) while PNIPAM exhibits a sharp

transition on heating and a broad hysteresis in the cooling process (Fig. 7). OEGMA-based polymers cannot form intermolecular hydrogen bonding and thus exhibit limited hysteresis (24).

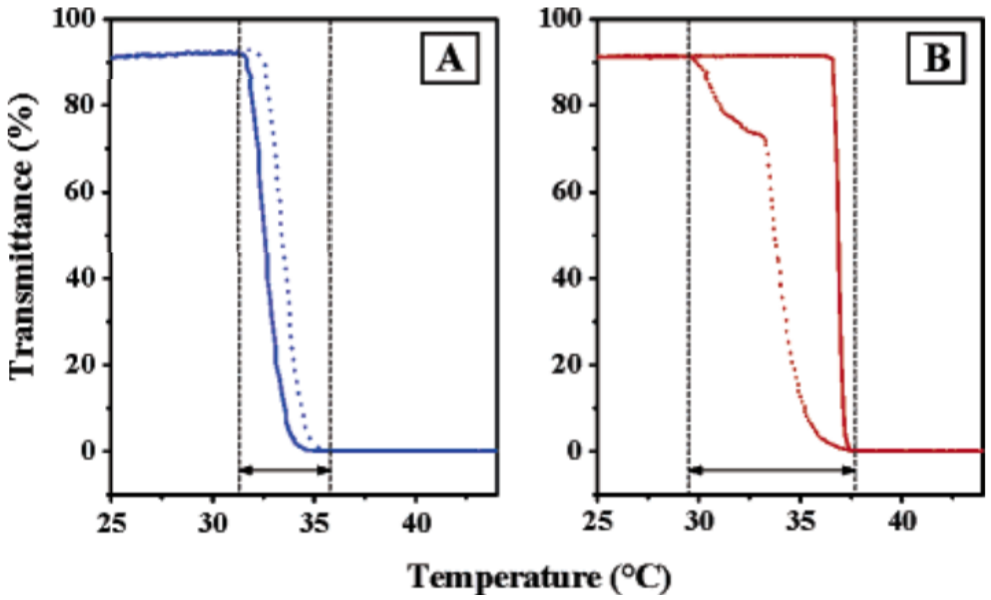

Figure 7. Plots of transmittance as a function of temperature measured for aqueous solutions (3 mg.mL^{-1}) of either (A) a copolymer P(MEO_2MA-*co*-OEGMA) containing 5 mol % of OEGMA per chain (DP ≈ 100; Mw/Mn = 1.34), and (B) a homopolymer PNIPAM (DP ≈ 100; Mw/Mn = 1.12): solid lines, heating cycles; doted lines, cooling cycles [42].

Finally, poly(oligo ethylene glycol (meth)acrylate)s, with tunable LCST, are based on neutral, water-soluble, nontoxic, biocompatible and commercially available oligo ethylene glycol segments, making them probably the most promising alternative to PNIPAM for use in diverse biologically relevant applications (46).

3.3. Poly (dimethylaminoethyl methacrylate)

Poly(dimethylaminoethyl methacrylate) (PDMAEMA) (Fig. 4) is another example of

thermoresponsive polymers with LCST behaviour. It exhibits a phase transition temperature ranging from 14–50 °C in pure water, depending on the molecular weight of the sample (47–49). It is also a weak polybase with a pKa of around 7.5 owing to a tertiary amine side group (50). The tertiary amine group is partially protonated under acidic condition and becomes deprotonated under basic condition. The different amine group protonated states, differing in the interactions between polymer and water, will result in different LCST values depending on the solution pH. The polymer's cloud point is shifted to a higher temperature with lowering pH due to the protonation, leading to increase in the electrostatic repulsive force and prevention of the phase transition. Therefore, the cloud point can be readily tuned by adjusting the pH of the solution and the molecular weight (51). The dual-responsiveness to pH and temperature has attracted widespread research on PDMAEMA in therapeutic and biomedical applications (50). Moreover, poly(N,N'-diethylaminoethyl methacrylate) (PDEAEMA), with longer hydrophobic groups at the end of the amine group, has stronger hydrophobic interactions at high pHs, Indeed, the polymer undergoes an abrupt precipitation above pH 7.5 due to the deprotonation of amino groups and the resulting hydrophobic interactions (52).

Interestingly, the tertiary amine groups of PDMAEMA can be quaternized with 1,3-propane sultone to a zwitterionic moiety. Then converting from LCST-type PDMAEMA, the formed poly(sulfobetaine methacrylate) (polySBMA) can display an UCST behavior (53). More details on UCST polymers are given below.

4. Polymers with UCST-type Thermoresponsiveness in Water

For UCST-type polymers, the solubility in water increases with temperature. Actually, many polymers are known to display UCST phase transition in organic solvents (54). Some classical examples include polystyrene in cyclohexane, polymethylmethacrylate in acetonitrile and polyethylene in diphenylether. Polymers with UCST in organic–water

mixtures are also studied in recent years. These polymers usually comprise good hydrogen bond accepting moieties, such as ester, ether or tertiary amide groups which have specific interactions with the co-solvent. For example, PNIPAM, the LCST polymer in water, has UCST behaviour in many mixtures of water and organic solvents including ethanol, propanol, and dimethyl sulfoxide (DMSO) at higher organic solvent concentrations (55). Polymers with UCST transition in alcohol–water mixtures were recently reviewed by Richard et al. (56).

Polymer solutions that show thermoresponsiveness in water are especially important since water, as a solvent, is cheap, safe and biologically relevant. However, in comparison to the widely studied LCST polymers, UCST polymers in aqueous solution are rarely investigated (18). While the LCST behavior of polymers in water is based on entropy driven dehydration, the UCST behavior in water requires strong supramolecular attraction of the polymer chains and an enthalpy driven solubility phase transition. The two main types of UCST polymers in water are charged zwitterionic polymers and polymers based on hydrogen bonding.

4.1. Zwitterionic polymers with UCST in water

Zwitterionic polymers have both positively and negatively charged moieties located either at the same monomer unit or at the pendant side chains of different monomer units. Among the well studied zwitterionic polymers, polysulfobetaines have received growing attention due to their thermoresponsivity. Since these polymers contain cationic or anionic groups, electrostatic dipole-dipole association is present (57,58). As such, strong molecular interactions based on intra- and intermolecular electrostatic interactions lead to collapsed structures at low temperature (Fig. 8) (18). Upon temperature increase, the thermally enhanced molecular motions will break the electrostatic interactions of zwitterionic charges resulting in dissolution of the polymer.

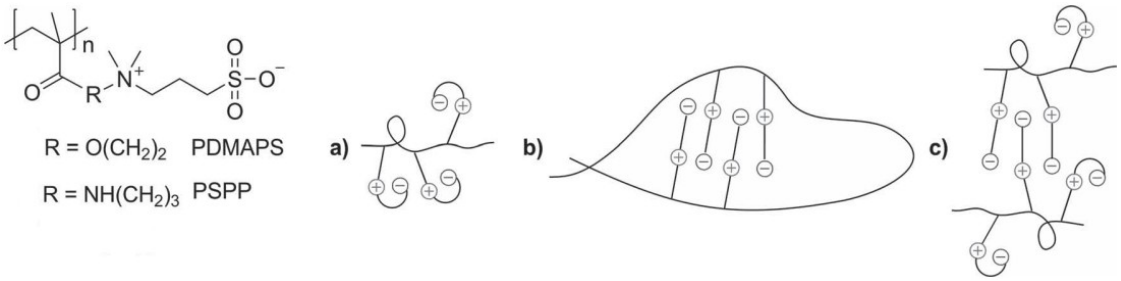

Figure 8. The UCST of zwitterionic polymers relies on intra- and intermolecular coulomb interaction: a) intragroup, b) intrachain, c) interchain [18].

Poly(3-[*N*-(3-methacrylamidopropyl)-*N*,*N*-dimethyl]ammoniopropanesulfonate (PSPP) (59) and poly-[3-dimethyl(methacryloyloxyethyl) ammonium propane sulfonate] (PDMAPS) (60,61) are the most common zwitterionic UCST polymers in water (Fig. 8). They are also the only two polymers where turbidity curves and partial phase diagrams of the homopolymers are available. Their phase separation temperature depends strongly on the molar mass of polymers, with the transition temperature decreasing upon decreasing molar masses. (59), To observe the UCST, the solution should be salt-free or contains low salt concentration. For PDMAPS, having the cloud point at 26 or 43 °C, the weight average molecular weight needs to be as high as 258 or 448 kg/mol, respectively; while a sample of 29 kg/mol has no measurable cloud point at all (62). Adding a salt into the polymer solution will enhance the solubility of polyzwitterions and lowers the UCST. For example, a 0.1 wt% solution of PDMAPS (710 kg/mol) showed a cloud point upon cooling of about 55°C in pure water, but upon increasing the NaCl concentration from 0.05 to 0.1 to 0.3 wt%, the cloud point dropped to 45, 39 and 18 °C, respectively (60). A recent paper reported that by incorporating a hydrophobic group, like benzyl, the UCST of zwitterionic polymers can be successfully tuned from 6 to 82 °C; the phase transition was also sharp, fully reversible and reproducible in low salt solutions (below 76 mM NaCl) (Fig. 9) (63). In addition to direct synthesis of UCST polymers from zwitterionic monomers, they can also be obtained by quaternization of the precursor polymers. As

stated above, PDMAPS can be obtained from PDMAEMA (a LCST polymer) after being quaternized with 1,3-propane sultone (53). The UCST could also be tuned by the degree of quaternization (64).

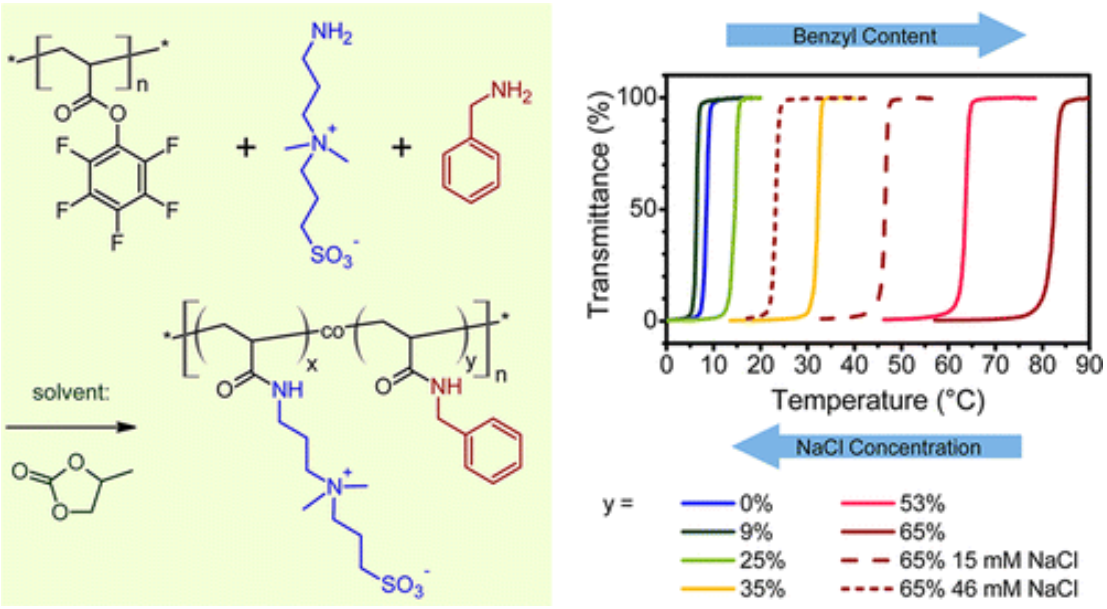

Figure 9. Synthetic route to hydrophobically modified zwitterionic copolymers and tunable UCST in aqueous solution under different conditions [63].

Since zwitterionic polymers have charged groups, their UCST are also greatly affected by the solution's pH which changes the intra- and intermolecular electrostatic interactions. It is known that changes in solution pH can act to screen the repulsive electrostatic forces between charged groups along the polymer chain of polyelectrolytes, resulting in shrinkage of the polymer coil. Usually, polymers exhibit the highest transition temperature when the solution's pH is around their isoelectric point, where the macromolecules exist in the zwitterionic form. Generally, the UCST decreases quickly when pH is below or above the isoelectric point. For PDMAPS, it showed the highest UCST at pH around 7.0. When pH was adjusted to 6.0 or 8.0, the UCST can drop by up to 30 °C within one pH unit (65). The similar phenomenon was found in other

zwitterionic UCST polymers, like poly(*L*-serinyl acrylate)s (66).

Statistical copolymers of zwitterionic moieties and NIPAM showed both UCST and LCST (67). The cloud point varied with the copolymer composition. Not only the copolymer can exhibit these two opposite thermoresponsive behaviour, but also the block copolymers. Laschewsky and co-workers reported the first reversed core-shell thermoresponsive diblock copolymer displaying both UCST and LCST by polymerization of NIPAM and the zwitterionic monomer 3-[*N*-(3-methacrylamidopropyl)-*N*,*N*-dimethyl]ammoniopropane sulfonate (SPP) (68). This structure combines two different thermo-sensitive hydrophilic blocks, enables one of the blocks to undergo a physical or a chemical transformation in aqueous solution, which renders it insoluble, while the copolymer stays in solution by virtue of the hydrophilicity of the other block. In this block copolymer, the PNIPAM block exhibits a LCST while the PSPP block shows an UCST. The bock copolymer can be stable in the full temperature range between 0 and 100 °C by appropriately designing of the block lengths. At low temperatures, the PSPP block forms the core of the aggregates that remain dispersed in solution by the PNIPAM block. At high temperatures, the PNIPAM becomes the hydrophobic block forming the core and the PSPP block constitutes the water-soluble corona. At intermediate temperatures, both blocks can be dissolved in water. In this way, colloidal aggregates which switch reversibly from their “inside” to the “outside”, and *vice versa*, can be prepared in water without any additives, just controlled by a simple thermal stimulus (Fig. 10). The mechanism of aggregation of PNIPAM-*b*-PSSP was studied in detail by Virtanen et al. (69). Their results reveal that salt and polymer concentration also have a big effect on the aggregation process in addition to the temperature. Other block copolymers consisting of a block of PDMAPS and a second block of PNIPAM (53) or poly(N,N-diethylacrylamide) (70) or POEGMA (64) were also reported in literature.

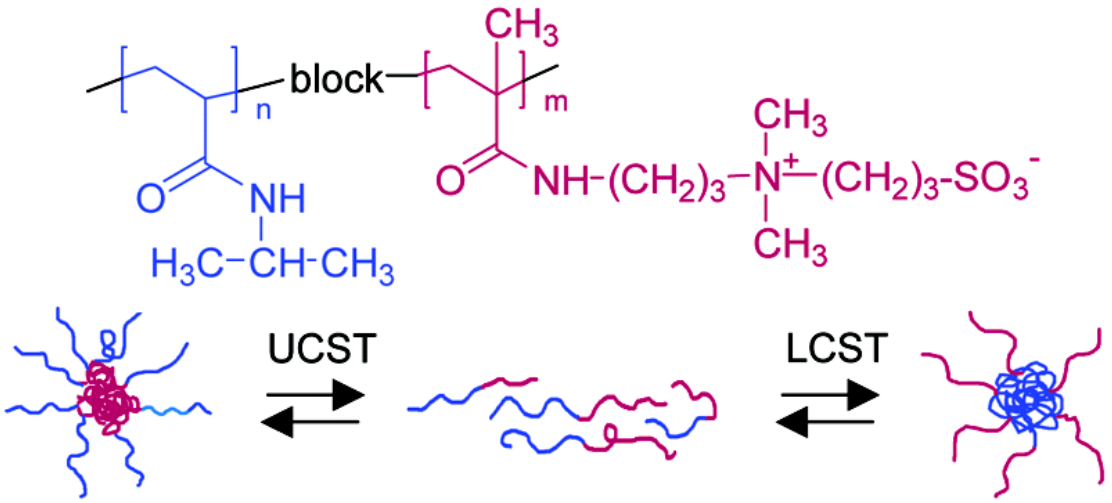

Figure 10. Chemical structure of PNIPAM-*b*-PSPP block copolymers and schematic illustration of the temperature-dependent association states [68].

Zwitterionic UCST polymers have great potential for applications in the smart material area. They can be used for preparation of thermoresponsive hydrogels (71–74), nanoparticles (62), hybrids containing biological molecules (75), surfaces with thermo-switchable wettability (76–78). Our group prepared UCST polymer-coated AuNPs (Fig. 11), for which AuNPs were firstly stabilized with a LCST diblock copolymer PEO-*b*-PDMAEMA with the PDMAEMA block tethered to the surface and then the PDMAEMA block was selectively quaternized to impart the UCST thermosensitivity (79).

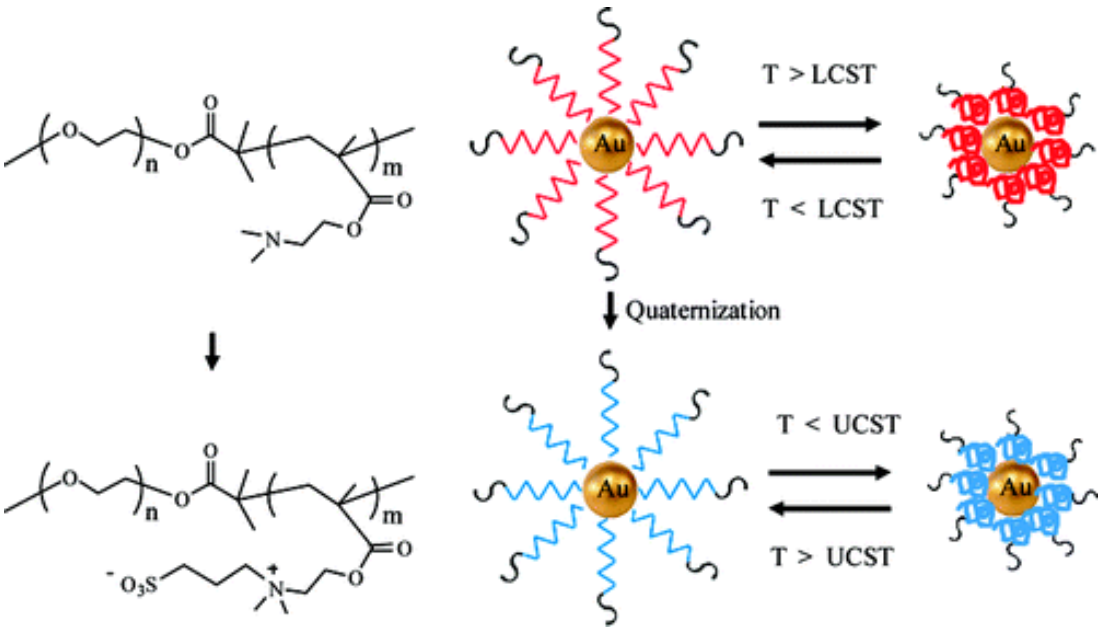

Figure 11. Chemical structures of the diblock copolymers tethered to gold nanoparticles (AuNPs) and schematic of both LCST and UCST thermal phase transitions on AuNP surface [79].

4.2. Hydrogen bonding based UCST polymers in water

Polymers with UCST in aqueous solution can also be based on hydrogen bonding interactions between polymer moieties and with water molecules. The UCST of this type of polymers is less sensitive to the salt concentration in water since hydrogen bonding is more stable against ions than the coulomb interactions in zwitterionic polymers. So far hydrogen bonding based UCST polymers are mainly featured with primary amide or ureido groups, except poly(acrylic acid) (PAAc), which are responsible for the hydrogen bonding formation (18). Some examples are outlined below.

PAAc was an extensively studied pH-responsive polymer and can actually display an UCST in aqueous solution of high ionic strength. Different from other hydrogen bonding based UCST polymers, its phase behavior was heavily influenced by the interaction with electrolytes (80). There was no UCST in pure water and the cloud point was observed for

the polymer solution with NaCl concentrations at least above 400 mM. The cloud point increased linearly with the NaCl concentration. Copolymers with AAc units can also show an UCST. An example was copolymer of AAc and NIPAM at different monomer ratios (81). With increasing the NIPAM content, the copolymer can change from showing only LCST to showing both UCST and LCST, in aqueous NaCl solution. The same behaviors were also found for copolymers of AAc and diethylacrylamide (82).

Poly(*N*-acryloyl glycinamide) (PNAGA), a polyacrylamide bearing a terminal amide group, is one of the most studied UCST polymers based on thermally reversible hydrogen bonding. It was first synthesized by Haas in 1964 for producing a thermo-reversible hydrogels in concentrated aqueous solutions (83). It was also found that the hydrogel could not be formed in the presence of hydrogen-bond interrupting agents like thiocyanate or urea and that the gel melting temperature increased with the molar mass and concentration of the polymer (84). However, PNAGA did not show thermoreversible gelation in dilute solutions. It was concluded that the gelation is based on the hydrogen bonding as supported by both calculation and experiments (85–88). Lutz and coworkers first prepared the PNAGA via RAFT polymerization by using ionic chain transfer agent and initiator (89). Agarwal *et al*. further investigated the UCST phase separation of PNAGA prepared using free radical polymerizaiton in DMSO using AIBN as initiator (90). It was demonstrated that the phase transition could be efficiently suppressed by ionic species that were introduced unintentionally from impurities present in the monomer, or ionic initiators or chain transfer agents, or as a result of the hydrolysis caused by the high polymerization temperature or sample preparation (Fig.12) (91). By taking precautions and designing the synthesis to limit the possibility of ionic impurities or end groups, the transition temperature of the polymer was clearly observed. Salt effect was also studied on the transition temperatures (92).

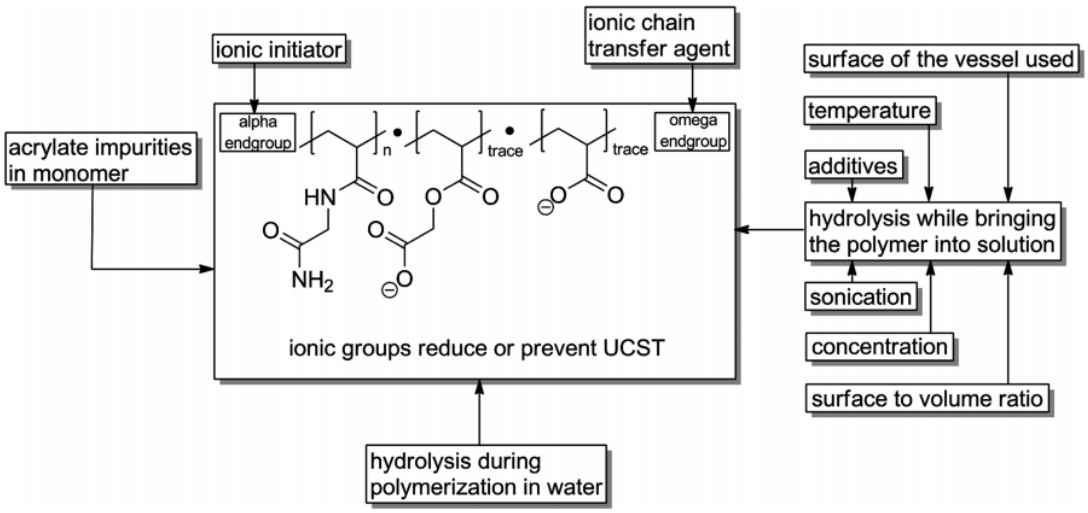

Figure 12. Pathways of unintentional introduction of ionic species into UCST polymers such as PNAGA [91].

Several copolymers based on NAGA were also reported such as poly(*N*-acryloylglycinamide-*co*-*N*-acetylacrylamide) (PNAGA-*co*-NAcAAm) (90), poly(*N*-acryloylglycinamide-*co*-butyl acrylate) (PNAGA-*co*-BA) and poly(*N*-acryloylglycinamide-*co*-styrene) (PNAGA-*co*-St) (93). The transition temperature of PNAGA-*co*-BA was found to decrease after each heating-cooling cycle due to increased hydrophilicity resulting from acrylic acid groups formed from the hydrolysis of butyl acrylate groups above 50 °C. By contrast, the UCST of (PNAGA-*co*-St) was found to be stable over nine consecutive heating-cooling cycles, because the comonomer of styrene does not undergo the hydrolysis reaction.

Some derivatives of PNAGA can display UCST-type thermoresponsivity, too. Ohnishi and coworkers first synthesized poly(*N*-aryloylasparagineamide) (PNAAAm), poly(*N*-methacryloylasparagineamide) (PNMAAAm) and poly(*N*-acryloylglutamineamide) (PNAGAAm) by free radical polymerization using ammonium peroxodisulfate as a radical initiator, and examined their phase transitions at the concentration of 0.2% (w/v) (94). PNAAAm showed cloud points of 22 and 25 °C in pure water and 20 mM Tris-HCl

buffer, respectively. In pure water, PNMAAAm showed both the UCST at 13 °C and LCST at 33 °C. When the polymer was dissolved in PBS, it displayed the UCST at 13 °C, as well as LCST at 30 °C. It was found that the cloud points of both PNAAAm and PNMAAAm did not change significantly upon addition of salt. For PNAGAAm, no cloud point was observed in pure water and the cloud points in 40 and 80 mM Tris-HCl buffer were very low at 2 and 3 °C, respectively. Different from PNAGA, PNAAAm and PNMAAAm show cloud points in pure water although they bear ion species derived from the charged initiator ammonium peroxodisulfate. Two explanations were proposed (18). First, in contrast to PNAGA, PNAAAm, and PNMAAAm may exhibit stronger interpolymer hydrogen bonding due to the second primary amide group. Theoretically, it was believed that a higher ΔH value resulted from increased interpolymer hydrogen bonding diminishes the negative impact of ionic groups. Second, free-radical polymerization used by Ohnishi et al. leads to a broad high molar mass distribution. The cloud points of high molar mass fraction are less affected by the ionic species. This was supported by Lutz and coworkers who examined the chain length-dependent UCST behavior of PNAAAM with a similar charged end group (95). The cloud point upon cooling of PNAAAM showed a clearly decreased trend with molar mass.

Maruyama et al. reported a series of ureido-derivatized polymers, such as poly(allylurea) (PU) and poly(L-citrulline) derivatives, and their UCST behavior under physiological buffer conditions (96). The modified PU derivatives with succinyl anhydride (PU-Su) and acetyl anhydride (PU-Ac) also showed UCST. The UCST of these type polymers can be controlled by their molecular weight, content of ureido groups, polymer concentration, and concentration of the added salt in the aqueous solution. In a following study, they used PU derivatives to examine the capture and separation of particular proteins from a protein mixture by cooling-induced phase separation (97). Selective and rapid capture of particular proteins from the protein mixtures was shown, indicating that the ureido-derivatized polymers are potential media for bioseparation under biofriendly

conditions. Lee and coworkers also synthesized a series of thermoresponsive ureido-derivatized polymers and further quaternization reactions with methyl iodide. By changing the degree of quaternization, the UCST could be precisely tuned (98). Very recently, Yusa et al. prepared a diblock copolymer composed of a biocompatible hydrophilic block and a ureido-derivatized block (99). Blow the UCST of the ureido-derivatized block, the micelles were formed. These UCST-type thermo-responsive polymer micelles are potentially used as a carrier for drug delivery system, because the polymer micelles can incorporate hydrophobic guest molecules with controlled-release, and their surface is covered with biocompatible shells.

Ritter et al. showed the UCST-type transition of poly(*N*-vinylimidazole-*co*-1-vinyl-2-(hydroxymethyl)imidazole) which can be tuned between 19 and 41 °C by copolymer composition (100). Later they further modified the copolymer with small amounts of adamantyl groups to make the UCST transition sensitive towards β-cyclodextrins (β-CD) by the host/guest interaction (101). Thus, they showed that the supramolecular control through β-CD is not limited to LCST polymers, but also possible for UCST polymers.

Arguably the most significant progress on H-bond-based UCST polymers was made by Agarwal's group. They showed that copolymers based on two commercially available monomers, acrylamide (AAm) and acrylonitrile (AN), can exhibit UCST thermosensitivity in water and PBS (Fig.13) (93). By simply adjusting the comonomer feed ratio that determines the random copolymer composition, the transition temperature of P(AAm-*co*-AN)s could easily be tuned. It increases with increasing the acrylonitrile content. Moreover, the hysteresis between the cloud point upon cooling and heating was very small, with only 1−2 °C in most cases, and the transition temperature can remain constant over several repeated cycles due to the hydrolytic stability of the monomers. Later, based on P(AAm-*co*-AN), they also reported a block copolymer with double

thermoresponsive behavior (LCST-UCST) (102) and a photo cross-linkable UCST-type thermo-responsive polymer that can be used for preparing thermophilic hydrogel films and fibers (103). Other groups in the world have also been working on this easily-accessible UCST polymer. Notably, Wu et al. observed that the transition temperature of P(AAm-co-AN) in D_2O was 10 °C higher than that in H_2O at the same concentration due to the solvent isotope effect (104). A potential application in drug delivery system of P(AAm-*co*-AN) was demonstrated using an UCST polymeric micelle (105). It was found that the polymer nanocarrier could effectively encapsulate doxorubicin and exhibited thermally sensitive drug release both *in vitro* and *in vivo*.

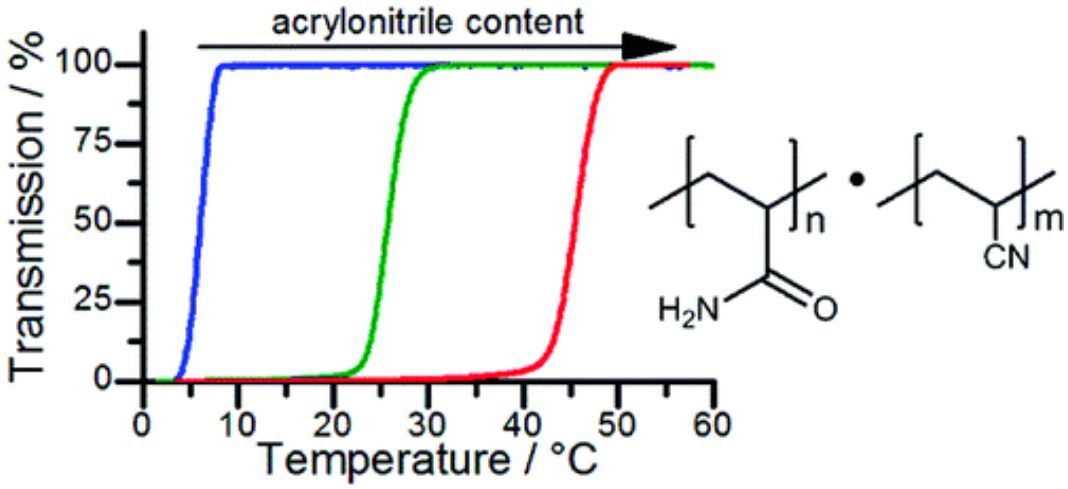

Figure 13. The cloud point of P(AAm-co-AN) in water or PBS buffer can be tuned by adjusting the comonomer ratio [93].

On the other hand, replacing the AN by another hydrophobic monomer, styrene, the copolymer, P(AAm-*co*-St), also displays UCST in water (106). Likewise, the homopolymer polymethacrylamide (PMAAm), having the additional methyl group in the monomer unit with respect to PAAm, shows a UCST, too (93).

5. Thermo-pH Responsive Polymer

As discussed above, thermoresponsive polymers are interesting because of the many potential applications, especially in the drug delivery area (5,6,15). The main rational for this use is the fact that the body or body-site temperature may change upon fever or local infections or diseases, and the drug may be released as a result of such trigger when the LCST or UCST of the polymer carrier is close to body temperature. For example, two different strategies can be used to control the delivery of drugs from the crosslinked LCST nanogel (107). When a hydrophilic drug is incorporated into the swollen nanocarrier, the diffusivity increases and the drug can be released below the LCST. The rate of the drug release depends on the swelling degree of the nanocarrier and the tortuosity of the pathway the drug taken (Fig. 14a). By contrast, when a more hydrophobic drug is incorporated in the nanogel below the LCST, it can be squeezed out above the LCST due to the pressure generated during hydrogel collapse (Fig. 14b).

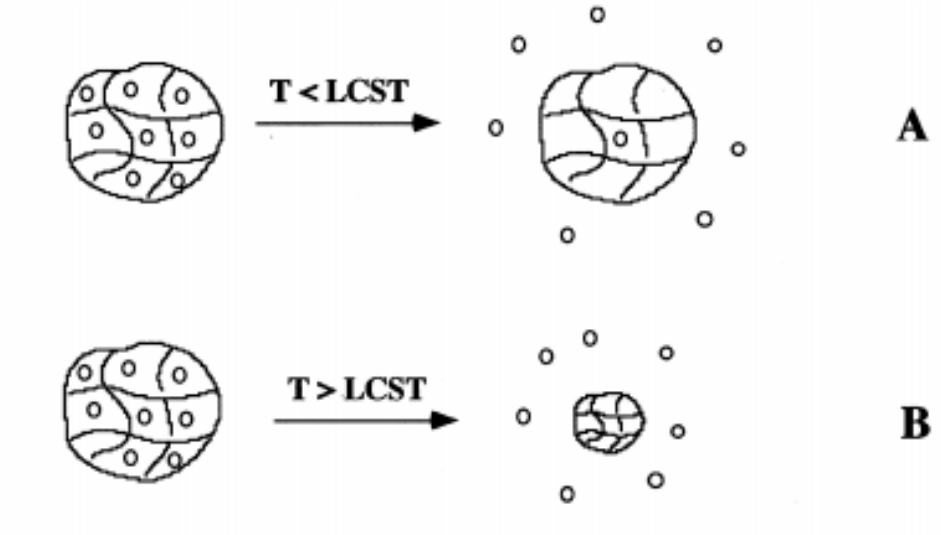

Figure 14. Schematic illustration of the strategies for controlling the delivery of drugs (circles) using thermoresponsive nanocarrier, A: diffusion-controlled release; B: drug release due to gel volume contraction. [107]

A very recent example was reported by Zhou and coworkers (Fig. 15) (108). They developed a thermoresponsive drug delivery system based on thermoresponsive Pluronic F127-poly(D,L-lactic acid) (FP) copolymer decorated with folate (FA) ligands for active targeting of folate receptor (FR)-overexpressed tumor cells. The nanocarrier assembled from the copolymer had a LCST of 39.2 °C which is close to body temperature. These micelles could remain stable at normal temperature (37 °C) with little amount of encapsulated anticancer drug Doxorubicin (DOX) released. At a slightly elevated temperature (40 °C), the shrinkage of thermoresponsive segments causes a rapid release of DOX and instantly increases the drug concentration locally. They also conducted the cytocompatibility analysis and measured the cellular uptake efficiency. The results showed that this nanocarrier has excellent cytocompatibility and a much better efficiency of cellular uptake, resulting in higher cytotoxicity to FR-overexpressed tumor cells.

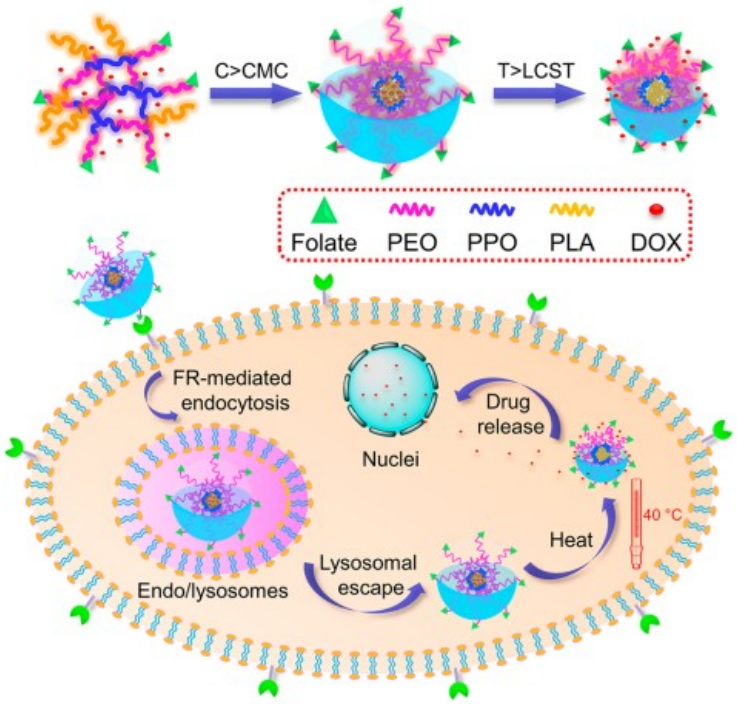

Figure 15. Schematic representation of thermosensitive nanocarrier working as a targeted drug delivery system with controlled drug release [108].

However, thermoresponsive polymers have some restrictions in practical applications with only a single stimulus, temperature. Biological systems are rich with nanoscale structures that selectively respond to multiple environmental changes rather than a single stimulus. Thus, in order to ideally mimic the complexity, and also to achieve a better control for drug release profile and improve the therapeutic efficacy, thermoresponsive polymers that can sense other stimuli (dual or multiple stimuli) in a predictable manner are of great interest. Therefore, fundamental research is required for engineering polymer structures that can combine the temperature stimulus with other stimuli, such as pH, light, ultrasound, electric/magnetic field, carbon dioxide, redox, *etc.* (5,109–111). Among these stimuli, pH is the most popular stimulus employed to combine with temperature to make a dual responsive polymer, that is, thermo-pH responsive polymer. Actually, an abnormal pH is also often observed, like temperature, in many diseased tissues and cellular compartments. For example, the intracellular compartments of cancer cells is more acidic (pH 4.5–6.5) than in healthy tissues (pH 7.4) (5). This difference in local pH values among various tissues and cellular compartments has frequently been the inspiration for designing thermoresponsive polymers with pH-sensitivity.

In fact, some homopolymers, such as PDMAEMA discussed in the previous section, not only show the thermoresponsive behavior, but also can respond to pH change (47,51). It displays a higher cloud point with decreasing the pH value of the polymer solution due to the protonation of the tertiary amine groups in side chains. Other thermo-pH dual responsive homopolymers were also developed, which include poly(N-acryloyl-N'-propylpiperazine) (PAcrNPP) (112), poly(N-ethylpyrrolidine methacrylate) (PEPyM) (113) and alkyne modified poly(2-hydroxyethyl methacrylate) (PHEMA) (114).

Although materials based on thermo-pH dual responsive homopolymers have already been much studied (115), the limited number of such polymers restricts the exploration

for applications. An obvious approach is to copolymerize a pH-responsive comonomer into the thermoresponsive polymer. The pH-responsive moieties usually are weak acids, like carboxylic acids, or bases like tertiary amines. Carboxylic acids are the most employed for this purpose. The earliest example was reported by Hoffman et al. who first developed a thermo-pH dual responsive copolymer of NIPAM and AAc for using as an oral matrix drug delivery system (116,117). The matrix was formed by physically mixing the copolymer and the drug. This matrix copolymer behaved similarly to the enteric copolymer coating, remaining insoluble at stomach temperature and acidic pHs, and later dissolving in the intestines. However, compared to enteric-coated tablet, where the drug would be rapidly released within the intestines once the coating is dissolved, the NIPAAm-AAc copolymer matrix released drug at intestinal pHs over several hours, and at rates that depended on the amount of AAc in the copolymer. In a more recent example, Jiang and coworkers constructed a thermo- and pH dual-responsive micelle based on poly(NIPAAm-*co*-acrylic acid)-*b*-polycaprolactone (P(NIPAAm-*co*-AA)-*b*-PCL) diblock copolymer (118). Interestingly, these nanoparticles could encapsulate up to 30 wt% of paclitaxel (PTX) and aggregated at pH 6.9 and body temperature. Faster drug release was observed at higher temperature and lower pH.

Chiu et al. prepared a pH and temperature dual stimuli-responsive nanogel from self-assembling of poly(acrylic acid-*co*-2-methacryloylethyl acrylate) (P(AAc-*co*-MEA)) grafted with either PNIPAM or PNIPAM with monomethoxypoly(ethylene glycol) (mPEG) followed by crosslinking via radical polymerization (Fig.16) (119). The drug, doxorubicin (DOX), can be effectively encapsulated into the nanogel at pH 7.4 and room temperature via electrostatic interactions with ionized AAc residues and hydrogen-bond pairings with grafted PNIPAM. Notably, the nanogel rapidly released the drug upon changing pH to 5.0 due to the extensive disruption of AAc/DOX complexes resulting from the reduced ionization of AAc residues within the gel layer and the pronounced shrinkage of the nanogel. Their *in vitro* experiments showed that the DOX-loaded

nanogel particles, after being internalized by HeLa cells via endocytosis, could rapidly release the payload within acidic endosomes or lysosomes. A significant drug accumulation in nuclei was observed and these drugs displayed comparable cytotoxicity to free DOX in the cells.

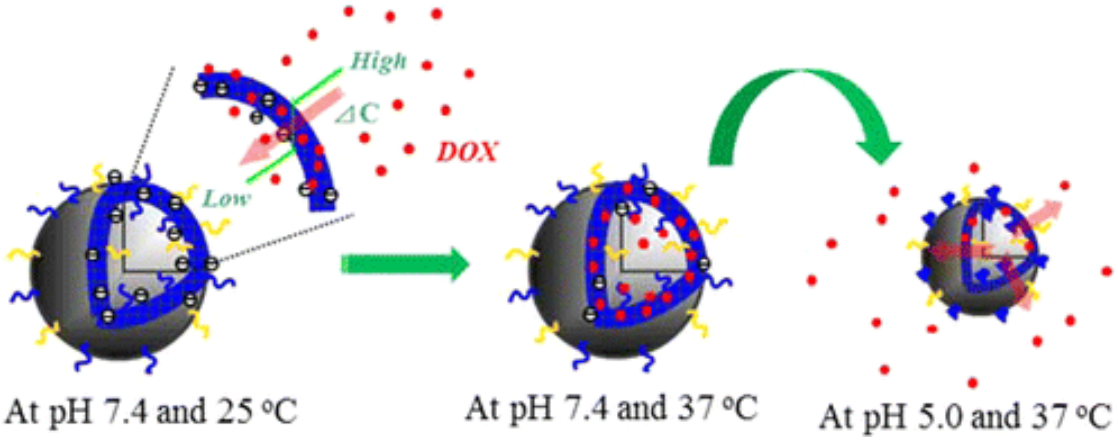

Figure 16. Schematic illustration of nanogels encapsulating and releasing the drugs [119].

6. Objective of the Thesis

The general objective of this thesis is to make contributions to our fundamental knowledge and understanding about thermoresponsive polymers in aqueous solution. More specifically, the research was conducted with the purpose of developing new strategies or approaches to use pH to control the water solubility of the polymers, which is the basis of many applications. To achieve the goal, rational polymer structural design was the emphasis of our studies. The research works described in this thesis can be divided into two parts.

In the first part, presented in Chapter 1, we developed a new comonomer design for enhancing the efficiency and sensitivity of the pH-induced LCST shift of thermosensitive polymers. The basic idea is to incorporate in the LCST polymer structure a comonomer bearing two acid groups of similar pKa. With respect to comonomers containing a single

acid group, the designed comonomer structure makes it more hydrophobic in the protonated state (pH < pKa) and more hydrophilic in the deprotonated state (pH > pKa). This feature leads to an increased LCST shift upon pH change. Our studies have validated this comonomer design as a general strategy to amplify the pH sensitivity of the LCST polymers.

The second part of the thesis, presented in Chapter 2 and Chapter 3, describes our research focused on the underexploited UCST polymers. In the study in Chapter 2, we synthesized a UCST copolymer P(AAm-*co*-AN) *via* RAFT polymerization, and used it as a macro-RAFT agent to synthesize three repersentive diblock copolymers. Owing to different designs, their self-assembled structures can exhibit a variety of thermally induced changes as dictated by the UCST of the P(AAm-*co*-AN) block, including reversible dispersion-aggregation of micelles, dissolution-formation of micelles, and reversal of micelle core and corona. The results demonstrated that P(AAm-*co*-AN) is a robust UCST polymer and can be introduced into controlled polymer architectures through the controlled radical polymerization. This is a significant achievement because it opens the door to developing new polymer materials with the UCST type thermosensitivity.

In the third project detailed in Chapter 3, we further explored UCST polymers for a new application. By taking advantage of the high sensitivity of UCST to charged groups in the polymer structure, we succeeded in preparing polymers that can undergo straightforward water solubility reversal in a wide accessible temperature range upon a slight pH variation. We demonstrated that micelles of this kind of polymers could be disrupted by a pH change as small as 0.25 unit. The underlying principle for such ultra-pH-sensitivity is general and might be extended to other UCST polymers.

CHAPTER 1 A NEW COMONOMER DESIGN FOR ENHANCING PH-TRIGGERED LCST SHIFT OF THERMOSENSITIVE POLYMERS

1.1 Introduction

PH-sensitive polymers have been the focus of a considerable amount of research and development effort. The interest is largely driven by the potential applications of this type of stimuli-responsive polymers in controlled drug delivery (120–123). Compared to the physiological pH of about 7.4, a wide range of acidic pH values can be found in tumor tissues (pH ~ 6.8) and in the intracellular compartments of cancer cells (pH 4.5-6.5). When a pH–sensitive polymer drug carrier (e.g. micelles), stable at pH 7.4, enters an acidic environment of either tumor tissues or inside cancer cells, with appropriate pKa, the polymer can sense the pH change, and its increased protonation can lead to structural disruption of the carrier and thus allows the drug to be released on the target site. Of the many pH-sensitive polymers that have been studied over the years, a group is particularly interesting. These are thermosensitive polymers whose water solubility features a lower critical solution temperature (LCST), basically being soluble in water at temperatures below LCST (coil chain conformation) and insoluble above LCST (globule) (8,30,40). Poly(N-isopropylacrylamide) (PNIPAM) is a representative example with a LCST of about 32 ^{o}C. This polymer is not pH-sensitive in the homopolymer form, but can be made responsive to pH change by incorporating a number of either acid or base comonomer units into the structure. Since the water solubility of the polymer is influenced by the hydrophilic or hydrophobic nature of the comonomer units, a change in protonation degree of acid or base groups upon pH variation can result in a reversible shift of the LCST. This means that the water solubility can now be controlled by a pH change at a constant temperature.

In the drug delivery application context, if the drug carrier is made of such a LCST polymer bearing acid or base comonomer units, a pH decrease can induce a drastic structural disruption, such as contraction of microgel (with acid comonomer) or dissolution of micelles (with base comonomer). Therefore, pH-triggered LCST shift is an important route towards developing pH-responsive polymers, and the comonomer used may play a key role in determining the polymer's sensitivity to pH change, the pH range where the sensitivity manifests as well as the extent of the LCST shift. Again, PNIPAM provides a telling case. For instance, with acrylic acid (pKa 5) units in PNIPAM, pH variation around 4-6 shifts reversibly the LCST over a temperature range generally above the initial LCST of PNIPAM, because acrylic acid in both the protonated neutral (COOH) and the deprotonated ionic form (COO^-) is more hydrophilic than NIPAM, (124–128) with few exceptions (129). By contrast, with propylacrylic acid, the protonated acid form is more hydrophobic than NIPAM due to the propyl group in the comonomer structure, while the deprotonated form is more hydrophilic than NIPAM; consequently, the pH-triggered LCST shift extends from below to above 32 ^oC (125,130). Similar effect was observed with pH-sensitive homopolymers containing side groups of different hydrophobicity (131).

Despite the advances achieved in LCST-based pH-sensitive polymers, there is still a need for more studies in order to further improve the ability to tailor or control the pH responsiveness to make the polymers better adaptable to specific uses. As a matter of fact, incorporating stimuli-reactive comonomer units into LCST polymers represents a general strategy to make polymers respond to stimuli such as pH, light or CO_2 (9,132–134), to name a few. A common fundamental question to address is how to reduce the amount of stimuli-reactive comonomer required to induce a significant responsiveness or, at a given comonomer content, how to increase the magnitude of the LCST shift. For a given LCST polymer, an adequate choice of the comonomer can make the difference. A more effective comonomer can give a greater swing in response to a stimulus by amplifying the shift of

LCST over a wider temperature range. This can be important for controlled drug delivery applications. For instance, nanogel carrier can be prepared using a polymer whose LCST decreases upon protonation of acid comonomer units. Upon pH decrease, the LCST needs to shift from above the body temperature (37 ^{o}C) to below it in order to allow the nanogel to undergo a volume transition (contraction) that leads to the payload release. It can be expected that a larger LCST decrease should be better than a smaller one, say, between LCST down to 10 ^{o}C or 30 ^{o}C, because a deeper LCST decrease means greater dehydration of the nanogel particle and thus more straightforward release. Being motivated by these considerations, in the present study, we propose and validate a general pH-reactive comonomer design for enhancing pH-induced LCST shift. A new comonomer bearing two carboxylic acid groups, which is the first of the kind to our knowledge, was synthesized and copolymerized with PNIPAM. We show that very large pH-triggered LCST shift can be obtained as a result of increase in both hydrophobicity and hydrophilicity of the acid groups upon protonation and deprotonation, respectively.

1.2. Results and Discussion

1.2.1 The Comonomer Design

The rationale of our comonomer design is schematically depicted in Figure 17. The host polymer, i.e., PNIPAM, has an initial LCST (curve 1). As mentioned above, it is known that having acid comonomer units can decrease the LCST at lower pH if the protonated form of the acid is more hydrophobic than the host (curve 2), and increase the LCST at higher pH if the deprotonated form is more hydrophilic (curve 3). Our hypothesis is that if, at a given amount of comonomer units, the protonated form of the acid can be made even more hydrophobic and the deprotonated form even more hydrophilic than the host, both the decrease (curve 4) and increase (curve 5) in LCST would be more prominent, thus further widening the gap between the LCST upon pH change. Scheme 1 shows the

chemical structure of the comonomer 4-((2-carboxyallyl)oxy)benzoic acid (CBA) designed to test the assumption. As is seen, the basic idea is to bring two acid groups of similar pKa into the comonomer structure. In the deprotonated form, the number of charges is doubled per comonomer unit, which would increase the hydrophilic power; whereas in the protonated form, the presence of the phenyl group should enhance the hydrophobic character. At this point, needless to emphasize that this comonomer design principle is general; different pairings of acid groups are possible, so are the pairings of two bases. In the latter case, the shift of LCST is simply reversed upon pH change, moving to higher LCST at the protonated state and lower LCST at the deprotonated state.

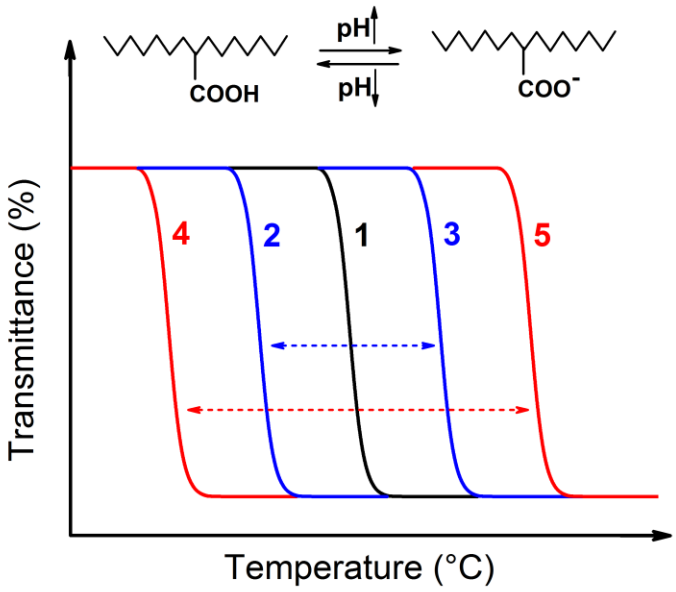

Figure 17. Schematic illustration of pH-induced LCST shifts upon protonation and deprotonation of acid comonomer units. Enhanced LCST shift means larger gap between the low and high LCST at the same acid comonomer content.

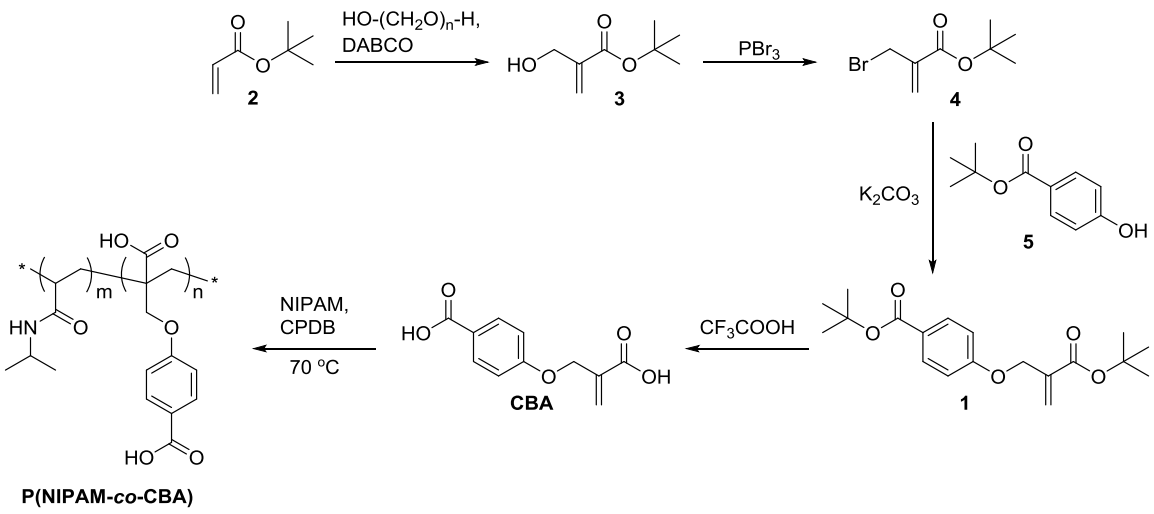

Scheme 1. Synthesis of the comonomer 4-((2-carboxyallyl)oxy)benzoic acid (CBA) and its copolymerization with *N*-isopropylacrylamide yielding P(NIPAM-*co*-CBA).

The Density Functional Theory (DFT) provides the ground state properties of a system knowing its electron density. A DFT analysis (this calculation was conducted by Prof. Armand Soldera's group; the details were described in our collaboration paper *Polym. Chem*. 2015, 6, 6644-6650 and will not be shown here) of the new comonomer was performed to reveal the effect of having two acid units in the structure on the solvation (or hydration) propensity in both the protonated and deprotonated state. It should be emphasized that the calculation was not meant to predict the LCST; rather it was used to have some insight into the possible impact of the comonomer on shifting the host polymer's LCST upon pH change. As a simple model, the calculation was focused on the hydration energy and the number of hydrogen bonds that are formed between the comonomer and water molecules. Since the comonomer can be considered as comprising a methacrylic acid (MAA) and a benzoic acid (BA), for the sake of comparison, the same analysis was also carried out on the two corresponding reference molecules, MAA and BA, separately. The main results are summarized in Table 1. In all cases, the deprotonated acid (pH 7) forms H-bonds with higher potential energy than the protonated state (pH 4),

meaning greater hydration energy with the ionized carboxylic acid. However, the difference in the hydration energy between the two states is significantly larger for CBA than for MAA or BA, which implies that the new comonomer could indeed be more hydrophobic in the protonated state and become more hydrophilic in the deprotonated state. Furthermore, in order to have a better insight on the polarity and hydrophilicity of the molecules, we also calculated the electrostatic potential (ESP) surfaces and logP that is a measurement of the difference in the Gibbs free energy of solvation in water and in n-octanol for a given compound (definition in Experimental Section). Despite the fact that values of logP stemming from DFT calculations do not agree quantitatively with the experimental data, the same tendency is observed. Roughly, logP of BA is twice that of MAA, due to the presence of aromatic cycle. LogP and ESP surfaces both reveal that the deprotonated state of CBA has much greater polarity and hydrophilicity than deprotonated MAA and BA (Table 1) (135,136). These results are in agreement with the calculated hydration energies. It should be noticed that the dependence of the LCSTs of charged PNIPAM-based copolymers on their charge fraction was investigated previously by an analytical theory on a macroscopic thermodynamic level (137).

Table 1. Hydration Energies, ESP surfaces and logP values from DFT Calculation (units in kJ/mol for hydration energies and ESP surfaces)

Molecules		CBA (MAA position)	CBA (BA position)	MAA	BA
Protonated state	Hydration energy	-289.6	-288.4	-287.7	-291.0
	ESP surfaces	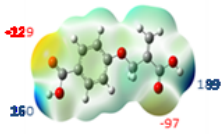		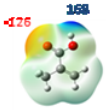	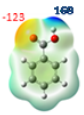
	logP	0.61		0.39 (0.93 exp.)	0.72 (1.87 exp.)
Deprotonated state	Hydration energy	-407.7	-441.1	-392.9	-382.4
	ESP surfaces	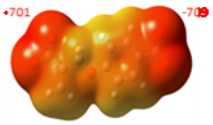			
	logP	-13.55		-7.33	-5.14
Difference in Hydration Energy between the two forms		118.1	152.7	105.2	91.4

1.2.2 pH-induced LCST Shift

As mentioned above, to experimentally test the effect of the new comonomer CBA on the pH-induced LCST shift, a series of random copolymer P(NIPAM-*co*-CBA) with various contents of CBA, were synthesized using RAFT polymerization. Table 2 summarizes the characteristics of the samples. As is seen, the copolymerization proceeds in a controlled way, yielding polymers with reasonably low polydispersity index (M_w/M_n) and general agreement between the feed and ^{1}H NMR-determined molar content of CBA units in the copolymers. The average molecular weights, as determined by SEC using PMMA standards, are relatively low for all samples. The effect of pH on the LCST was investigated by measuring the cloud points of P(NIPAM-*co*-CBA) solutions under the same conditions. Unless otherwise stated, each solution was prepared by dissolving the

polymer (0.2 wt%) in cold PBS (stirring in the ice-water bath), and the solution transmittance (at 500 nm) was recorded as a function of temperature upon heating the solution at a rate of 0.5 ^{o}C/min. For a given polymer solution, the pH was adjusted by using HCl or NaOH, ranging from 4.0 to 7.0 with an interval of 0.5.

Table 2. Characteristics of Synthesized P(NIPAM-*co*-CBA) Random Copolymers

Sample	CBA in feed (mol%)	CBA in polymer (mol%)[a]	M_n (g/mol)[b]	PDI
P1	1.0	2.1	7490	1.16
P2	2.4	4.3	7530	1.12
P3	4.8	7.6	6850	1.21
P4	7.0	10.0	6360	1.23
P5	13.0	17.3	4590	1.32

[a]Calculated by ^{1}H NMR in d_6-DMSO; [b]determined by size exclusion chromatography.

Figure 18 shows the plots of transmittance vs. temperature for the solutions of all P(NIPAM-*co*-CBA) samples, measured at four different pH values: 4.5, 5.0, 5.5 and 6.0. In case no data are shown for a given P(NIPAM-*co*-CAB) sample, it means that at that particular pH no transmittance drop (cloud point) could be detected over the temperature range used for the measurements (10-60 ^{o}C), i.e., the polymer remains either soluble (below LCST, P5 in Figs. 18c and 18d) or insoluble (above LCST, P4 and P5 in Fig.18a). At pH 4.5 (Fig.18a), all samples display a cloud point below 30 ^{o}C, which decreases with increasing the CBA content. This result indicates that at this pH, the acid comonomers are essentially protonated (pH<pKa) and the CBA exerts a hydrophobic comonomer effect on PNIPAM, bringing down the LCST. With pH up to 5.0 (Fig.18b), the situation is drastically reversed, as more acid comonomer groups are deprotonated (pH approaching

pKa). While all samples see their cloud points shifted to higher temperatures, the magnitude of increase is greater with increasing the CBA content, so that the actual cloud points are in the ascending order of the CBA content. At this point, the cloud points of P2 and P3 are only slightly above that of P1, suggesting counterbalance between the hydrophobic and hydrophilic comonomer effects. With pH further raised to 5.5 and 6.0, the cloud points of all samples continue to increase in a pace proportional to the CBA content, widening their differences in cloud point. At these two pH values, the acid groups are mainly deprotonated (pH>pKa) and CBA acts predominantly as hydrophilic comonomer whose effect raises the LCST of P(NIPAM-*co*-CBA).

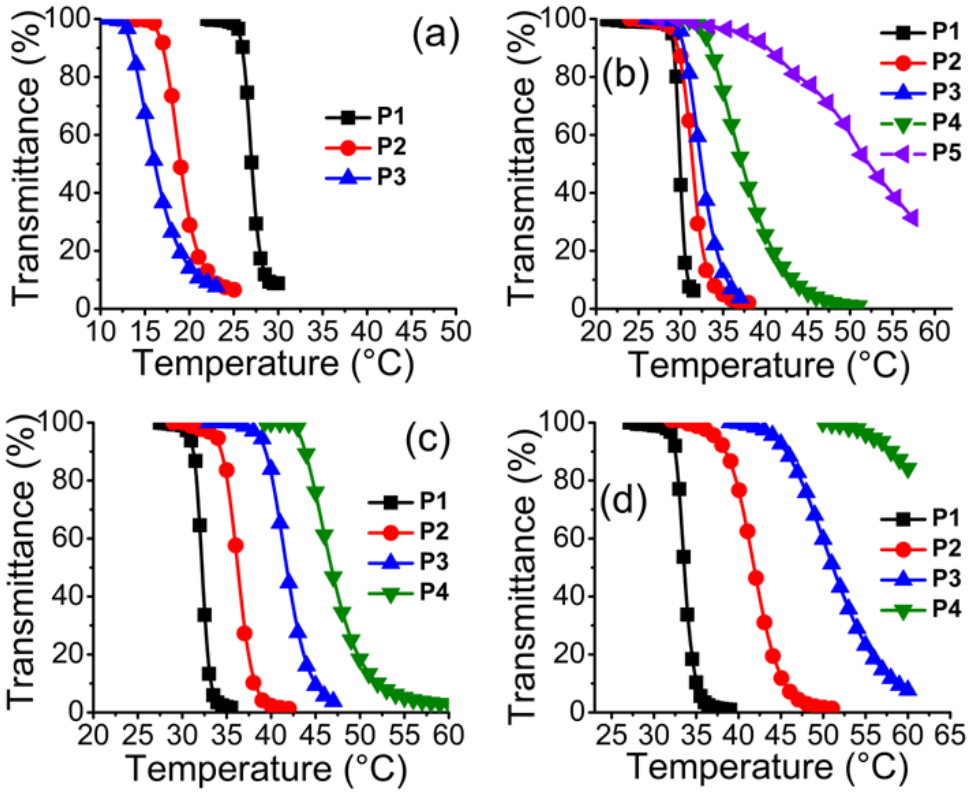

Figure 18. Plots of transmittance vs. temperature for the solutions of different P(NIPAM-*co*-CBA) samples obtained at: a) pH 4.5, b) pH 5.0, c) pH 5.5 and d) pH 6.0

Analyzing the data in Figure 18, it becomes already clear that the width of LCST shift

upon protonation and deprotonation of CBA units is proportional to the content of the comonomer. To better illustrate this result, Figure 19 shows the plots of transmittance vs. temperature for two samples, P1 and P2, over the pH range 4-7 at an interval of 0.5. Data of the cloud points for all samples over this pH range are collected in Table 3. With P1, the sample having the lowest CBA content of 2.1 mol%, the cloud point difference between pH 4 and 7 is about 10 ^{o}C (Fig.19a). By contrast, P2 has a higher CBA content of 4.3 mol%, the variation of cloud point reaches about 32 ^{o}C (Fig.19b). The effect of the comonomer content on the LCST shift is understandable. A higher content of CBA means greater switch between "hydrophobic" and "hydrophilic" comonomer effect on LCST in response to the switch between the neutral (protonated) and ionic (deprotonated) forms of the acid comonomer. Obviously, the efficiency of acid comonomers for shifting LCST over pH-induced protonation and deprotonation should be compared at the same comonomer content. Such a comparison with comonomers investigated in the literature is difficult to make due to often different comonomer contents as well as different experimental conditions used to measure the cloud point (polymer concentration, heating rate, etc.). Nevertheless, the 32 ^{o}C cloud point shift obtained at CBA content of 4.3 mol% and polymer concentration of 2 mg/mL is among the largest variation (124–130), indicating the high efficiency of CBA for the targeted comonomer effect. For instance, Stayton et al. investigated pH-induced LCST (cloud point) shift of random copolymers of NIPAM and propylacrylic acid, P(NIPAM-*co*-PAA) under basically the same conditions as those used in the present study (130). At the comonomer content PAA of about 2.6 mol%, the largest cloud point shift is about 18 ^{o}C over pH rage 5.0-7.0. With the PAA content at 9 mol%, the shift is about 17 ^{o}C over pH 5.0-6.5. For comparison, with our P(NIPAM-*co*-CBA), the sample P4, having about 10 mol% CBA, displays cloud point shift of larger than 50 ^{o}C over pH range 4.5-6.0 (Table 3).

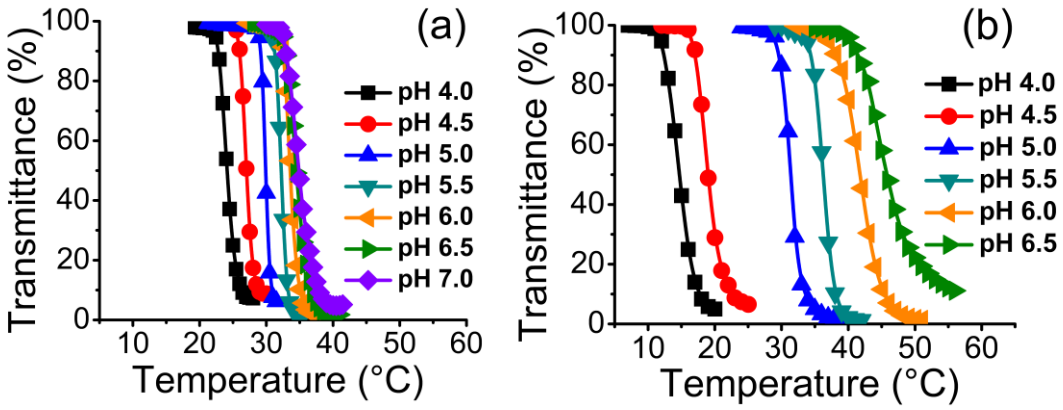

Figure 19. Plots of transmittance vs. temperature obtained at different pH values for the solutions of two P(NIPAM-*co*-CBA) samples: a) P1 and b) P2.

Table 3. Cloud Points (^{o}C) of Various Copolymer Solutions

pH	Cloud Points (^{o}C)				
	P1	**P2**	**P3**	**P4**	**P5**
4.0	24.1	14.6	a	a	a
4.5	26.9	18.9	15.8	a	a
5.0	29.9	31.4	32.3	36.9	51.3
5.5	32.2	36.2	41.7	46.6	b
6.0	33.6	41.7	50.8	b	b
6.5	34.5	45.3	b	b	b
7.0	34.8	b	b	b	b

a < 10 ^{o}C; b > 60 ^{o}C

Comparing different carboxylic acid comonomers, in addition to their different pH-induced LCST shift efficiencies, they may also impart different pH sensitivities to the LCST polymers. In other words, the question of interest is how small is the pH variation required for turning the polymer from soluble to insoluble state in water or vice versa. A comonomer like CBA exhibiting greater switch between hydrophobic and hydrophilic states associated with the protonation-deprotonation transition would give rise to higher sensibility. To better illustrate this feature, Figure 20a plots the cloud points (LCST) vs. pH for the solutions of all P(NIPAM-*co*-CBA) samples (graphical presentation of data in Table 3). The apparent slope, d*LCST*/d*pH*, around pH 4.5-5.0 increases with the content of CBA in the copolymer (as stated above, the cloud point at pH 4.5 for samples P4 and P5 could not be measured for being below 10 ^{o}C). This result implies that with increasing the content of CBA, the required pH variation for switching the polymer water solubility became increasingly smaller. As an example, Figure 20b shows the change in transmittance of the solution of P5 (0.2 mg/mL) at 37 ^{o}C as a function of pH at an interval of 0.2. The copolymer is soluble at pH 5.1 but becomes insoluble at pH 4.8, meaning that a pH variation of about 0.3 unit is enough to switch the water solubility. In the context of possible drug delivery applications, if nanogel is made with this polymer, it should remain stable even at pH 5.1, and the volume transition (collapse) of the nanogel would take place only inside intracellular compartments with a pH below 5 (122). In principle, this feature can be exploited for payload release specifically within a narrow range of acidic pHs.

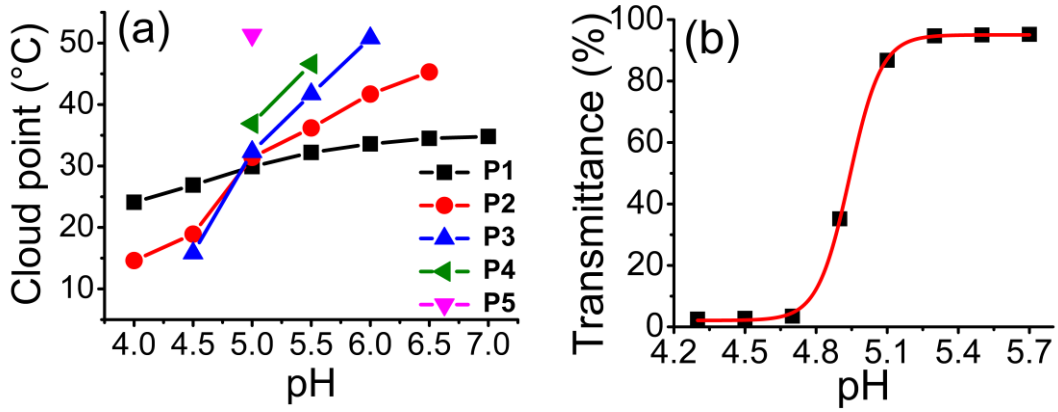

Figure 20. a) Plots of cloud point vs. pH for the solutions of different (NIPAM-*co*-CBA) samples. b) Transmittance change as a function of pH for the solution of P5 measured at 37 ^{o}C.

Finally, it should be mentioned that the present study focuses on only pH-induced LCST shift. Reversely, since the polymer undergoes a phase transition between hydrated and dehydrated state, the dielectric constant of the local environment surrounding the acid groups may change, resulting in change in the actual pKa. In other words, the pH responsiveness of the polymer may be affected by the changing thermosensitivity.

1.3 Experimental Section

1.3.1 Materials

Unless otherwise stated, all chemicals were purchased from Aldrich and used as received. The monomer, N-isopropylacrylamide (NIPAM), was recrystallized from hexane prior to use; whereas the designed comonomer, 4-((2-carboxyallyl)oxy)benzoic acid (CBA), was synthesized according to Scheme 1 (details below). The reversible addition fragmentation chain transfer (RAFT) agent, 2-(2-cyanopropyl) dithiobenzoate (CPDB), was synthesized using a reported method (138). The initiator, 2,2'-azobis(2-methylpropionitrile) (AIBN), was purified by recrystallizations from ethanol.

1.3.2 Synthesis of the Comonomer CBA

The whole synthetic route of the monomer CBA was shown in Scheme 1. Firstly, the fully *t*-butyl protected monomer **1** was prepared following a three-step sequence amenable to the preparation of large quantities if necessary. Briefly, the allylic alcohol **3** was synthesized following a Baylis-Hillman procedure from *t*-butyl acrylate **2** and in 75% yield (139,140). The alcohol **3** was then transformed into its corresponding allylic bromide **4** by means of phosphorus tribromide (PBr_3) (75%) (140). **4** was used as an alkylating agent for the phenolate ion of commercially available or easily prepared phenol **5** (141). Finally, treatment of **5** with potassium carbonate followed by addition of **4** in acetone under reflux yielded the methacrylate derivative **1** (yield: 86%), which was readily converted to the comonomer CBA upon hydrolysis of the two ester groups. The following are the specific procedure of this synthesis.

t-Butyl 2-(hydroxymethyl)acrylate **3**. Water (30 mL), paraformaldehyde (3.03 g, 100 mmol) then acetonitrile (MeCN) (50 mL) were successively added to 1,4-diazabicyclo[2.2.2]octane(DABCO) (5.6 g, 50 mmol) in a 250 mL round-bottom flask and with stirring. The resulting mixture was heated at 80 °C until the reaction mixture became homogeneous. *t*-Butyl acrylate **2** (7.3 mL, 6.4 g, 50 mmol) was then added all at once. The solution was heated at 80 °C for 2.5 h and left to cool down to room temperature. The reaction mixture was extracted twice with dichloromethan (DCM) (2 × 100 mL). The combined DCM layer was washed with 1 N aqueous HCl (100 mL) followed by brine (50 mL); it was dried ($MgSO_4$) and the solvent was removed under reduced pressure. The crude oil was purified by flash chromatography (hexane: ethyl acetate 8:2) to yield the title product as a colorless liquid (5.9 g, 75%).

^{1}H-NMR (300 MHz, $CDCl_3$): δ = 1.45 (s, 9H), 2.90 (t, *J* = 6.0 Hz, 1H), 4.25 (d, *J* = 6.0 Hz, 2H), 5.75 (s, 1H), 6.16 (s, 1H). **^{13}C-NMR** (75 MHz, $CDCl_3$): δ = 28.00, 62.30, 81.20,

124.00, 140.90, 165.60. **IR**: 3400, 2975, 2931, 1703, 1639, 1460, 1370, 1314, 1283, 1260, 1145, 1050, 945, 846, 820, 760 cm^{-1}. **HRMS** (EI, 70eV): calcd for $C_7H_{11}O_3$: 143.0708; found :143.0630 [M^+ - CH_3].

t-Butyl 2-(bromomethyl)acrylate **4**. PBr_3 (1.4 mL, 3.97 g, 14.66 mmol) was added, with stirring, to a cold (-30 °C) solution of alcohol **3** (5.8 g, 36.70 mmol) in anhydrous diethyl ether (40 mL). The mixture left to warm up to 0 °C over a 3 h period, then cooled again to -10 °C. Water (2.5 mL) was added and the resulting mixture was allowed to reach room temperature. The organic layer was collected, dried ($MgSO_4$.) and the solvent was removed under reduced pressure. The residue was purified by chromatography on silica gel (hexane:EtOAc 5:1) to afford the title product (6.1 g, 75 %) as a colorless liquid.

^{1}H-NMR (300 MHz, $CDCl_3$): δ = 1.45 (s, 9H), 4.07 (d, J = 1.0 Hz, 2H), 5.78 (d, *J* = 1.0 Hz, 1H), 6.15 (d, *J* = 1.0 Hz, 1H). **^{13}C-NMR** (75 MHz, $CDCl_3$): δ = 27.90, 29.80, 81.70, 127.80, 138.60, 163.90. **IR**: 2970, 2930, 1710, 1635, 1390, 1370, 1340, 1320, 1226, 1148, 950, 845, 810, 720 cm^{-1}.

t-Butyl 4-(3-(*t*-butoxy)-2-methylidene-3-oxopropoxy)benzoate **1**. Potassium carbonate (3.50 g, 51.60 mmol) and allylic bromide **4** (5.70 g, 25.80 mmol) were added to a solution of *t*-butyl *p*-hydroxybenzoate **5** (5.00 g, 25.80 mmol) in acetone (50 mL). The mixture was refluxed for 3h with stirring. The solvent was removed under reduced pressure and the residue was purified by flash chromatography (hexane:EtOAc 9:1) to give the title compound as a white solid (7.42 g, 86%).

^{1}H-NMR (300 MHz, $CDCl_3$): δ = 1.54 (s, 9H), 1.60 (s, 9H), 4.78 (s, 2H), 5.91 (d, *J* = 1.3 Hz, 1H), 6.33 (d, *J* = 1.3 Hz, 1H), 6.95 (d, *J* = 9.0 Hz, 2H), 7.96 (d, *J* = 9.0 Hz, 2H). **^{13}C-NMR** (75 MHz, $CDCl_3$): δ = 28.09, 28.26, 66.27, 80.57, 81.48, 114.17, 124.87, 125.52, 131.39, 136.88, 156.72, 164.58, 165.52. **HRMS** (ESI-Q-Tof): calcd for [MNa^+]: 357.1672; found: 357.1664.

4-((2-Carboxyallyl)oxy)benzoic acid **CBA**. A solution of diester **1** (1.00 g, 2.99 mmol) in a mixture of trifluoroacetic acid (TFA) and DCM (1:1, 18 mL) was stirred at room temperature for 2 h. The solvent was removed under reduced pressure 3 times after addition of some toluene each time. The residue was purified by flash chromatography (CH_2Cl_2:MeOH 95:5) to give the title compound as a white solid (651 mg, 98%). The ^1H NMR spectra of the synthesized monomer CBA and polymers are shown in Figure 21.

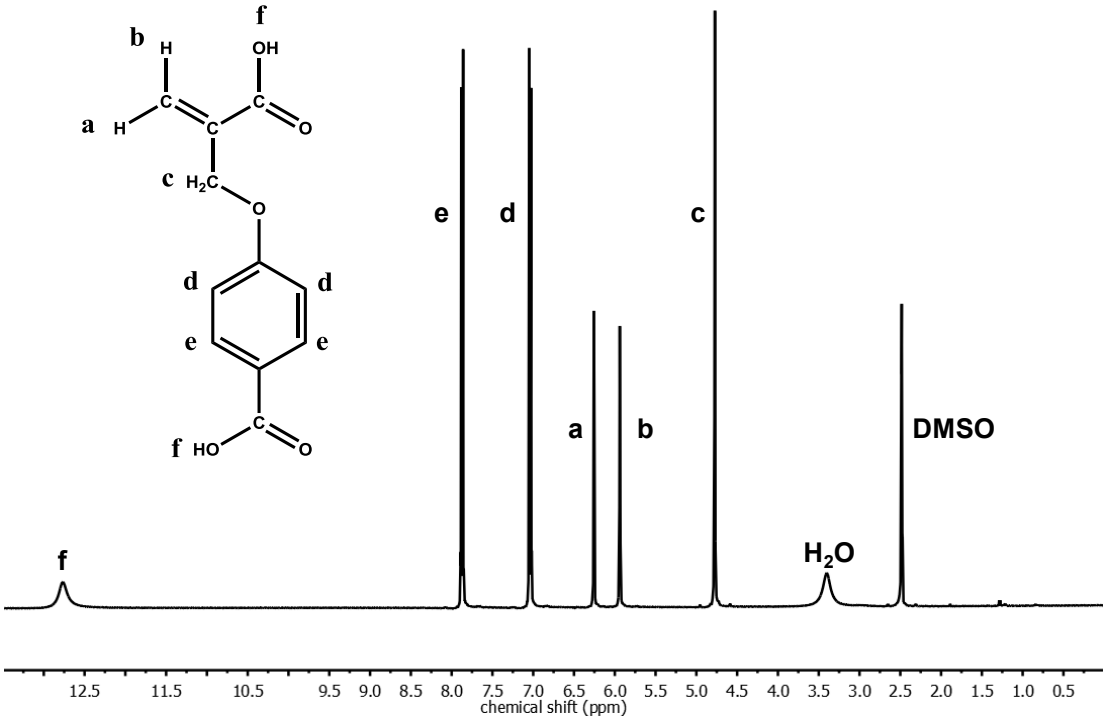

Figure 21. The ^1H NMR spectrum of synthesized CBA monomer in d_6-DMSO.

1.3.3 Synthesis of the Random Copolymer P(NIPAM-*co*-CBA)

RAFT polymerization was utilized to prepare the random copolymer P(NIPAM-*co*-CBA) having different CBA contents (Scheme 1). Using the copolymer containing about 2.1 mol% CBA as example, the synthetic details are as follows. A 10 mL round-bottom flask was charged with NIPAM (0.5 g, 4.4 mmol), CBA (9.8 mg, 0.044 mmol), AIBN (1.5 mg),

CPDB (9.8 mg, 0.044 mmol) and dioxane (1 mL). The mixture was degassed by three times freeze-thaw cycles; then it was placed into an oil bath preheated to 80 ^{o}C. The polymerization was allowed to proceed for 2.5 h with the mixture under stirring. After polymerization, the mixture was cooled to room temperature and precipitated into ethyl ether. The purification was repeated three times. The final product was dried to constant weight under vacuum. The ^{1}H NMR spectra of the synthesized polymers are shown in Figure 22.

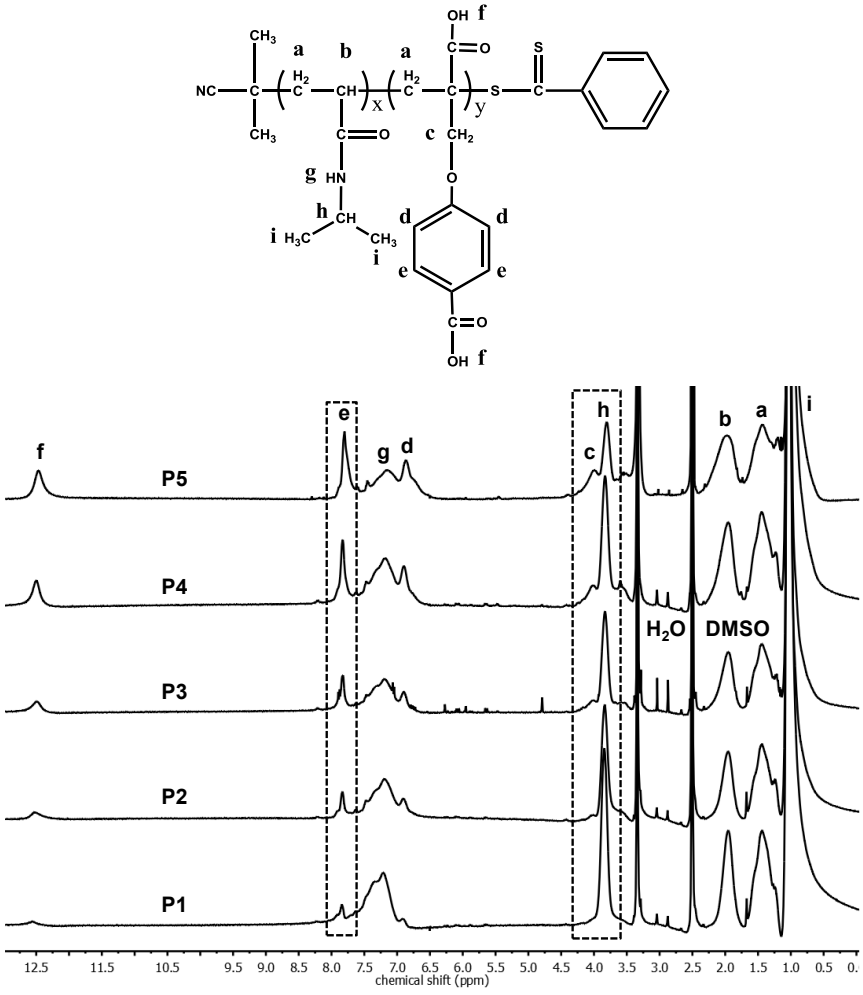

Figure 22. The ^{1}H NMR spectra of synthesized copolymers (P1-P5) in d_6-DMSO.

1.3.4 Characterizations

^{1}H-NMR spectra were recorded on a Bruker AC 400, using DMSO-d_6 as the solvent. The spectra of the monomer CBA and the random copolymer P(NIPAM-*co*-CBA) are shown in above Figure 21 and Figure 22, respectively. The compositions of the various copolymer samples were determined from the ^{1}H NMR spectra by comparing the integral of peak *h* (3.8 ppm, from the tertiary carbons of NIPAM side groups) with the integral of either peak *e* (7.8 ppm, from the aromatic protons of CBA) or peak *c* (4.0 ppm, assigned to ethyl groups of CBA); similar results were obtained from the different resonance signals. The increased intensity of peaks *e* and *c* with respect to peak *h* reflects the increased percentage of CBA in the samples P1-P5. Size exclusion chromatography (SEC) was performed on Tosoh EcoSEC GPC system, equipped with three TSK-GEL Super AWM-H columns (6x150mm). The measurements were conducted at 50 ^{o}C using dimethylformamide (DMF) containing 1 g/L of LiBr as the eluent (flow rate: 0.5 mL/min) and poly(methyl methacrylate) (PMMA) as standards. The cloud points of P(NIPAM-*co*-CBA) solutions at a polymer concentration of 0.2 wt% were measured using an Agilent Cary Series UV-Vis-NIR spectrophotometer by monitoring the solution transmittance (measured at wavelength of 500 nm) as a function of temperature upon heating at a rate of 0.5°C/min. The transmittance curves were normalized to 100% for clarity. The cloud point of a given solution was taken as the temperature corresponding to the inflection point of the changing transmittance that was graphically determined from the maximum value of the first derivative of the heating curve. For the cloud point measurements of the solutions at different pH values, P(NIPAM-*co*-CBA) samples were first dissolved in 0.15 mol L^{-1} phosphate-buffered saline (PBS) (pH 7.4, under stirring in the ice-water bath), with the solution pH then adjusted to a desired value by adding NaOH (0.1N, 1N) or HCl (0.1N, 1N). The pH was measured using a Fisher Scientific Accumet AB 15 pH Meter with 13-620-223A Accumet glass pH electrode.

1.4 Conclusions

We have reported the design and synthesis of a polymerizable compound bearing two carboxylic acid groups of similar pKa in the structure, and showed that using it as comonomer in PNIPAM could enlarge the reversible shift of LCST upon pH change. Both the cloud point measurement and DFT calculations suggest that the wide swing of LCST is due to the comonomer structure that can increase both the hydrophobicity and hydrophilicity with protonated and deprotonated acid groups, respectively. Having two (or even more) acid or base groups in the comonomer structure may present a general approach to increasing the sensitivity and efficiency of pH-induced water solubility switch for thermosensitive polymers like PNIPAM. Obtaining the same shift of LCST with a lower content of the comonomer may be regarded as an amplification mechanism, and it is of interest for different reasons. First, it allows fine-tuning of the phase (or volume) transition temperature of the polymer in response to pH change. With respect to a constant solution (or body) temperature, a deeper decrease below or greater increase above for the LCST means different dehydration or hydration state of the polymer, respectively, which would result in different degrees of disruption for nanocarriers (e.g., nanogel or micelle) built with the polymer. Secondly, it may give rise to great pH sensitivity of the polymer water solubility. As shown, for the P(NIPAM-*co*-CBA) sample containing 17.3 mol% CBA, a pH change of about 0.3 unit is sufficient for switching the polymer between soluble and insoluble state. Thirdly, the ability of reducing the amount of comonomer while retaining the pH-induced LCST shift may be beneficial depending on the sought applications. This would be desirable in case the comonomer causes toxicity. Moreover, by limiting the structural and chemical perturbation of the thermosensitive polymer, it would be possible to diminish the comonomer's effect of slowing down the thermal phase transition, which is noticeable with P5 (Fig.18b).

1.5 Statement of Contribution

This work was published in Polymer Chemistry, 2015, 6, 6644-6650 by Hu Zhang, Thomas Marmin, Étienne Cuierrier, Armand Soldera, Yves Dory and Yue Zhao. This research work was carried out in the Université de Sherbrooke under the supervision of Prof. Zhao. The acid monomer was synthesized by Thomas Marmin and Prof. Yves Dory. The theoretical calculation was conducted by Étienne Cuierrier and Prof. Armand Soldera. I performed all the other experiments reported in the paper.

CHAPTER 2 UNCHARGED UCST BLOCK COPOLYMERS AND THEIR DIVERSE THERMORESPONSIVE MICELLES IN PHYSIOLOGICAL MEDIUM

2.1. Introduction

In the broad field of stimuli-responsive materials, thermosensitive polymers displaying a lower critical solution temperature (LCST) in water arguably have been the most studied. Basically they are soluble in cold water at temperatures below LCST but become insoluble above LCST. The enormous interest generated by LCST polymers stems from their applications in many areas including drug delivery, bioseparation, tissue engineering, and biomedical soft materials (10,26,142–144). Applications can also be envisioned where the reversed thermosensitivity, i.e., insoluble in cold water and soluble at higher temperatures, is required or preferable. For instance, if a block copolymer (BCP) micelle needs to be simply dissolved above a certain temperature, the micelle core-forming block should have the thermosensitivity opposite to LCST. Despite this fact, studies on such polymers, especially BCPs, with an upper critical solution temperature (UCST)(53,58,59,62–64,67–74,79,85,89,90,92,93,95–98,100,145–158) have been rare as compared to their LCST counterparts. The main reason is that polymers with UCST in water are not only limited in number but also, generally, difficult to access in terms of monomer and polymer synthesis. As a matter of fact, most studies on polymers exhibiting a UCST in water dealt with zwitterionic (charged) polymers with a UCST sensitive to electrolytes (ions), which limits their potential utility for applications in physiological medium (53,58,59,62–64,67–74,79,146,147,149,151–153,155,158). In recent years, significant progress has been made on the discovery of hydrogen bond-based uncharged UCST polymers whose thermosensitivity is little affected or unaffected by the presence of ions, thereby making them more suitable for biomedical applications

(85,89–93,95–98,100,106,145,150,156,157). The most notable contribution is a recent report by Seuring and Agarwal who showed that free radical copolymerization of commercially available acrylamide and acrylonitrile could yield random copolymers P(AAm-*co*-AN) with a sharp UCST in water or electrolyte solution tunable by varying the composition of the monomers (93). Despite this finding, up to now, by no means could UCST polymers, especially BCPs, match their LCST counterparts for generated interest.

Our motivation in the present study was to first apply the reversible addition–fragmentation chain-transfer (RAFT) polymerization to prepare P(AAm-*co*-AN), then use this UCST polymer as a macromolecular chain transfer agent (macro-CTA) to grow BCPs of different kinds, and finally investigate the thermoresponsive behaviors of BCP micelles. To demonstrate the versatility, three representative BCPs were synthesized by coupling P(AAm-*co*-AN) with hydrophobic polystyrene (PS), hydrophilic poly(dimethylacrylamide) (PDMA) and LCST-exhibiting poly(*N,N*-dimethylaminoethyl methacrylate) (PDMAEMA), respectively. Our study found that the BCP micelles in water or phosphate buffered saline (PBS) could exhibit diverse UCST-dictated behaviors in a way that is as robust as LCST-based BCPs. The message we hope to convey is that by making use of P(AAm-*co*-AN) the same way as, say, the extensively studied LCST poly(*N*-isopropylacrylamide) (PNIPAM), UCST polymers of engineered or controlled architectures like the BCP examples investigated in this study, are now very accessible through RAFT, which means that the door is wide open to exploring new smart materials and devices with the reversed thermosensitivity.

2.2. Experimental Section

2.2.1. Synthesis of P(AAm-*co*-AN) and its Diblock Copolymers

Materials. All reagents were purchased from Sigma-Aldrich. *N*-Acrylamide (AAm) was

recrystallized in chloroform prior to use; acrylonitrile (AN), styrene (ST), *N*,*N*′-dimethylacrylamide (DMA) and *N,N*-dimethylaminoethyl methacrylate (DMAEMA) were purified by passing through a column filled with basic alumina. 2,2′-Azobis(2-methylpropionitrile) (AIBN) was purified by recrystallizations from ethanol. The used RAFT chain transfer agent (CTA), 2-(2-cyanopropyl) dithiobenzoate (CPDB), was synthesized according to a reported method (138).

Synthesis of P(AAm-*co*-AN) of Various AN Contents. As an example, the synthesis of P(AAm-*co*-AN) with an AN feed content of 22 mol % was conducted as follows. A 50 mL round-bottom flask was charged with AAm (3.324 g, 46.76 mmol), AN (700 mg, 13.19 mmol), CPDB (13.25 mg, 0.060 mmol), AIBN (1.96 mg, 0.012 mmol), and dimethyl sulfoxide (DMSO, 14.12 mL). The mixture was degassed by three freeze-thaw cycles and then placed into an oil bath preheated to 70 ^{o}C. The polymerization was allowed to proceed for a predetermined time with the mixture under stirring. After the polymerization reaction, the polymer was purified by precipitation from a DMSO solution into methanol twice. In order to completely remove DMSO, the polymer dissolved in DMSO was dialyzed against deionized water for 3 days (with 3000 MWCO dialysis tubing from Spectra/Por) and then recovered by lyophilization. All RAFT polymerizations were carried out at a 4.0 M total monomer concentration and the total monomer to CPDB ratio $[M]_0/[CTA]_0$ was held constant at 1000/1. Samples of P(AAm-*co*-AN) with different AN contents were obtained by varying the feed content of AN in the mixture of the two monomers. The characteristics of the P(AAm-*co*-AN) samples are summarized in Table 4.

Table 4. Summary of the Characterization of the UCST Random and Block Copolymers

Sample number	Polymer	AN in feed (mol%)	AN in polymer (mol%)[a]	Reaction time(h)	M_n (g/mol)[b]	Cloud point (°C)[c]	
						Cooling	Heating
P1	Poly(AAm_{231}-co-AN_{76})	22	25.4	12	20779	28.3	30.6
P2	Poly(AAm_{260}-co-AN_{87})	22	25.1	18	23318	29.0	29.9
P3	Poly(AAm_{317}-co-AN_{102})	22	24.4	24	28166	25.6	27.3
P4	Poly(AAm_{238}-co-AN_{108})	25	30.6	24	22834	35.1	36.5
P5	Poly(AAm_{165}-co-AN_{94})	28	33.8	24	18358	47.5	49.2
P6	P(AAm_{231}-co-AN_{76})-*b*-PS_{42}	—	—	12	25153	48.2[d]	50.0[d]
P7	P(AAm_{231}-co-AN_{76})-*b*-$PDMA_{425}$	—	—	10	62309	14.3	14.9
P8	P(AAm_{231}-co-AN_{76})-*b*-$PDMAEMA_{619}$	—	—	12	70929	20.7/44.8[e]	20.9/45.8[e]

[a]Determined by IR spectroscopy; [b]calculated by ^{1}H NMR in d_6-DMSO; [c]5 mg/ml in PBS; [d]0.5 mg/ml in PBS due to the solubility; [e]the first value is for the P(AAm-co-AN) block and the second for the PDMAEMA block.

Synthesis of Diblock Copolymers of P(AAm-*co*-AN)-*b*-PS, P(AAm-*co*-AN)-*b*-PDMA and P(AAm-*co*-AN)-*b*-PDMAEMA. The RAFT polymerization procedures for obtaining the three diblock copolymers used in the present study were the same except for slight variations in the reaction temperature and reaction time. In all cases, the concentration of the monomer for the second, non-UCST block (either ST or DMA or DMAEMA) was 1 M in DMSO. All three BCPs were synthesized by using the same P(AAm-*co*-AN) sample (P1 in Table 4) as the macro-CTA. Using the synthesis of P(AAm-*co*-AN)-*b*-PS as example: P(AAm-*co*-AN) (200 mg), ST (540.89 mg), AIBN (0.56 mg), and DMSO (4.6 mL) were added into a 25 mL round-bottomed flask with a magnetic stirring bar. After three freeze-thaw cycles, the flask was sealed under vacuum and then immersed in an oil bath thermostated at 100 ^{o}C. The polymerization reaction was stopped after 12 h. The resulting polymer was purified by 3-fold precipitation from a DMSO solution into methanol. The final product was collected and dried in a vacuum oven at room temperature for 3 days. In the case of P(AAm-*co*-AN)-*b*-PDMA, the polymerization temperature was set at 70 ^{o}C and the polymerization time was 10 h. As for P(AAm-*co*-AN)-*b*-PDMAEMA, the polymerization temperature was 90 ^{o}C and the reaction time was 12 h.

2.2.2. Characterizations

^{1}H NMR spectra were recorded on a Varian 600 MHz spectrometer (INOVA system) using deuterated DMSO (d_6-DMSO) as solvent at 70 ^{o}C. For the variable-temperature ^{1}H NMR measurements, the spectra were recorded with polymers in deuterium oxide (D_2O) using a temperature interval of 3 ^{o}C and a thermal equilibrium time of 5 min at each temperature before taking the spectrum. For the measurements of solution transmittance (at 500 nm), absorption spectra were recorded on an Agilent Cary Series UV-Vis-NIR spectrophotometer as a function of the solution temperature. Normally, the measurements were carried out by first cooling the solution from the used highest temperature under a constant cooling rate of 1.0 °C/min and then heating the solution back to the starting temperature at the same rate. The inflection point of the transmittance curve was considered as the UCST-related cloud point. It was graphically determined by the maximum of the first derivative of the heating or cooling curve, respectively. In the case of P(AAm-*co*-AN)-*b*-PDMAEMA, the solution was equilibrated at 40 °C, cooled to 5 °C, then heated to 70 °C, and finally cooled to 5 °C again. Dynamic light scattering (DLS) measurements were performed on a Malvern Zetasizer Nano ZS ZEN3600 system with a helium–neon laser (wavelength, λ = 633 nm). All measurements were carried out at a scattering angle of 173°. Infrared spectra were recorded on an ABB MB104PH FTIR spectrometer using the diffuse reflection technique. Samples were milled with potassium bromide (KBr) to form a fine powder for testing. The calibration curve used to determine the AN contents in the P(AAm-*co*-AN) samples was obtained with the spectra of a series of known-composition mixtures of polyacrylamide and polyacrylonitrile homopolymers; the error bars are the standard deviation of the determined absorption integral ratios from 10 measurements (Fig.23) (93). A Waters size exclusion chromatograph (SEC) instrument, equipped with a 410 refractive index detector and a 996 photodiode array detector, was also utilized to measure the molecular weights using poly(methyl methacrylate) (PMMA) standards. The SEC measurements were conducted at 35 ^{o}C using a single column

(Styragel HR4, 7.8 mm × 300 mm, 5 µm beads) and a mixed solvent of dimethylformamide (DMF)/DMSO (50:50, v:v) containing 1 g/L of LiBr as the eluent (flow rate: 0.5 mL.min^{-1}). Finally, atomic force microscope (AFM) observations were conducted on a Veeco's Nanoscope V Dimension Icon, equipped with a Nanoscope V controller. The ScanAsyst mode in air, with a SCANASYST-AIR cantilever having a force constant of 0.4 N/m and resonance frequency of 50-90 kHz, was used for imaging the micellar aggregation. The tapping-mode in air, with a TESPA cantilever having a force constant of 20–80 N/m and resonance frequency of 343–399 kHz, was performed for observing the microphase separation in BCP thin films.

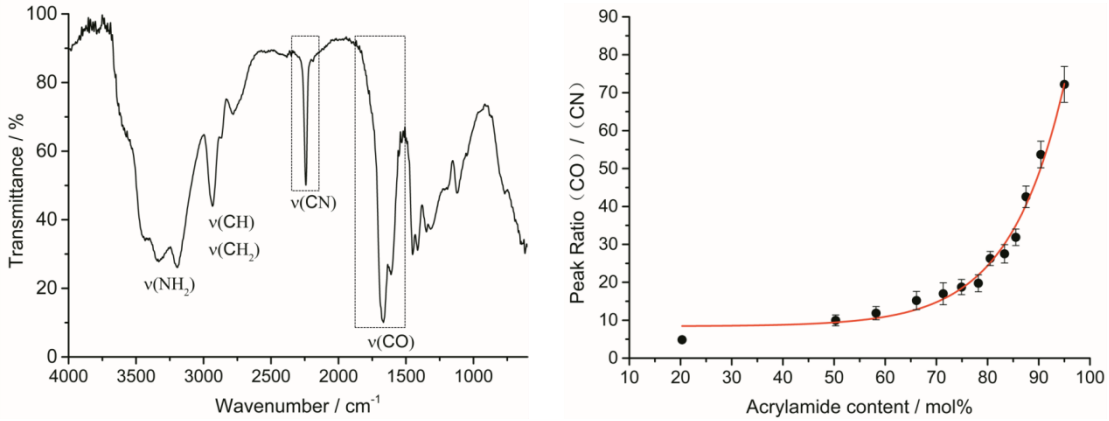

Figure 23. Left: Infrared spectrum of the sample P1 in Table 4 showing the characteristic absorption band of CN in acrylonitrile (AN) and that of CO in acrylamide (AAm). Right: Calibration curve obtained by plotting the integral ratio of the CO absorption band to the CN band vs. known content of AAm in mixtures of PAAM and PAN homopolymers (93).

2.3. Results and Discussion

2.3.1. RAFT Synthesis, Characterization, and UCST Behavior

By varying the feed ratio of AAm/AN in the monomer mixture and the RAFT reaction time, a series of P(AAm-*co*-AN) random copolymers of different molecular weights and

compositions was prepared. They all displayed a sharp and reversible UCST both in water and in PBS. It should be noted that not all RAFT agents are suitable to polymerize the acrylamide monomer (159). The RAFT agent used in this study, CPDB, was demonstrated to give good control not only for polymerization of acrylamide (160), but also for acrylonitrile (161). To synthesize three types of representative diblock copolymers for investigation of their diverse UCST-controlled thermosensitive micelles both in water and in PBS, we chose to use a P(AAm-*co*-AN) sample with a UCST around 30 ^{o}C as the macro-CTA. Therefore, the same UCST P(AAm-*co*-AN) block (P1 in Table 4) was utilized to grow a second block of either PS or PDMA or PDMAEMA, giving rise to P(AAm-*co*-AN)-*b*-PS, P(AAm-*co*-AN)-*b*-PDMA and P(AAm-*co*-AN)-*b*-PDMAEMA, respectively. The characterization results of all the P(AAm-*co*-AN) samples as well as the three BCPs are summarized in Table 4.

Before discussing the UCST behaviors of P(AAm-*co*-AN) and the various types of thermoresponsive BCP micelles containing the UCST P(AAm-*co*-AN) block, the characterization of the samples, especially their compositions and molecular weights given by the numbers of all constituting monomer units in the acronyms, needs explanation. In particular, the determination of the BCP compositions is not trivial. First, the composition of each P(AAm-*co*-AN) sample was determined by means of infrared spectroscopy (93), using a calibration curve that plots known AAm molar content versus integral ratio from the characteristic absorption bands around 1659 cm^{-1} and 2242 cm^{-1} assigned to the carbonyl and nitrile group in AAm and AN, respectively (Fig.23). Then, the compositions of all samples in Table 4 were obtained by combining the infrared data with the ^{1}H NMR spectra. Since the three diblock copolymers were synthesized using the same P(AAm-*co*-AN) macro-CTA (P1 in Table 4), Figure 24 shows the ^{1}H NMR spectra of the four samples. For P(AAm-*co*-AN) (Fig.24a), using the small resonance peak *a* (7.8 ppm, from two aromatic protons of the RAFT CTA end group) as reference, the ratio of integrals of peaks *g* and *h* (1–2 ppm, from the methylene group in

all monomer units and the two methyl units at the chain end) to peak *a* led to the total number of AAm and AN units in the sample P1. Knowing the composition (infrared result), the numbers of AAm and AN could be calculated. To determine the BCP compositions, in the case of P(AAm-*co*-AN)-*b*-PS (P6 in Table 4) (Fig.24b), the small peak *a* was still visible, which is indicative of a short PS block. The peaks in the region of 6.2–7.8 ppm are from the aromatic protons of PS and those of the acrylamide groups of AAm. As it should be, the ratio of the integral covering the 6.2–7.8 ppm region to that of peak *a* is much higher than the ratio of integrals at the same resonances for P1 (Fig.24a); the difference allowed us to deduce the number of ST units in the PS block. By contrast, for both P(AAm-*co*-AN)-*b*-PDMA (Fig.24c) and P(AAm-*co*-AN)-*b*-PDMAEMA (Fig.24d), peak *a* was hardly discernible, which implies longer PDMA and PDMAEMA blocks. For P(AAm-*co*-AN)-*b*-PDMA (sample P7), the integral of the peaks in the 6.2–7.8 ppm region (from AAm) was compared to the integral of the peaks in the 1–2 ppm region (mainly from the methylene units in the chain backbone), and the difference with respect to P1 was used to estimate the number of DMA units. Finally, the situation of P(AAm-*co*-AN)-*b*-PDMAEMA is relatively easier. Comparing the 1–2 ppm peak integral with that of peak *k* at 3.9 ppm (characteristic of DMAEMA) yielded the number of DMAEMA units.

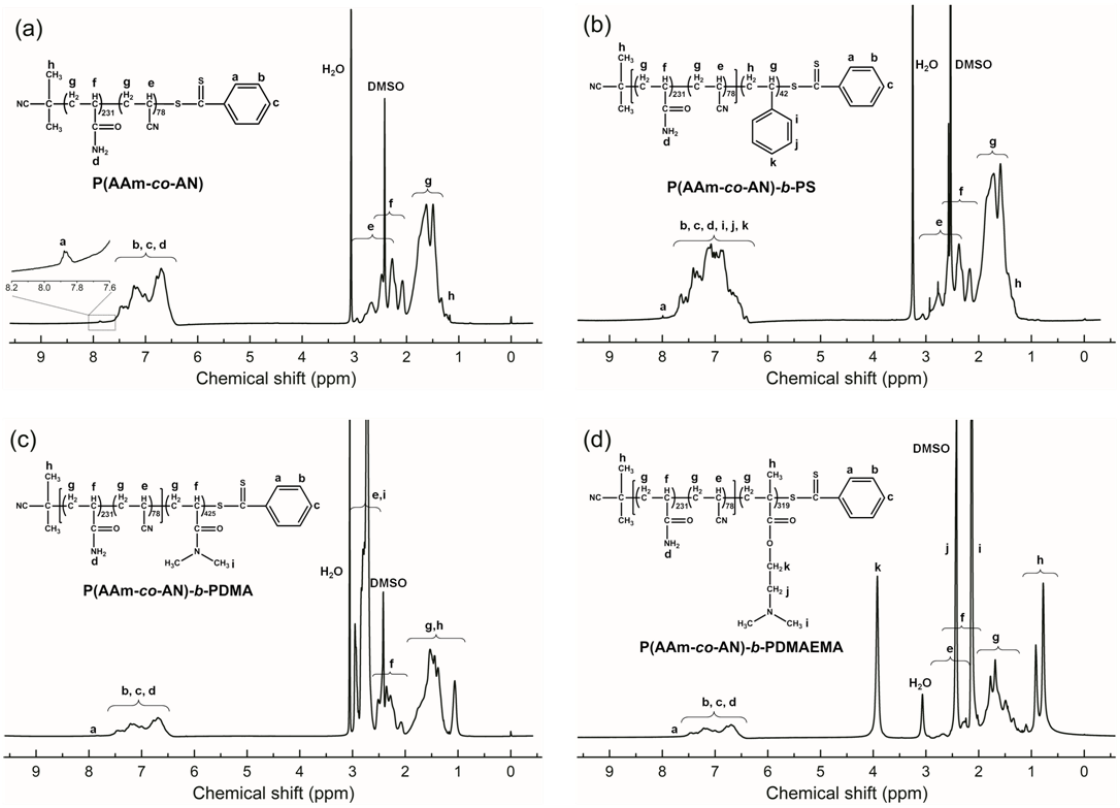

Figure 24. 1H NMR spectra in d_6-DMSO at 70 ^{o}C for the P(AAm-*co*-AN) macro-CTA (a) and the three diblock copolymers: P(AAm-*co*-AN)-*b*-PS (b), P(AAm-*co*-AN)-*b*-PDMA (b) and P(AAm-*co*-AN)-*b*-PDMAEMA (c).

Figure 25 shows the SEC measurement results, using a mixture of DMSO and DMF (50:50, v:v) as the eluent, for three P(AAm-*co*-AN) samples synthesized under the same conditions except the RAFT reaction time (Fig. 26a, P1–P3 in Table 4) and for the three BCPs obtained with the same macro-CTA, P1 (Fig.25b, P6–P8). For P(AAm-*co*-AN), the controlled chain extension with increasing the reaction time is visible for P1 through P3 as revealed by a decreased retention time. By contrast, in the case of BCPs, the results are less clear. Of them, P(AAm-*co*-AN)-*b*-PDMA displays shorter retention times; while the elution peak of P(AAm-*co*-AN)-*b*-PS shifts very slightly, which qualitatively is consistent with the short PS block as revealed by ^{1}H NMR, P(AAm-*co*-AN)-*b*-PDMAEMA apparently shows negligible changes. Similar results

were obtained with DMF or DMSO as the eluent. The second block of PDMA is a polyacrylamide, similar to AAm in the P(AAm-*co*-AN) block; the fact that all P(AAm-*co*-AN) samples and the diblock copolymer P(AAm-*co*-AN)-*b*-PDMA display resolved SEC traces implies that the used eluent is appropriate for them but may not be good for P(AAm-*co*-AN)-*b*-PS and P(AAm-*co*-AN)-*b*-PDMAEMA, of which the second block, PS or PDMAEMA, is not a polyacrylamide. One possibility is that in those two cases, different intermolecular interactions between the two blocks affect their hydrodynamic volume, which offsets the effect of an increased molecular weight for the two BCPs. Moreover, using PMMA standards, the SEC-based M_n values for P1–P3 are about 77 360, 89 600, and 104 900 g/mol, respectively, with low polydispersity index (PDI) between 1.15 and 1.21. The M_n data are not reliable because they are greater than what would be even assuming 100% monomer conversion. In the end, due to the uncertainty in using SEC to measure the molecular weights of P(AAm-*co*-AN) and the BCPs, we chose to the report the characterization results obtained with ^{1}H NMR and infrared spectroscopy in Table 4. However, it should be emphasized that despite the difficulty with SEC, the obtaining of uncharged UCST BCPs through RAFT leaves no doubt. To make sure of this claim with P(AAm-*co*-AN)-*b*-PDMAEMA, AFM analysis was carried out on thin film and only the microphase separation characteristic of a diblock copolymer was observed, displaying domain sizes around 16–18 nm (Fig.26). As shown below, the three BCPs, representing three types of amphiphilic BCP design, all form micellar aggregates in either pure water or PBS, and exhibit robust thermally induced and UCST-governed morphological changes and transitions.

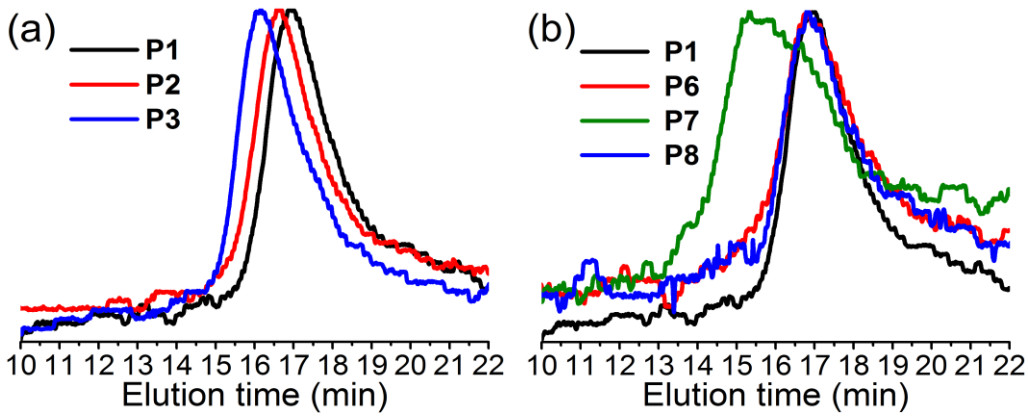

Figure 25. SEC traces at 35 °C with polymers dissolved in DMF/DMSO (50:50): (a) three P(AAm-*co*-AN) samples, and (b) three diblock copolymers and the used macro-CTA.

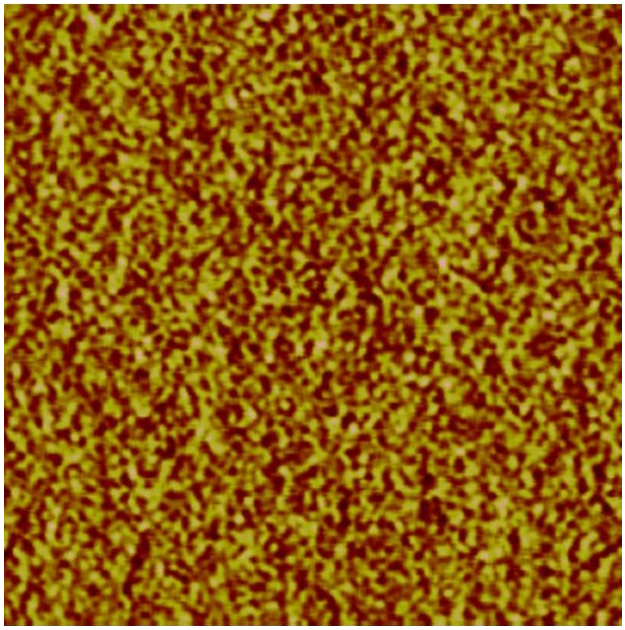

Figure 26. AFM phase image (tapping mode) of P(AAm-*co*-AN)-*b*-PDMAEMA thin film (image size: 1μm x 1μm). The film was prepared by spin-coating the block copolymer DMSO solution onto a mica substrate, followed by annealing in a vacuum oven at 145 °C for 4 days. The thickness of the film is about 70 nm, the surface roughness about 0.22 nm and the average sizes for the bright domains (harder P(AAm-*co*-AN)) and the dark domains (soft PPDMAEMA) are about 18 nm and 16 nm, respectively.

The various P(AAm-*co*-AN) samples of different molecular weights and compositions in Table 4 all display excellent UCST both in water and in PBS (such as an example shown in Figure 27). Figure 28 shows the results obtained with the polymers in PBS at a concentration of 5 mg/mL, plotting the solution transmittance as a function of temperature on cooling and subsequent heating (1 ^{o}C/min). As seen from Figure 28a, all samples exhibit a sharp UCST transmittance change with very slight hysteresis between cooling and heating. Comparing P1, P2, and P3, which have a similar AN content, the molecular weight of the polymer seems to affect little the UCST. By contrast, comparing P1, P4, and P5, which have similar molecular weights but different compositions, it is clear that the UCST is sensitive to the content of AN comonomer units, shifting to a higher temperature with increasing the AN content. These results are consistent with the report of Agarwal et al. on P(AAm-*co*-AN) samples prepared using conventional free radical copolymerization (93). Presented in Figure 28b are the results of 10 consecutive cooling and healing cycles of the P1 solution. The almost superimposed curves indicate excellent thermal stability of the UCST behavior for the P(AAm-*co*-AN) samples. The UCST transition of the copolymer is also confirmed by the changes of the integral of the corresponding peaks and the plot of this change versus temperature, obtained from variable-temperature ^{1}H NMR spectra (Fig.29).

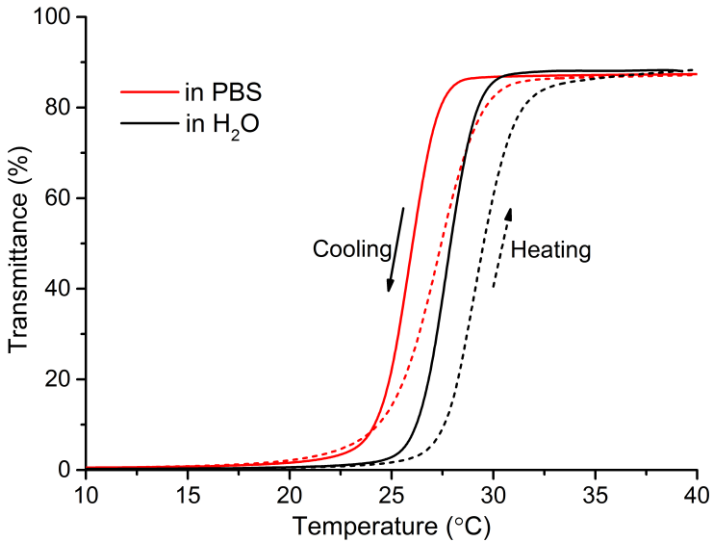

Figure 27. Transmittance change vs. temperature for a representative P(AAm-*co*-AN) (P3 in Table 4) both in pure water and in PBS (5 mg/mL). The difference in UCST is slight as compared to poly(N-acryloyl glycinamide) (89,91).

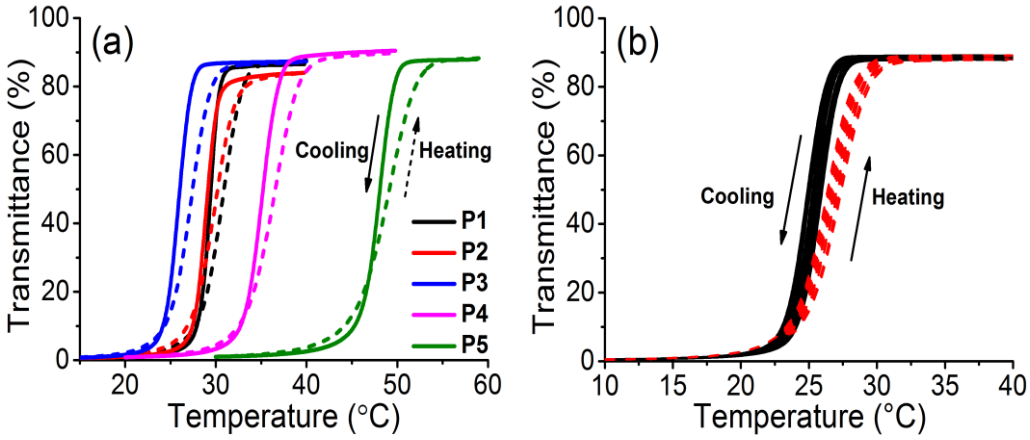

Figure 28. Plots of solution transmittance vs. temperature showing the UCST behavior in PBS solution (polymer concentration at 5 mg/mL; heating and cooling rate at 1 ^{o}C/min; solid and dotted lines for cooling and heating scan, respectively): (a) P(AAm-*co*-AN) samples of different molecular weights and compositions; and (b) the same P(AAm-*co*-AN) sample (P1) subjected to ten consecutive heating and cooling cycles.

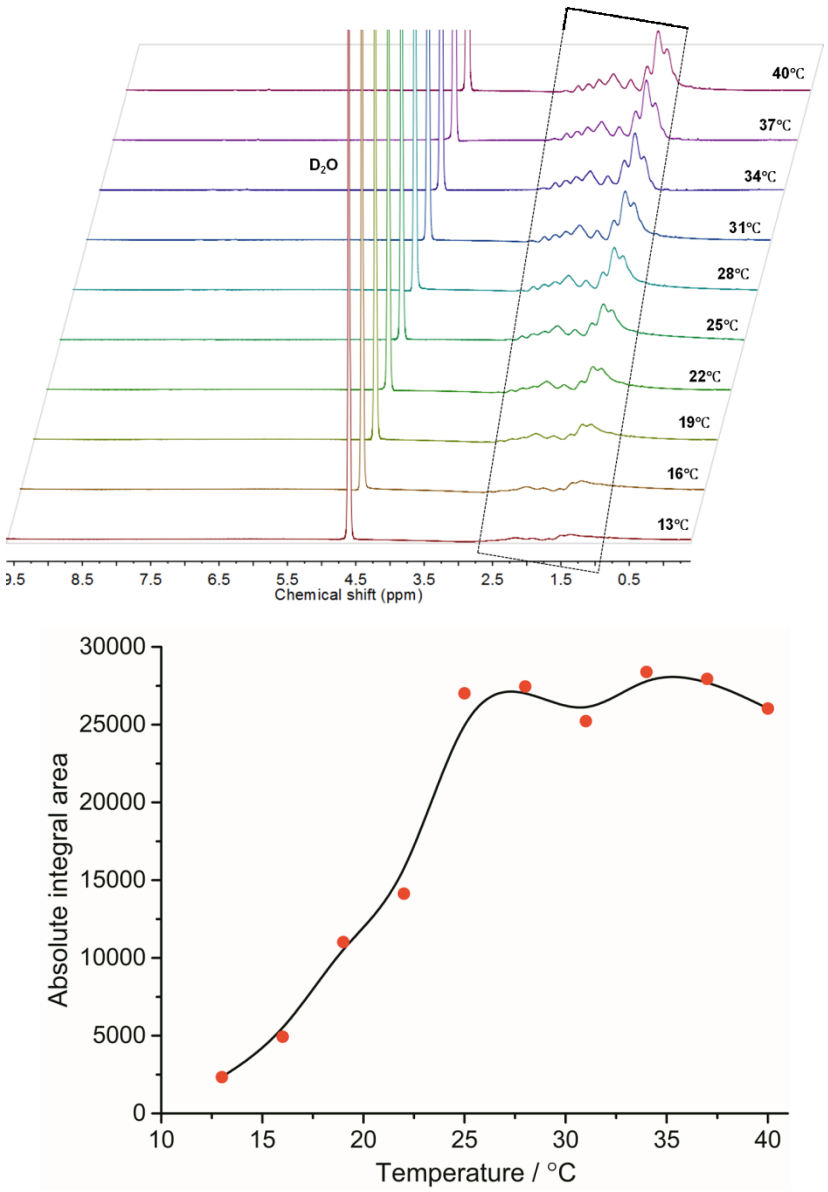

Figure 29. Top: Variable-temperature ^{1}H-NMR spectra of P(AAm-*co*-AN) (P3 in Table 4) in D_2O recorded from 13 ^{o}C to 40 ^{o}C with an interval of 3 ^{o}C. Down: Change in the integral of the resonance peaks from 0.5 to 3 ppm as a function of temperature, indicating the UCST-determined water solubility.

2.3.2. Diversiform UCST-Dictated Thermosensitivity of P(AAm-*co*-AN)-Based Block Copolymer Micelles

After having confirmed the robust UCST behavior in water and PBS of the RAFT-synthesized P(AAm-*co*-AN), diblock copolymers were further synthesized using P(AAm-*co*-AN) as macro-CTA. As mentioned above, the main purpose of this work is to investigate whether controlled radical polymerization techniques like RAFT can be applied to construct various BCPs comprising an uncharged UCST block, which is a crucial step toward exploitation of polymers having a thermosensitivity opposite to the LCST counterparts. Figure 30 shows the chemical structures of the three synthesized BCPs samples (P6–P8 in Table 4) and the expected thermoresponsive behaviors of their micelles if the P(AAm-*co*-AN) block does manifest the UCST solubility change in aqueous solution.

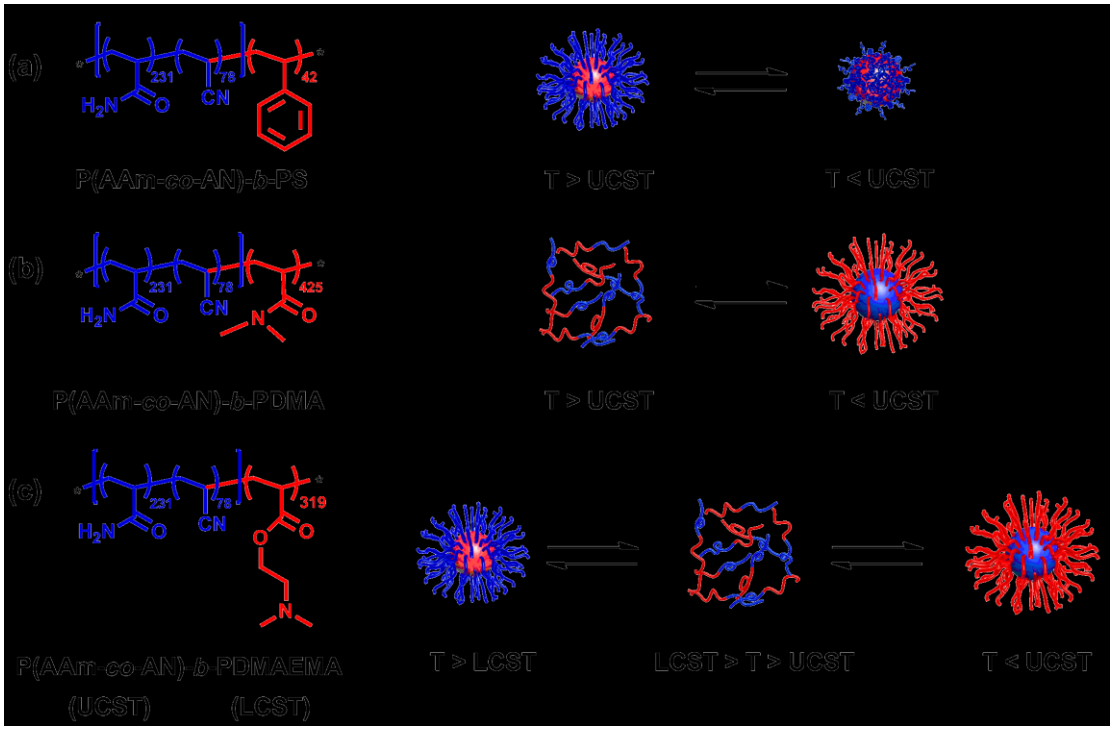

Figure 30. Left side: chemical structures of three diblock copolymers composed of the same UCST P(AAm-*co*-AN) block and a block of hydrophobic PS (a), hydrophilic PDMA (b) and LCST PDMAEMA (c). Right side: schematic illustration of the expected diverse thermoresponsive behaviors of their micelles.

In the case of P(AAm-*co*-AN)-*b*-PS (Fig.30a), micelles in aqueous solution should be expected at $T >$ UCST with PS core and P(AAm-*co*-AN) corona; while when the solution is cooled below UCST, collapse of the micelle corona with dehydrated P(AAm-*co*-AN) chains should take place. As for P(AAm-*co*-AN)-*b*-PDMA (Fig.30b), micelles should be formed only at $T <$ UCST with P(AAm-*co*-AN) core and PDMA corona, and they should be totally dissolved if the solution temperature goes up above the UCST because the two blocks are water-soluble. In the last case of P(AAm-*co*-AN)-*b*-PDMAEMA (Fig.30c), since the LCST of PDMAEMA (about 45 °C) is higher than the UCST of the P(AAm-*co*-AN) block, the reversed core-shell micelles can be expected; that is, micelles formed at $T >$ LCST would have the PDMAEMA core and P(AAm-*co*-AN) corona reversed to the P(AAm-*co*-AN) core and PDMAEMA corona at $T <$ UCST. Such micelle core–corona switching was demonstrated with BCPs bearing a zwitterionic UCST block in water (not in PBS) (53,64,68,69,151). As shown below, the three types of thermally induced micellar changes dictated by UCST either in water or in PBS have been confirmed by experiments using a number of characterization methods.

Of the three BCPs, P(AAm-*co*-AN)-*b*-PS is the only one that cannot be dissolved in water. At $T >$ UCST of the P(AAm-*co*-AN) block, it is a typical amphiphilic BCP. To prepare the micelles, a sample was first dissolved in hot DMSO (50 ^{o}C, good solvent for both blocks), and hot water (50^{o}C) was then added under stirring to induce the formation of micelles that were finally dispersed in aqueous solution after dialysis against hot water to remove DMSO. Figure 31 shows a collected set of characterization results. The response of the micelles in aqueous solution to temperature change was assessed by solution transmittance measurements (Fig.31a). The BCP solution was first equilibrated at 70 °C, where micelles with PS core and P(AAm-*co*-AN) corona should form; and it was then subjected to a cooling and heating cycle (1 °C/min). As can be seen, the initial transmittance depends on the BCP concentration, but for the two solutions the transmittance drops on cooling as the P(AAm-*co*-AN) chains become insoluble at $T <$

UCST, likely resulting in aggregation of the micelles. At the low BCP concentration of 0.5 mg/mL, the transmittance change is reversible upon the subsequent heating, indicating redispersion of the micelles when the P(AAm-*co*-AN) chains recover the soluble state at $T >$ UCST. However, at the higher BCP concentration of 5 mg/mL, on heating through the phase transition, the transmittance appears higher than the initial level. Visual examination found that part of the aggregates could not be redispersed on heating and remained at the bottom of the cuvette, resulting in a lower actual concentration of micelles in the solution. Dynamic light scattering (DLS) was used to monitor the change in the size (hydrodynamic diameter D_H) of the micelles on cooling from 60 to 20 ^oC (Fig.31b). In this experiment, over the temperature range around the UCST, the measurement was taken at an interval of 1 ^oC (solution held at each temperature for 3 min prior to the measurement). It is visible that the phase transition occurs at about 43 ^oC, and that before the average D_H increases from ~150 to 210 nm, the size of the micellar aggregates decreases at the beginning of the phase transition, which indicates a collapse of the P(AAm-*co*-AN) chains upon the hydration–dehydration transition surrounding the PS micelle core. Since the micelles with insoluble P(AAm-*co*-AN) corona are instable, aggregation of the micelles follows. As can be seen from the distribution of sizes measured at 50 and 30 ^oC, the thermally induced change from dispersed micelles at $T >$ UCST to aggregated micelles at $T <$ UCST is reversible and can be repeated over several temperature shift cycles (Fig.31c).

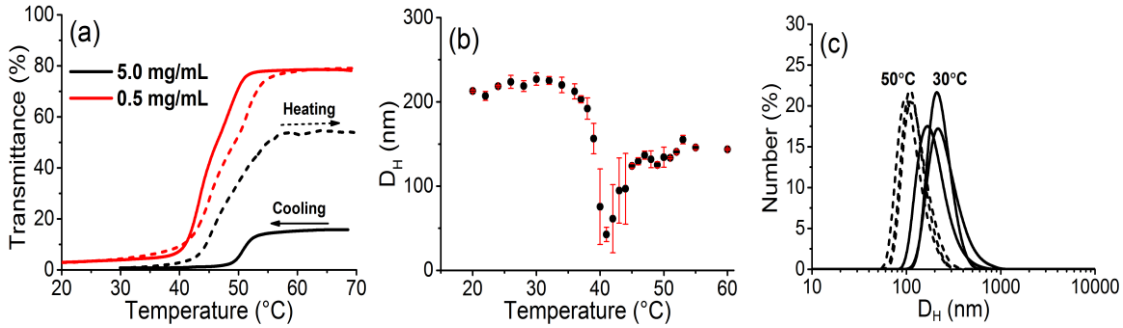

Figure 31. Characterization results for P(AAm-*co*-AN)-*b*-PS. (a) Transmittance change of the BCP micellar solution at two polymer concentrations upon a cooling-heating cycle (1 ^{o}C/min). (b) Change in the hydrodynamic diameter, D_H, on cooling of a micellar solution (0.5 mg/mL). (c) Reversible change in the size distribution of the micellar aggregates in water (0.5 mg/mL) upon temperature shift between 50 ^{o}C (>UCST) and 30 ^{o}C (<UCST).

The case of P(AAm-*co*-AN)-*b*-PDMA is more interesting. The BCP is totally soluble in water at $T >$ UCST while micelles with P(AAm-*co*-AN) core and PDMA corona should be formed on cooling the solution below the UCST. The utility of this type of BCP micelles for temperature-controlled release of payload is different from LCST polymer-based BCPs. The micelles with a UCST block core can simply be dissolved upon temperature rise to $T >$ UCST. The results in Figure 32 confirm the UCST-governed micellar change. The transmittance changes observed with two solutions of different BCP concentrations are characterized by a decrease around 18 ^{o}C on cooling, arising from the formation of micelles from the dissolved state (Fig.32a). The dissolution of the micelles on heating is revealed by the recovered high transmittance. It is noticeable that as compared to P(AAm-*co*-AN)-*b*-PS, the UCST of P(AAm-*co*-AN)-*b*-PDMA appears at lower temperature, likely and understandably due to the influence of the water-soluble PDMA block. Indeed, the formation of micelles on cooling is visible from the change in the hydrodynamic diameter as D_H jumps from about 10 nm (dissolved state) to 160 nm at the UCST phase transition temperature (Fig.32b). Likewise, from the changes in the distribution of sizes measured at 10 and 40 ^{o}C in both pure water and PBS (Fig.32c), the

reversible formation and dissolution of the micelles below and above the UCST of the P(AAm-*co*-AN) block, respectively, leaves no doubt. With P(AAm-*co*-AN)-*b*-PDMA soluble in water, we recorded variable-temperature ^{1}H NMR spectra in a D_2O solution of the BCP. The three spectra at 7, 19, and 31 °C (Fig.32d), chosen as examples, also indicate the micellization, since the characteristic signals of P(AAm-*co*-AN) from about 1 to 1.6 ppm, very much visible at 31 ^{o}C, see their intensities significantly reduced at 7 ^{o}C as a result of the aggregation of the P(AAm-*co*-AN) chains in the micelle core. The plot of the integral of the peaks versus temperature, obtained from a complete set of variable-temperature ^{1}H NMR spectra, clearly shows the UCST transition (Fig.33).

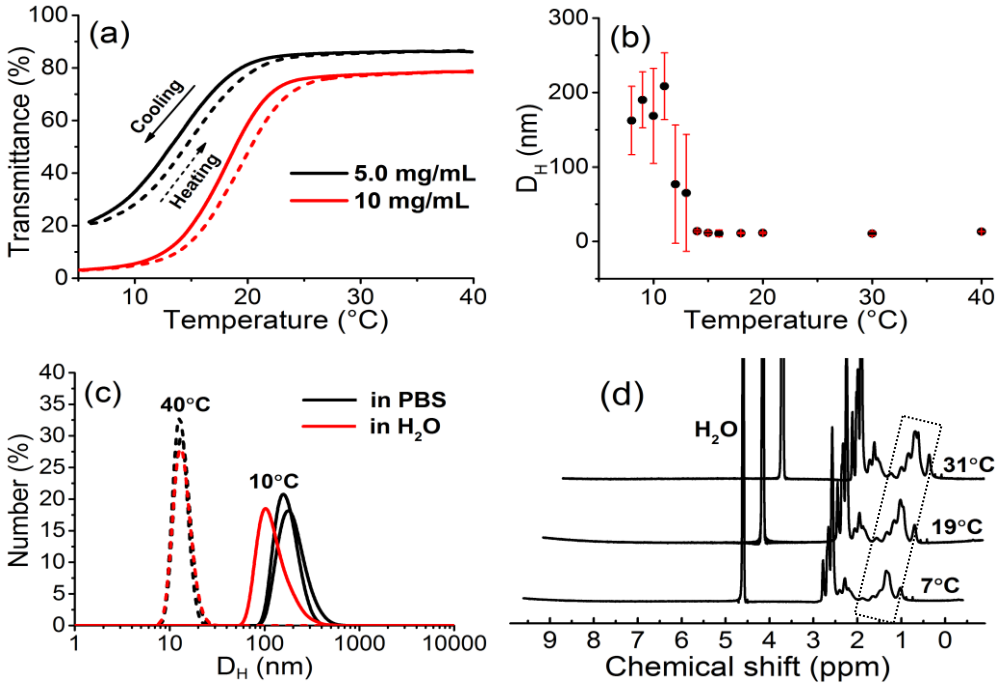

Figure 32. Characterization results for P(AAm-*co*-AN)-*b*-PDMA. (a) Transmittance change of the BCP micellar solution at two polymer concentrations upon a cooling-heating cycle (1 ^{o}C/min). (b) Change in the hydrodynamic diameter, D_H, on cooling of the micellar solution (1 mg/mL). (c) Reversible change in the size distribution of the solution (1 mg/mL) in PBS or in water upon temperature shift between 40 ^{o}C (>UCST) and 10 ^{o}C (<UCST). (d) Variable-temperature ^{1}H NMR spectra in D_2O.

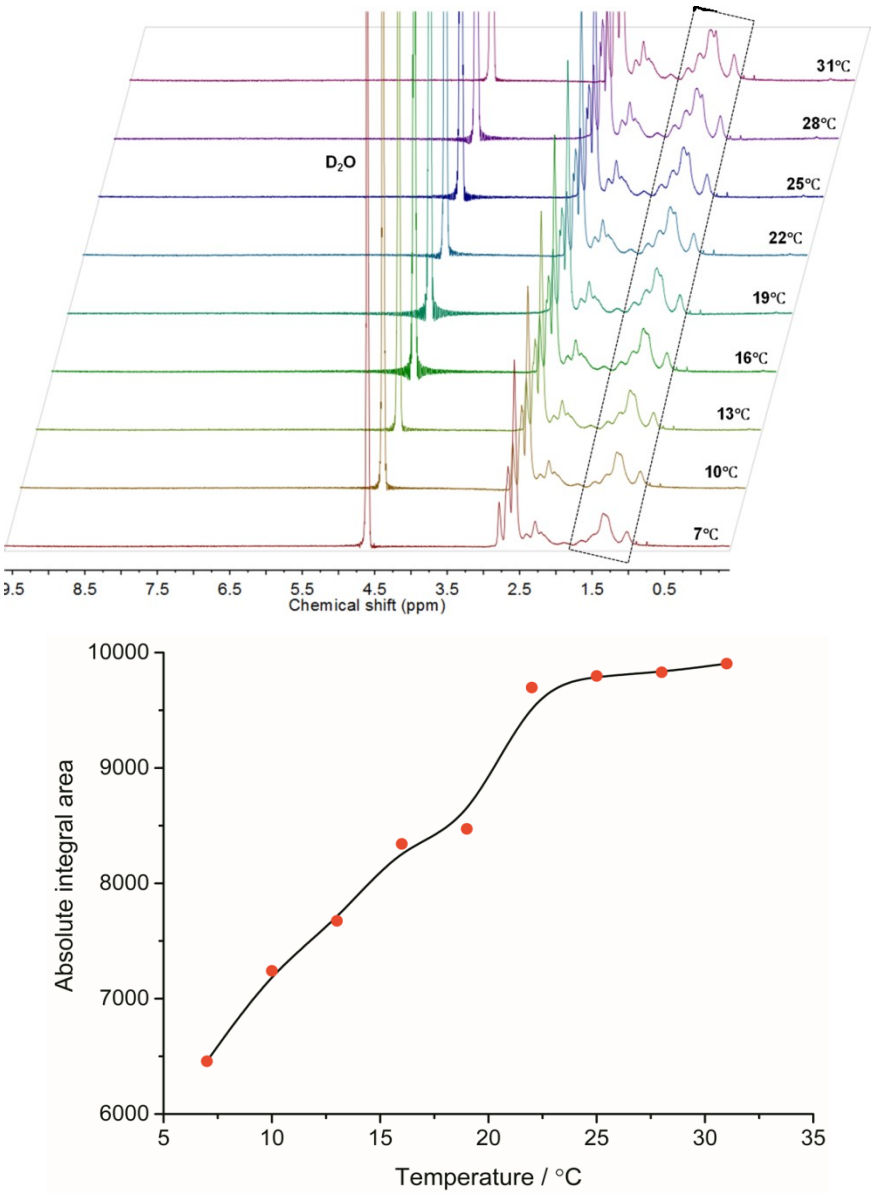

Figure 33. Top: Variable-temperature ^{1}H-NMR spectra of P(AAm-*co*-AN)-*b*-PDMA (P7 in Table 4) in D_2O recorded from 7 ^{o}C to 31 ^{o}C with an interval of 3 ^{o}C. Down: Change in the integral of the resonance peaks from 1 to 1.8 ppm as a function of temperature, showing the UCST behavior of the P(AAm-*co*-AN) block in the diblock copolymer.

As pointed out above, the last diblock copolymer of P(AAm-*co*-AN)-*b*-PDMAEMA

should, by design, form micelles at $T >$ LCST of the PDMAEMA block and, necessarily, $T >$ UCST of the P(AAm-*co*-AN) block, with the insoluble PDMAEMA chains making the micelle core and the soluble P(AAm-*co*-AN) chains forming the corona. However, when the solution is cooled to $T <$ UCST of the P(AAm-*co*-AN) block, meaning necessarily $T <$ LCST of the PDMAEMA block, micelles with reversed core and corona should be formed. Indeed, such thermally induced "reversed core-shell" behavior was readily observed, as seen in Figure 34. First, the transmittance change of a PBS solution of the BCP (Fig.34a) indicates that P(AAm-*co*-AN)-*b*-PDMAEMA is soluble over a temperature range of about 22–41 °C (high transmittance), and that the transmittance drop results from the formation of micelles at temperatures either higher than 41 °C (>LCST of PDMAEMA) or lower than 22 °C (<UCST of P(AAm-*co*-AN)). Variable-temperature DLS measurements on cooling the solution from 70 to 10 °C confirmed the above analysis (Fig.34b). The BCP in an aggregated state at the high-temperature end (D_H around 200 nm) becomes dissolved at temperature below 62 °C (D_H drops to 10 nm), while upon further cooling to the low-temperature side, aggregation of the BCP reappears at temperatures below 18 °C (D_H hundreds of nm). With respect to the transmittance measurements, the apparently larger temperature range for the soluble state is caused by the lower BCP concentration used for the DLS experiments. The reversible changes upon "switching" the solution temperature between 70 °C (micelle with PDMAEMA core), 40 °C (dissolved state), and 10 °C (micelle with P(AAm-*co*-AN) core) in either PBS or water can be seen from Figure 34c. Likewise, variable-temperature ^{1}H NMR spectra recorded in the three regions further confirmed the reverse of the blocks in the micelle core and corona (Fig.34d). While the characteristic resonance signals for both P(AAm-*co*-AN) and PDMAEMA are visible at 34 °C, upon cooling the solution to 10 °C, the peaks of P(AAm-*co*-AN) from 1.3 to 2 ppm are much reduced due to aggregation of the P(AAm-*co*-AN) chains in the micelle core; by contrast, with the solution heated to 70 °C, it is the peak of PDMAEMA around 4 ppm that is

much disappeared, indicating the aggregation of the PDMAEMA chains in the micelle core. The plot of the integral of the resonance peaks of the two blocks vs temperature shows the UCST and LCST transitions (Fig.35). As compared to the micelle of P(AAm-*co*-AN)-*b*-PDMA (Figure 32 and Figure 33), the NMR peak intensity of either P(AAm-*co*-AN) or PDMAEMA in the micelle core is much more lowered, suggesting a more dehydrated state. It should be emphasized that these variable-temperature ^{1}H NMR measurements provide crucial evidence for the formation of micelles. It is possible that the formation of colloidal particles detected by DLS or solution turbidity is caused by a macroscopic phase separation of the polymer solution giving rise to a more concentrated phase in the form of particles (162–164). However, in such a case, the polymer chains in the two phases should remain hydrated or solvated so that no or little ^{1}H NMR spectral changes (dropped peak intensity and peak broadening) can be observed (162).

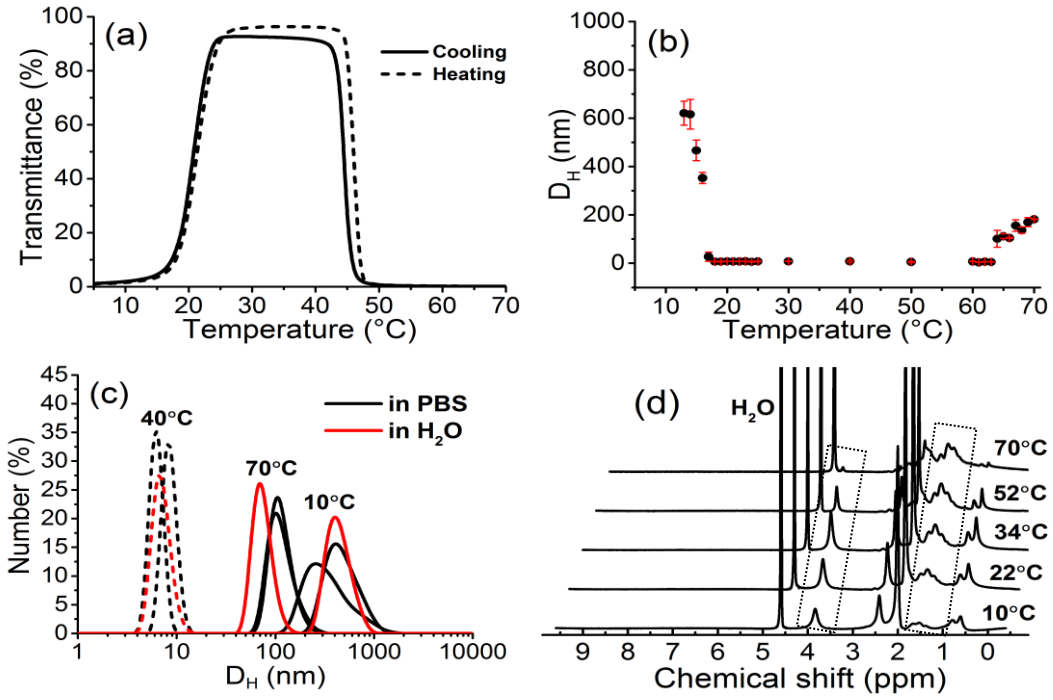

Figure 34. Characterization results for P(AAm-*co*-AN)-*b*-PDMAEMA. (a) Transmittance change of the BCP micellar solution (polymer concentration: 5 mg/mL) upon a cooling-heating cycle (1 ^{o}C/min). (b) Change in the hydrodynamic diameter, DH, on cooling of the micellar solution (0.8 mg/mL). (c) Reversible change in the size distribution of the micellar aggregates in PBS or in water (0.8 mg/mL) upon temperature shift between 10 ^{o}C (UCST>T<LCST), 40 ^{o}C (LCST>T>UCST) and 70 ^{o}C (UCST<T>LCST). (d) Variable-temperature ^{1}H-NMR spectra in a D_2O solution.

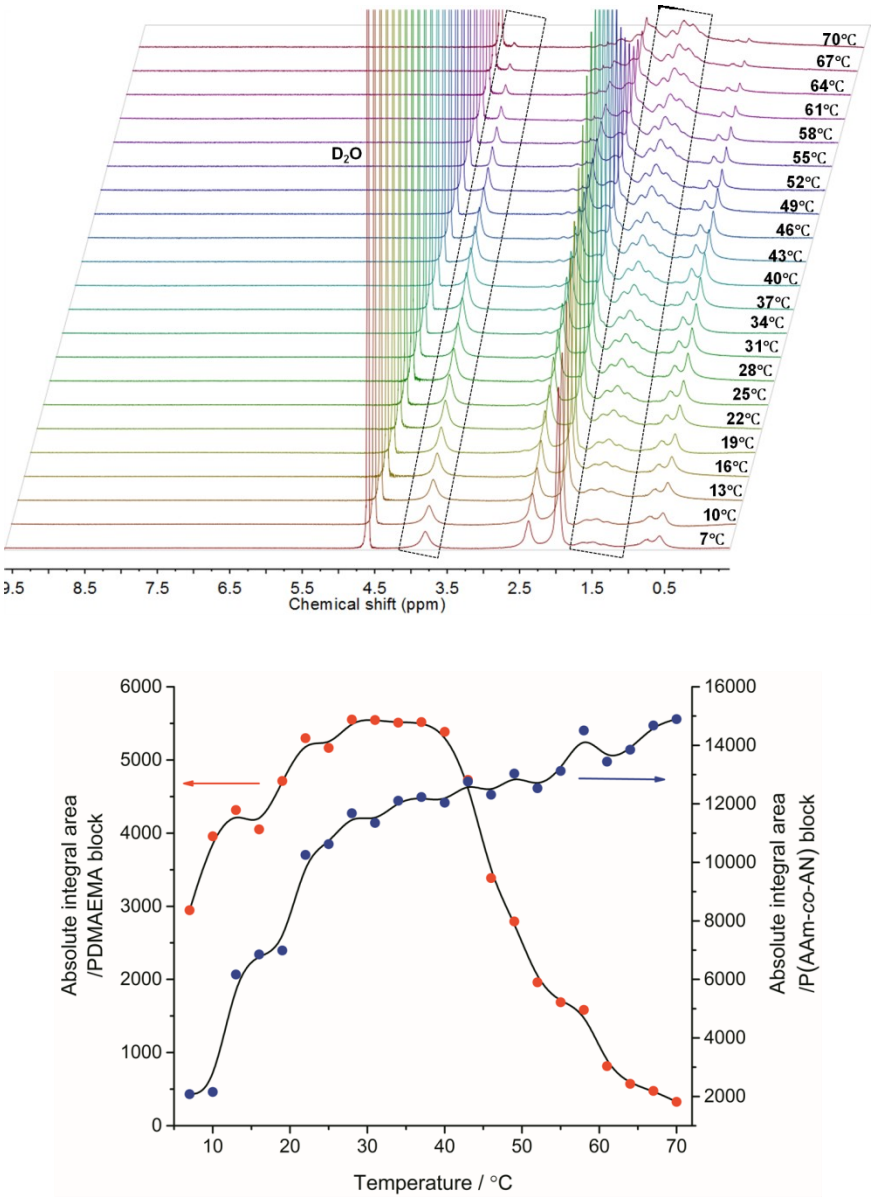

Figure 35. Top: Variable-temperature ^{1}H-NMR spectra of P(AAm-*co*-AN)-*b*-PDMAEMA (P8 in Table 4) in D_2O recorded from 7 ^{o}C to 70 ^{o}C with an interval of 3 ^{o}C. Down: Change in the integral of the resonance peak of PDMAEMA (3.8-4.1 ppm) as well as that of P(AAm-*co*-AN) (1.3-2.0 ppm) as a function of temperature, showing the LCST behavior of the PDMAEMA block and the UCST of the P(AAm-*co*-AN) block in the diblock copolymer.

AFM observation was also carried out to confirm the formation and the various

thermoresponsive behaviors of the micelles of the three BCPs. Figure 36 shows representative images. In all cases, although the size of micellar aggregates viewed on AFM generally appears smaller than the average hydrodynamic diameter measured by DLS, which is common, the thermally induced formation or dissolution or size change of the micelles are clearly observable and in agreement with the DLS results. For P(AAm-*co*-AN)-*b*-PS (Fig.36a), on cooling the micellar solution from 50 °C (hydrophobic PS with hydrophilic P(AAm-*co*-AN)) to 20 °C (two hydrophobic block), the average size of the micellar aggregates is about doubled (from 32 to 61 nm), indicating agglomeration of initial micelles as a result of the hydration–dehydration transition of the P(AAm-*co*-AN) chains. For P(AAm-*co*-AN)-*b*-PDMA (Fig.36b), micelles (about 30 nm) formed at 10 °C (hydrophobic P(AAm-*co*-AN) with hydrophilic PDMA) are totally disappeared upon heating of the solution to 50 °C (two hydrophilic blocks), indicating the dissolution of the micelles due to the dehydration–hydration transition of the P(AAm-*co*-AN) chains. Likewise, in the case of P(AAm-*co*-AN)-*b*-PDMAEMA (Fig.36c), on heating the micellar solution from 10 °C (hydrophobic P(AAm-*co*-AN) with hydrophilic PDMAEMA) to 35 °C (two hydrophilic blocks), the micellar aggregates (average size 223 nm) are basically dissolved; further temperature increase to 70 ^{o}C (hydrophilic P(AAm-*co*-AN) with hydrophobic PDMAEMA) results in new micelles of smaller sizes (average 163 nm). The different sizes of the two types of micelles with reversed core and corona are consistent with the DLS measurements.

(a)P(AAm-*co*-AN)-*b*-PS **(b)P(AAm-*co*-AN)-*b*-PDMA**

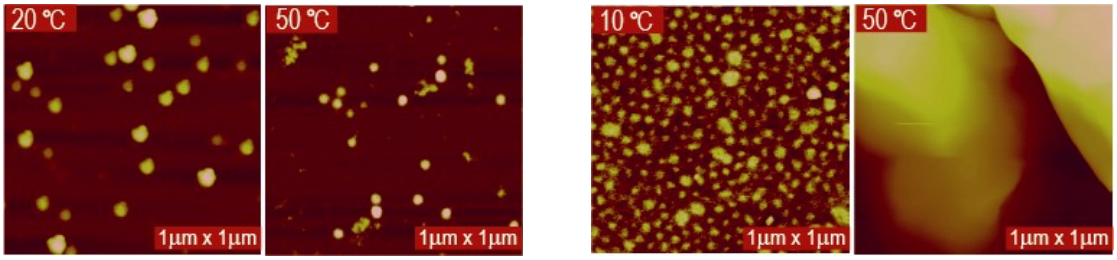

(c) P(AAm-*co*-AN)-*b*-PDMAEMA

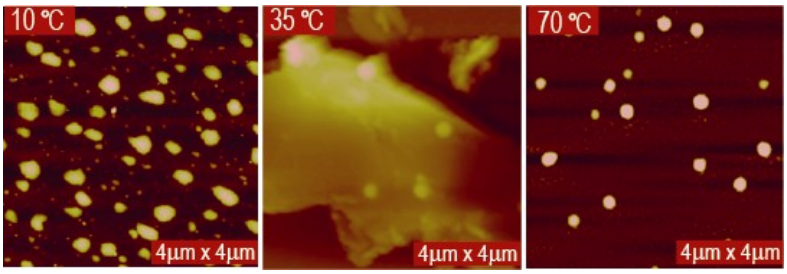

Figure 36. AFM images of the thermosensitive micellar aggregates of the three UCST diblock copolymers: (a) P(AAm-*co*-AN)-*b*-PS, showing that micelles formed at T>UCST of the P(AAm-*co*-AN) block (image at 50 ^{o}C) aggregate at T<UCST (20 ^{o}C); (b) P(AAm-*co*-AN)-*b*-PDMA, showing that micelles formed at T<UCST of the P(AAm-*co*-AN) block (image at 10 ^{o}C) dissolve at T>UCST (50 ^{o}C); and (c) P(AAm-*co*-AN)-*b*-PDMAEMA, showing that micelles formed at T>LCST of the PDMAEMA block (micelle core) and T>UCST of the P(AAm-*co*-AN) block (micelle corona) (image at 70 ^{o}C) can reverse the micelle core and corona at T<LCST and T<UCST (10 ^{o}C), with micelles dissolved at temperatures between LCST and UCST of the two blocks (35 ^{o}C).

2.4. Conclusions

We have shown that P(AAm-*co*-AN) with a sharp and stable UCST in aqueous solution can be synthesized using RAFT, and that the as-prepared P(AAm-*co*-AN) can be utilized

as macro-CTA to grow a second polymer of choice for BCP synthesis. To demonstrate the great potential of incorporating the uncharged UCST P(AAm-*co*-AN) in polymers of controlled structures or architectures producible with RAFT, we used the same P(AAm-*co*-AN) to synthesize three amphiphilic diblock copolymers that are representative of three types of BCP constructions, with P(AAm-*co*-AN) linked to hydrophobic PS, hydrophilic PDMA and LCST-exhibiting PDMAEMA, respectively. We found that the three BCPs of different designs can all exhibit thermally induced changes as dictated by the UCST of the P(AAm-*co*-AN) block, in a reversible and robust way in both pure water and PBS. Considering the fact that P(AAm-*co*-AN) is synthesized from two commercially available monomers and has composition-tunable UCST, and that RAFT is a versatile polymerization method for macromolecular and materials engineering, our study shows that the uncharged P(AAm-*co*-AN) can be used to construct UCST-based polymers of controlled architectures, much the same way as using LCST polymers like, say, PNIPAM. This ability may open the door to in-depth exploitation of new smart polymer materials and devices based on the thermosensitivity opposite to the much-developed LCST polymers.

2.5. Statement of Contribution

This work was published in *Langmuir* 2014, 30, 11433–11441 by Hu Zhang, Xia Tong, and Yue Zhao. This research work was conducted in Université de Sherbrooke under the supervision of Prof. Zhao. Xia Tong did the AFM measurements. I synthesized all the samples and performed all the other characterizations reported in this publication.

CHAPTER 3 ULTRASENSITIVE PH-INDUCED WATER SOLUBILITY SWITCH OF UCST POLYMERS

3.1. Introduction

Thermosensitive polymers exhibiting an upper critical solution temperature (UCST) in aqueous solution have not been studied with the same widespread interest as for polymers displaying a lower critical solution temperature (LCST). Basically the two groups of polymers undergo opposite water solubility switch (from soluble to insoluble state or vice versa) upon temperature change across the phase separation temperature (LCST or UCST). Most reported UCST polymers are zwitterionic (58,59,62–64,66–74,79,146,147,149,151–153,155,158,165–172), for which charged groups make the UCST sensitive to salts or electrolytes (ionic strength). This feature is thought to be undesirable for applications in physiological medium because of an unstable UCST (59,63,66,67,69,71,152,155,158,166,169). To this regard, uncharged UCST polymers may be advantageous. Although some polymers whose intermolecular interactions in water are predominated by H-bonding (polymer-polymer, polymer-water) are known to show an UCST, they have instigated little interest because their UCSTs are outside the accessible temperature range for liquid water (18). Recent studies by Agarwal's group (90–93,102,103,106,145,173) and others (85,89,94–100,104,105,150,156,157,174–178) demonstrated that with appropriate choices of monomers H-bonding-based polymers can display easily accessible and stable UCSTs in physiological medium. Among the uncharged UCST polymers, particularly interesting is the random copolymer of acrylamide and acrylonitrile (two commercially available monomers), denoted as P(AAm-*co*-AN) hereafter. As revealed by the cloud point (solution transmittance drop) measurement, the UCST of P(AAm-*co*-AN) is not only tunable by varying the copolymer composition, it is also sharp, insensitive to salt

and has little hysteresis upon cooling and heating cycles (93,104,179). Furthermore, the use of controlled radical polymerization such as RAFT to prepared P(AAm-*co*-AN) makes it easy to have the uncharged UCST P(AAm-*co*-AN) in block copolymer structures of various designs, (179) showing the perspective of exploring UCST polymers of controlled architectures. To obtain H-bonding-based UCST polymers with accessible phase separation temperatures in water, the absence of charged groups in the polymer structure is necessary, because even a few ions beard by the polymer may bring the UCST down to a temperature that is too low to be readily observable (89,91). This high ion-sensitivity of UCST is believed to originate from the polymer solution enthalpy that is initially small so that the presence of even a few charged groups interacting with water molecules may result in a significant variation in solution enthalpy and thus in phase separation temperature (18,148).

In this paper, we demonstrate that one can take advantage of the high sensitivity of UCST to charged groups to prepare polymers that can undergo straightforward water solubility switch in a wide accessible temperature range upon slight pH change. We synthesized UCST random copolymers comprising acrylamide, acrylonitrile and a third pH-responsive monomer, namely, acrylic acid or 4-pyridine, which are referred to P(AAm-*co*-AN-*co*-AAc) and P(AAm-*co*-AN-*co*-4VP), respectively. The introduction of AAc or 4VP comonomer units into P(AAm-*co*-AN) obviously has the purpose of shifting the UCST upon pH-induced protonation or deprotonation of the weak acid or base units leading to change in the number of charged groups. Indeed, we found that the cloud point of P(AAm-*co*-AN-*co*-AAc) or P(AAm-*co*-AN-*co*-4VP) in phosphate buffered saline (PBS) solution could shift considerably in response to small pH change over a certain range, especially with 4VP in the structure. For one sample of P(AAm-*co*-AN-*co*-4VP), it displays a cloud point shift of 57 ^{o}C over pH variation of 0.25 unit, and, from the solution transparency change, its solubility switch at room temperature is visible over a pH variation as little as 0.05 unit! Furthermore, to demonstrate the possible applications of

such ultrasensitive pH-induced water solubility switch, we synthesized an ABA-type triblock copolymer of P(AAm-*co*-AN-*co*-4VP)-*b*-PDMA-*b*-P(AAm-*co*-AN-*co*-4VP) whose middle PDMA block is "permanently" water soluble (PDMA stands for poly(dimethylacrylamide)). The micelle of this block copolymer in PBS at 37 ^{o}C can be stable from pH 7.00 down to pH 4.75 but undergoes abrupt dissociation at pH 4.50 as a result of the solubility reversal of the P(AAm-*co*-AN-*co*-4VP) micellar core (from about 30 ^{o}C below the UCST at pH 4.75 to more than 30 ^{o}C above the UCST at 4.50). This micellar disruption over a tiny pH change contrasts with the much more gradual change found for most pH-sensitive polymer assemblies based on LCST polymers (49,51,114,180,181).

3.2. Experimental Section

3.2.1. Materials

All reagents were purchased from Sigma-Aldrich. N-acrylamide (AAm) was recrystallized in chloroform prior to use; acrylonitrile (AN), 4-vinylpyridine (4VP) and N,N'-dimethylacrylamide (DMA) were purified by passing through a column filled with basic alumina; acrylic acid (AAc) was distilled under reduced pressure to remove the inhibitor. 2,2'-Azobis(2-methylpropionitrile) (AIBN) was purified by recrystallizations from ethanol. The RAFT chain transfer agent, S, S'-bis(α, α'-dimethyl-α"-acetic acid)trithiocarbonate (BTC), was synthesized according to a reported method (182). Other chemicals were used as received. Dimethyl sulfoxide (DMSO) was HPLC grade. Dialysis membrane tube with molecular weight cut-off (MWCO) of 3000 was purchased from the Spectrum Laboratories (USA).

3.2.2. Synthesis of UCST Random Copolymers and Triblock Copolymer

A total of six polymers were synthesized using RAFT polymerization. Figure 37 shows

their chemical structures, and Table 5 lists their acronyms and main characteristics. Since the samples were prepared with RAFT, they all bear a trithiocarbonate moiety at the middle of polymer chain.

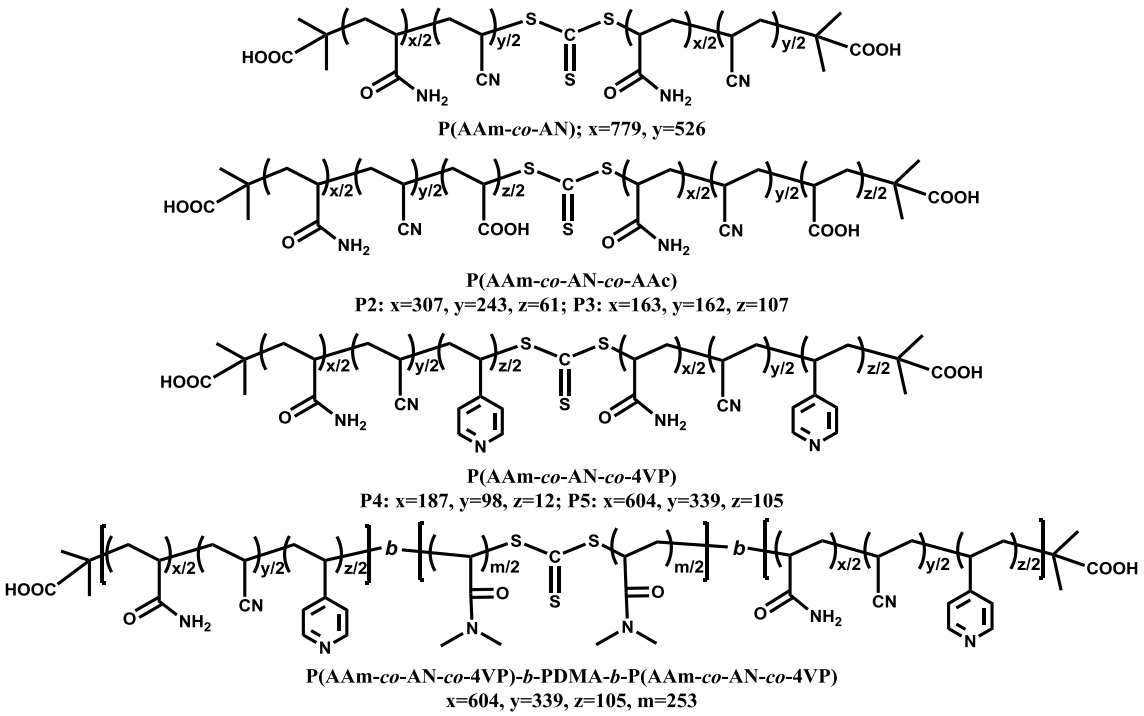

Figure 37. Chemical structures of the UCST random and block copolymers synthesized using RAFT polymerization.

Table 5. Characteristics of synthesized copolymers

Sample number	Polymer	AN in feed (mol%)	AN in polymer (mol%)[a]	AAc or 4VP in feed (mol%)	AAc or 4VP in polymer (mol%)[a]	M_n (g/mol)[b]	M_w/M_n[b]
P1	P(AAm-*co*-AN)	26.5	33.5	—	—	83275	2.6
P2	P(AAm-*co*-AN-*co*-AAc)	26.6	32.9	5.0	11.3	39120	1.9
P3	P(AAm-*co*-AN-*co*-AAc)	25.2	30.7	10.0	27.7	27926	2.4
P4	P(AAm-*co*-AN-*co*-4VP)	26.6	26.2	5.0	6.5	19779	2.8
P5	P(AAm-*co*-AN-*co*-4VP) (also used as macro-CTA for **P6**)	25.2	25.0	10.0	15.4	72024	1.8
P6	P(AAm-*co*-AN-*co*-4VP)-*b*-PDMA-*b*-Poly(AAm-*co*-AN-*co*-4VP) (DMA in polymer: 25.8 mol %)	—	18.6	—	11.4	97148	2.3

[a]Calculated by IR spectroscopy and ^{1}H NMR in d_6-DMSO; [b]determined by size exclusion chromatography.

Synthesis of P(AAm-*co*-AN) (P1 in Table 5). A 25 mL round-bottom flask was charged with AAm (2.8 g), AN (760.0 mg), BTC (74.4 mg), AIBN (8.7 mg) and DMSO (12.3 mL). The mixture was degassed by freeze-thaw cycles (3 times) and then placed into an oil bath preheated to 70 ^{o}C. The polymerization was allowed to proceed for 2h with the mixture under stirring. Afterwards, the polymer was purified by precipitation from the DMSO solution into methanol twice. To completely remove DMSO, the polymer re-dissolved in DMSO was dialyzed against deionized water for 3 days and then recovered by lyophilization. Figure 38 shows the ^{1}H NMR spectrum of **P1**.

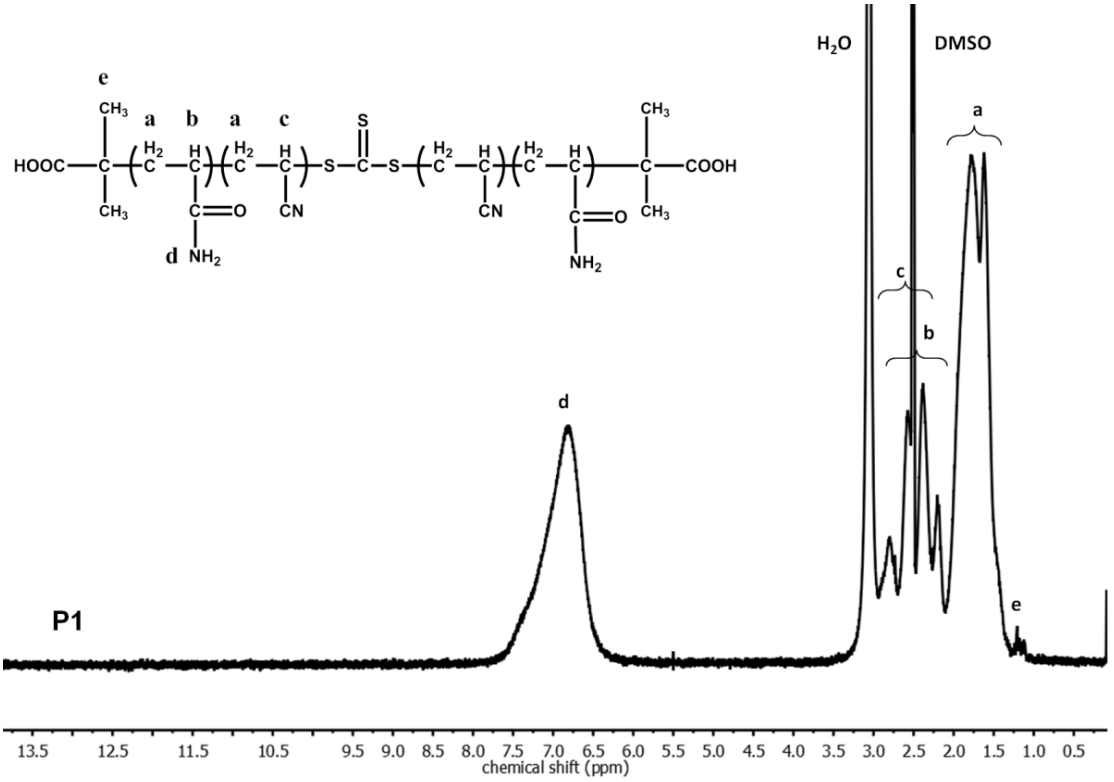

Figure 38. The ^{1}H NMR spectrum of P1 (in d_6-DMSO).

Synthesis of P(AAm-*co*-AN-*co*-AAc) and P(AAm-*co*-AN-*co*-4VP) copolymers (P2-P5 in Table 5). The RAFT polymerization procedures for obtaining these four copolymers were similar except for slight variations in the reaction time. In all cases, the same amounts of AAm (2411.0 mg) and AN (700.0 mg) were used; the total concentration of the monomers (AAm, AN, AAc or 4VP) was 4.0 M in DMSO and the total monomer to BTC ratio $[M]_0/[CTA]_0$ was held constant at 300/1. Using the synthesis of P(AAm-*co*-AN-*co*-AAc) with 5 mol% AAc in feed (**P2**) as example: AAm (2411.0 mg), AN (700.0 mg), AAc (179.0 mg), AIBN (5.4 mg) and DMSO (12.3 mL) were added into a 25 mL round-bottomed flask with a magnetic stirring bar. After three freeze-vacuum-thaw cycles, the flask was sealed and then immersed in an oil bath thermostated at 70 ^{o}C for polymerization. The reaction was stopped after 6h and the resulting polymer was purified by three times of precipitation from the DMSO solution

into methanol. The polymer re-dissolved in DMSO was dialyzed against deionized water for 3 days and then recovered by lyophilization. The reaction time was the same, 6 h, for P(AAm-*co*-AN-*co*-AAc) with 10 mol% AAc in feed (**P3**). In the case of P(AAm-*co*-AN-*co*-4VP) with 5 and 10 mol% in feed (**P4**, **P5**), the polymerization time was 4h. The ^{1}H NMR spectra of these four copolymers, P2-P5, are shown in Figure 39 and Figure 40.

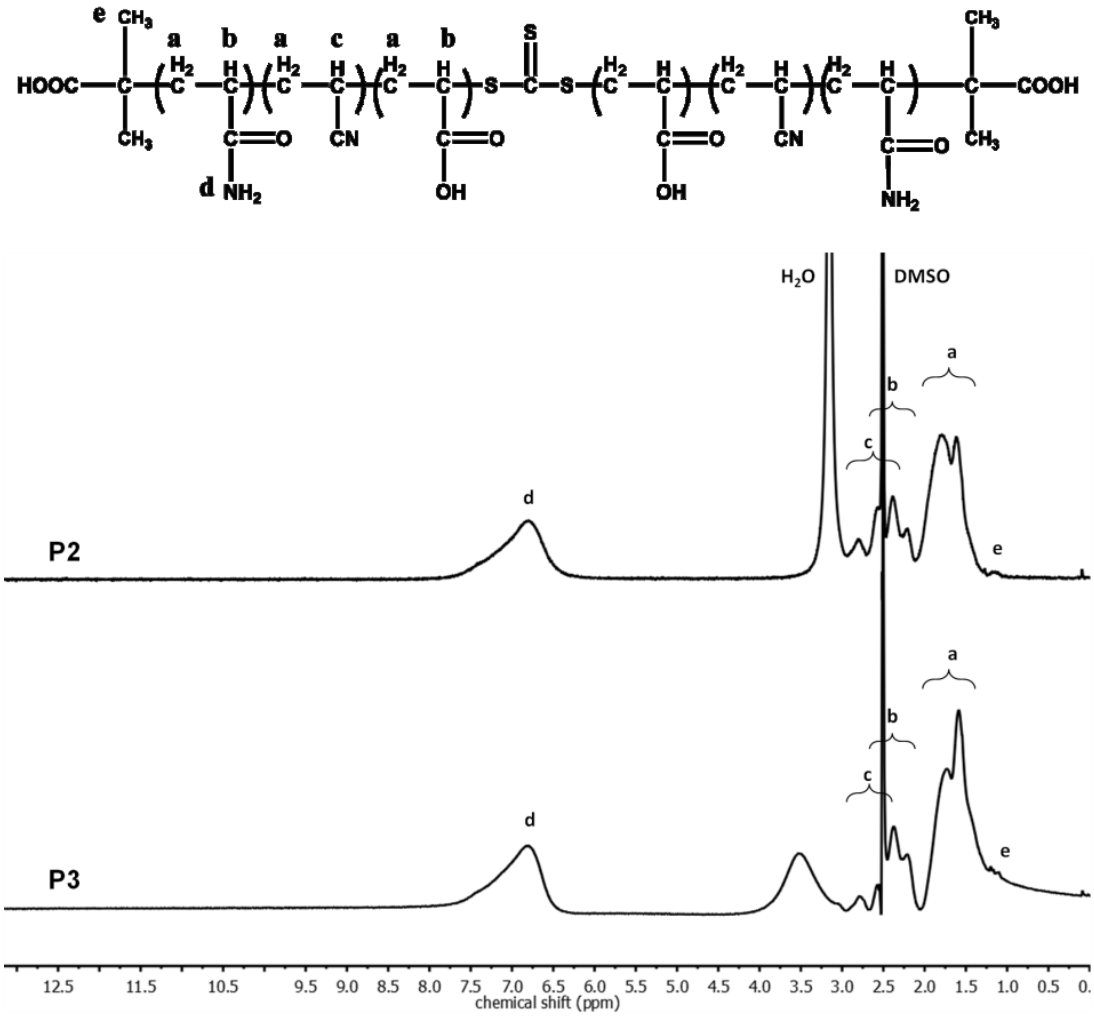

Figure 39. The ^{1}H NMR spectra of P2 and P3 (in d_6-DMSO).

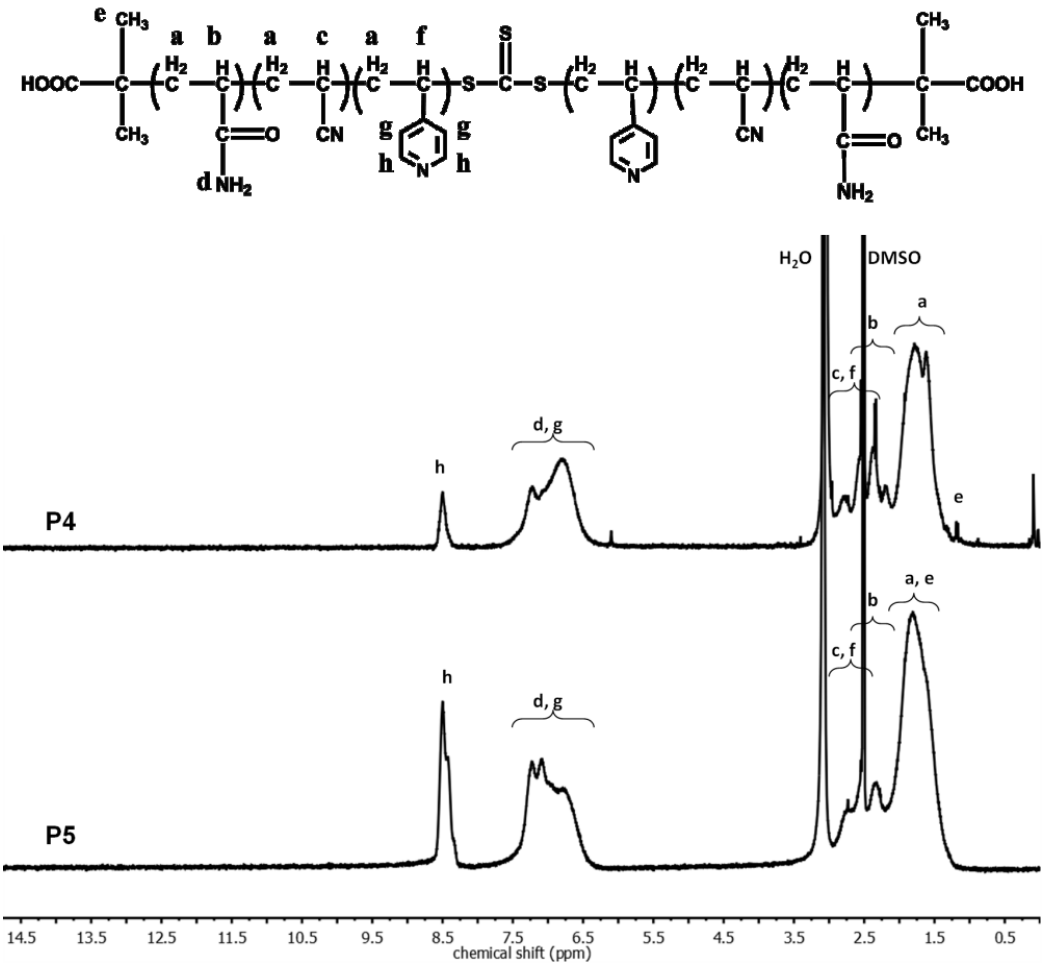

Figure 40. The ^{1}H NMR spectra of P4 and P5 (in d_6-DMSO).

Synthesis of P(AAm-*co*-AN-*co*-4VP)-*b*-PDMA-*b*-P(AAm-*co*-AN-*co*-4VP) (P6 in Table 5). The triblock copolymer was synthesized by using the P(AAm-*co*-AN-*co*-4VP) with 10 mol% in feed (**P5**) as the macromolecular chain transfer agent. DMA (2107.0 mg), **P5** (223.0 mg), AIBN (1.2 mg) and DMSO (22.0 mL) were added into a 50 mL round-bottomed flask. The reaction mixture was degassed by pouring N_2 flow for 1h, then sealed and placed in an oil bath thermostated at 60 °C for 18 h. It was then diluted with DMSO and directly dialyzed against deionized water for 3 days and then recovered by lyophilization. Since DMA is highly water-soluble, unreacted DMA could be removed during dialysis. The ^{1}H NMR spectrum of **P6** is shown in Figure 41.

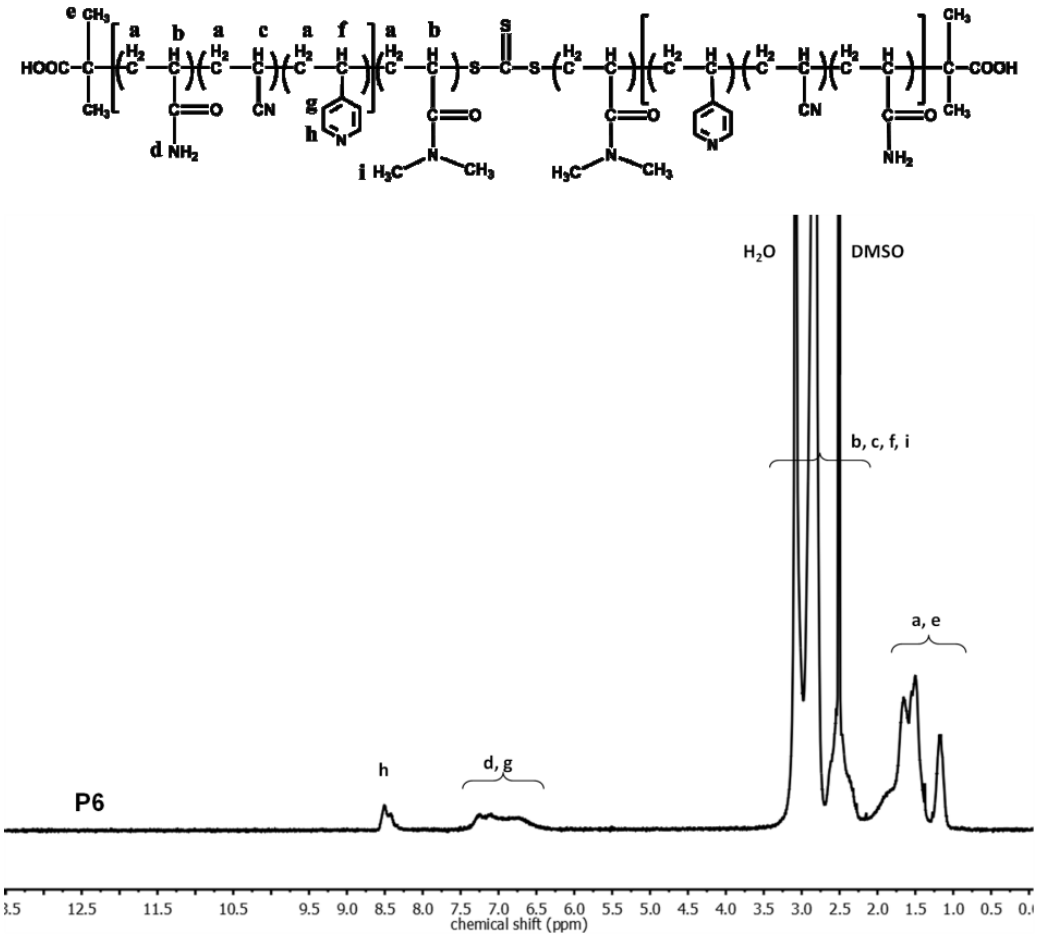

Figure 41. The ^{1}H NMR spectrum of P6 (in d_6-DMSO).

3.2.3. Characterization methods

^{1}H NMR spectra were recorded on a Bruker Advance III HD 300 MHz spectrometer using deuterated DMSO (d_6-DMSO) as solvent at 80 ^{o}C. Dynamic light scattering (DLS) measurements were performed on a Malvern Zetasizer Nano ZS ZEN3600 system with a helium−neon laser (wavelength: 633 nm), at a scattering angle of 173°. Infrared spectra were recorded on an ABB MB104PH FTIR spectrometer using the diffuse reflection technique. Samples were milled with potassium bromide (KBr) to form a very fine powder for testing. The calibration curve used to determine the AN contents in the various samples was obtained with the spectra of a series of known-composition mixtures

of polyacrylamide and polyacrylonitrile homopolymers (93,179). Size exclusion chromatography (SEC) measurements were carried out on Tosoh EcoSEC GPC system, equipped with three TSK-GEL Super AWM-H columns (6x150mm), at 45 ^{o}C using DMSO containing 1.25 mg.mL^{-1} of LiBr as the eluent (flow rate: 0.3 mL/min) and poly(methyl methacrylate) (PMMA) as standards. The results are shown in Figure 42. Fluorescence emission spectra were recorded using a Varian Cary Eclipse fluorescence spectrophotometer. The used excitation wavelengths were 339 nm for pyrene (excitation and emission slit widths set at 5 nm) and 540 nm for Nile Red (excitation and emission slit widths set at 20 nm). Micellar aggregates were examined using a Hitachi H-7500 transmission electron microscope (TEM) operating at 80 kV. Samples for TEM observations were prepared by casting one drop of the micellar solution on a carbon-coated copper grid, followed by drying at room temperature.

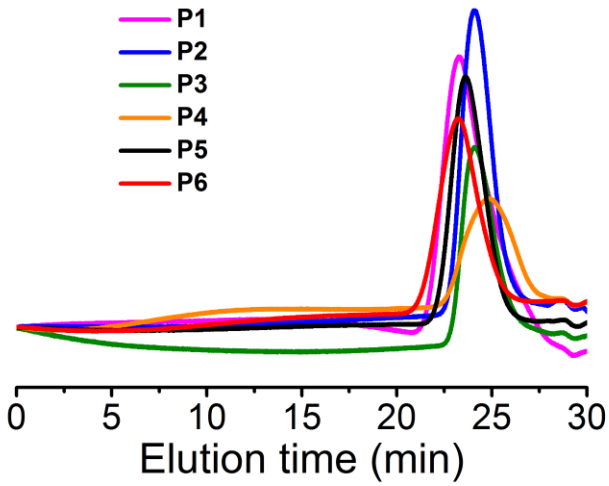

Figure 42. Size exclusion chromatography (SEC) traces of the various polymers (P1-P6) dissolved in DMSO. All the polymers show a unimodal distribution. The sample P6 (triblock copolymer) was synthesized using P5 as macromolecular chain transfer agent, and its SEC trace shows shorter retention time, indicating chain growth.

The UCST shift was investigated by monitoring the change in cloud point of a given polymer solution, which was taken as the inflection point of the transmittance vs. temperature curve. The transmittance was measured at 500 nm. To measure the transmittance as a function of temperature for solutions at various pH values, P(AAm-*co*-AN) (**P1**) and P(AAm-*co*-AN-*co*-AAc) (**P2**, **P3**) samples were first dissolved in 0.15 mol L^{-1} phosphate-buffered saline (PBS) at pH 7.40. By contrast, the samples of P(AAm-*co*-AN-*co*-4VP) (**P4**, **P5**) and P(AAm-*co*-AN-*co*-4VP)-*b*-PDMA-*b*-P(AAm-*co*-AN-*co*-4VP) (**P6**) were first dissolved in 0.15 mol L^{-1} PBS at pH 2.00 to ensure complete dissolution of the polymers. Then the solution pH was adjusted to a desired value by adding either NaOH (0.1 N) or HCl (1 N). The solution pH was measured using a pH-meter (Fisher Scientific™ accumet™ AB 15 pH-meter with 13-620-223A accumet glass pH electrode). Transmittance spectra were recorded on an Agilent Cary Series UV-Vis-NIR spectrophotometer as a function of the solution temperature. Normally, the measurements were carried out by first cooling the solution from the used highest temperature under a constant cooling rate of 1.0 °C/min and then heating the solution back to the starting temperature at the same rate. In case a polymer solution at room temperature was turbid at certain pH (below UCST), it was heated to transparent state (above UCST) before being transferred to a quartz cuvette preheated above UCST in the instrument.

3.2.4. Determination of copolymer compositions

For **P1**, the AN content was directly obtained from a calibration curve with the spectra of a series of known-composition mixtures of polyacrylamide and polyacrylonitrile (93,179). The calibration curve was based on the integral ratio from the characteristic absorption bands around 1659 cm^{-1} and 2242 cm^{-1} assigned to the carbonyl and nitrile group in AAm and AN, respectively. For **P2**-**P3**, the AN content in polymer was obtained the same way. Then, by comparing the integral of peak d (from the NH-protons of AAm side

groups) with the integral of peak a (assigned to methylene groups in all monomer units), the AAm content was obtained (Fig.39). This allows the content in AAc to be calculated. Note that due to partial deuterium exchange of the NH-protons in the 1H NMR spectrum, the AAm content would be higher than in reality, meaning that the actual content AAc would be lower. For **P4-P5**, the calibration curve gives the ratio of AN over the sum of AN and AAm (not the real AN in polymer). We firstly used the integral of peak h (from the aromatic protons of 4VP) with the integral of peak a (assigned to methylene groups in all monomer units) to calculate the 4VP content in polymer (Fig.40). The sum of the AN and AAm can then be calculated, and knowing the ratio of AN over the sum of AN and AAm know from the IR spectra and calibration curve, the respective amount of AN and AAm can be obtained. For **P6**, the 4VP content can be obtained using the NMR spectra Figure 41, the same way as for P4 and P5. Since P6 was synthesized using P5, the ratio of AN with AAm or 4VP should be the same. By using these information the amount of each constituent could be estimated (AN, AAm, 4VP, and DMA: 18.6%, 44.2%, 11.4% and 25.8%, respectively).

3.2.5. Determination of critical micelle concentration of P6 triblock copolymer

Critical micelle concentration (CAC) of the polymer was determined by fluorescence spectroscopy using pyrene as a hydrophobic probe. 1 mL of pyrene solution in THF ($1x10^{-5}$ M) was taken in different vials, and the solvent was removed by blowing argon. A stock solution of the P6 triblock polymer (1 $mg.mL^{-1}$) was prepared in PBS (pH was adjusted to 2.0 to make the polymer completely dissolved) and different volumes of this stock solution were added to the vials containing pyrene. The final volume was adjusted with PBS to obtain a series of solutions with constant pyrene concentration ($1x10^{-6}$ M) and varying polymer concentrations ($1x10^{-6}$ $mg.mL^{-1}$ to 1 $mg.mL^{-1}$). Each solution was adjusted to pH 7.0, sonicated for 30 min and allowed to equilibrate for 12 h at 37 ^{o}C. The emission spectrum was recorded. The ratio of the emission intensities of **I1** (at 373 nm)

and **I3** (at 384 nm) was plotted against logarithmic polymer concentrations as shown in Figure 43.

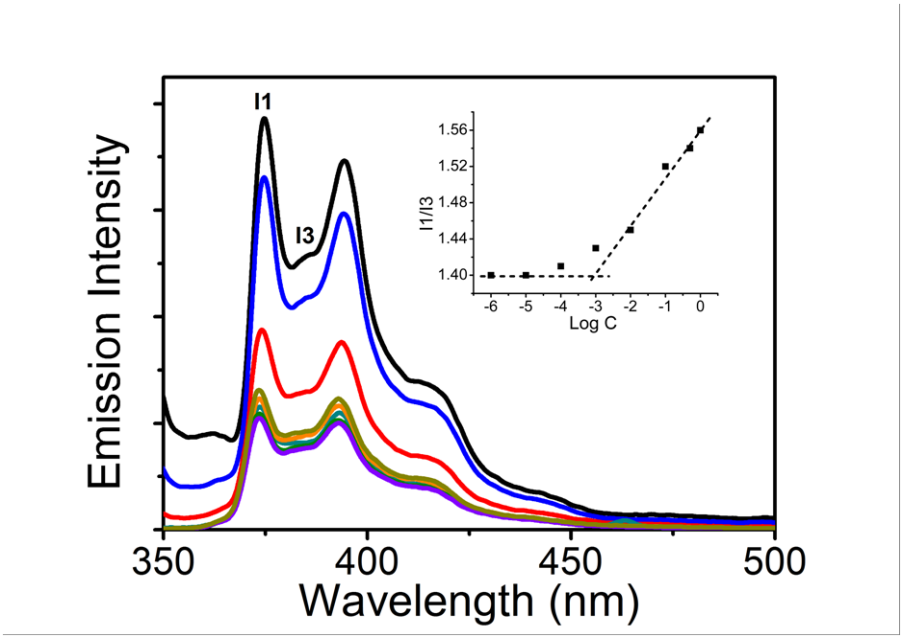

Figure 43. Emission spectra of pyrene dissolved in aqueous solution of P6 at varying concentrations; inset: variation of **I1**/**I3** in pyrene emission spectra as a function of polymer concentration. The critical micelle concentration, determined as the intersection of the two lines, is about 1.0×10^{-3} mg.mL^{-1}.

3.2.6. Preparation of Pyrene-loaded Micellar Solution

Triblock copolymer micelles (1 mg.mL^{-1}) loaded with the pyrene dye (1×10^{-6} M) were prepared using the same method as that described above for the determination of CMC.

3.2.7. Preparation of Nile Red-Loaded Micelles

Triblock copolymer micelles loaded with the NR dye were prepared in the following way. **P6** (10 mg) was first dissolved in DMSO (1.0 mL) and 0.1 mL of NR solution in DMSO (10 mg.mL^{-1}) was added in the polymer solution. DMSO is a good solvent for the

polymer and the dye. Then, the whole solution was added quickly to PBS buffer (9 mL) under ultrasonic agitation using an ultrasonic cleaner (Fisher Scientific FS20, 42 kHz). The solution was dialyzed against PBS for 3 days (with 3000 MWCO dialysis tubing from Spectra/Por) at 37 ^{o}C. The obtained aqueous solution was then filtered through a filter paper (0.45 μm pore size) to remove NR not solubilized by the micelles. The final dye-loaded micellar solution was stored in dark at 37 ^{o}C in water bath before use.

3.3. Results and Discussion

3.3.1. Water Solubility Switch Due to pH-Induced UCST Shift

Of the six samples synthesized for this study (Table 5 and Figure 37), **P1** is the UCST P(AAm-*co*-AN) without acid or base comonomer and used as reference. **P2** and **P3** are P(AAm-*co*-AN-*co*-AAc) with 5 and 10 mol% of acrylic acid in the feed, respectively. As for **P4** and **P5**, they are P(AAm-*co*-AN-*co*-4VP) with 5 and 10% of 4VP in the feed respectively. The actual contents of AAc and 4VP as revealed by infrared and ^{1}H NMR spectra appear to be higher than the feed amount. The last sample, **P6**, is P(AAm-*co*-AN-*co*-4VP)-*b*-PDMA-*b*-P(AAm-*co*-AN-*co*-4VP) triblock copolymer obtained by using **P5** as the macromolecular chain transfer agent, meaning that each of its two end UCST blocks has the half length of **P5** while having the same composition. At T<UCST of the two end blocks, as the middle PDMA block is water soluble, the block copolymer is amphiphilic.

The pH-induced UCST shift was investigated by monitoring the change in cloud point of the solution. In all cases, the measurements were carried out in PBS solution with a polymer concentration of 5 mg/mL and a cooling or heating rate of 1 ^{o}C/min. The results are shown in Figures 45-47 for all samples except the block copolymer. Having the same solution temperature range on abscissa, their different pH dependence or sensitivity of the cloud point is visible. For P(AAm-*co*-AN) (sample **P1**), Figure 44 shows that the

transmittance vs. temperature curves recorded at three representative pH (3.00, 7.00, 10.00) are almost superimposable (1-2 ^{o}C difference), indicating that the polymer's UCST is unaffected by the solution pH. These results are consistent with a previous report with checked pH from 5.0 to 9.0 (104). By contrast, for both P(AAm-*co*-AN-*co*-AAc) (Fig.45) and P(AAm-*co*-AN-*co*-4VP) (Fig.46), the UCST is very sensitive to pH change in the vicinity of pKa of AAc or 4VP groups. In Figure 45, the cloud point of **P2** (with less AAc) already decreases quickly with increasing pH from 3.0 to 4.5 (Fig.45a), and it can no longer be detected at pH 5.0 over the temperature range, as the polymer remains soluble. As expected, the effect is even more prominent for **P3** (with more AAc) (Fig.45b); the cloud point drops by 20 ^{o}C when pH increases from 3.0 to 3.5 and is out of the detectable temperature range at pH 4.0. Bearing AAc in the UCST polymer structure, an increase in pH means more ionized COO- groups, enhanced water solubility and thus decrease in UCST. On the other hand, as seen in Figure 46, P(AAm-*co*-AN-*co*-4VP) displays the opposite cloud point shift upon pH variation due to the base comonomer groups of 4VP. In this case, an increase in pH means less charged (protonated) 4VP groups, which reduces the polymer water solubility and thus results in increase in UCST. From the data obtained with **P4** (Fig.46a) and **P5** (Fig.46b), it is easy to notice that as with AAc, a higher 4VP content in the polymer gives rise to a larger cloud point shift upon the same pH change due to a greater change in the number of ionic groups. Comparing P(AAm-*co*-AN-*co*-AAc) with P(AAm-*co*-AN-*co*-4VP), it appears that the incorporation of 4VP into P(AAm-*co*-AN) gives rise to greater UCST shift than with AAc. At the same content in the feed and apparently lower measured content in the polymer (Table 5), the cloud point shift is larger for P(AAm-*co*-AN-*co*-4VP). In particular, for **P5**, a slight pH variation of 0.25 unit, from 4.50 to 4.75, results in a cloud point shift of 57 ^{o}C (Fig.46b). It is also notable that for all samples at all pH values with a detectable cloud point, the transition between the soluble and insoluble state remains as sharp as with the non-pH-sensitive P(AAm-*co*-AN), with little hysteresis upon the

cooling and heating cycle. This result implies that at a given feed of the three monomers, the random copolymer chains formed at different times over the reaction had a similar composition.

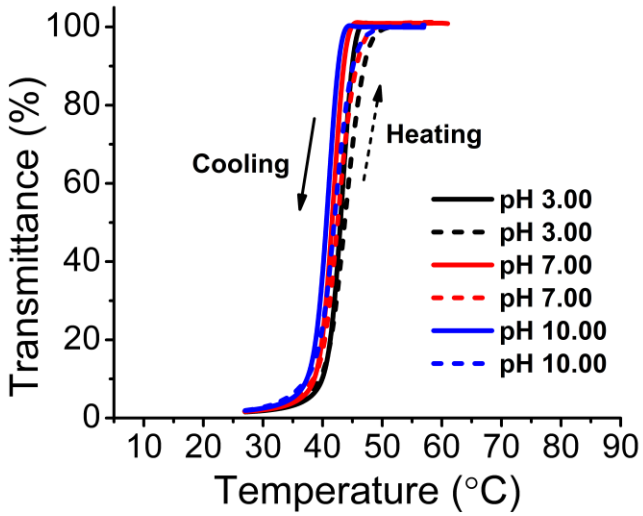

Figure 44. Plots of solution transmittance vs. temperature for P(AAm-*co*-AN) (sample **P1**) in PBS solution at different pH values (polymer concentration: 5 mg/mL; heating and cooling rate: 1 ^{o}C/min; solid and dotted lines: cooling and heating runs respectively).

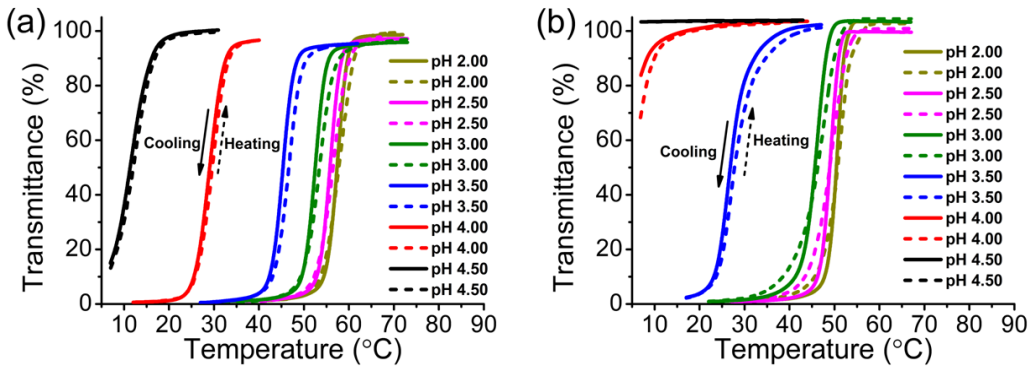

Figure 45. Plots of solution transmittance vs. temperature for P(AAm-*co*-AN-*co*-AAc) in PBS solution at different pH values (polymer concentration: 5 mg/mL; heating and cooling rate: 1 ^{o}C/min): a) sample **P2**, and b) sample **P3**.

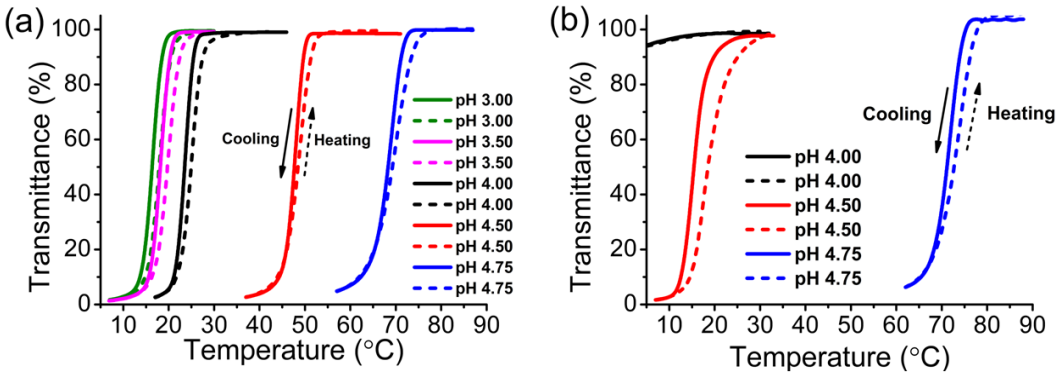

Figure 46. Plots of solution transmittance vs. temperature for P(AAm-*co*-AN-*co*-4VP) in PBS solution at different pH values (polymer concentration: 5 mg/mL; heating and cooling rate: 1 ^{o}C/min): a) sample **P4**, and b) sample **P5**.

To recapitulate the above results, Table 6 collects the cloud points of all samples, being taken as the maximum of the first derivative of the transmittance vs. temperature curves. Figure 47 gives a graphical presentation of the data. The cloud point (CP) of **P1** solution remains essentially unchanged over a large pH range. For **P2** and **P3**, the apparent slope, dCP/dpH, is negative and small around pH 2.00-3.00, but increases drastically with pH above 3.00. As for **P4** and **P5**, the apparent slope is positive and small for pH 3.00-4.00, and then rises for pH 4.00-4.75. In this pH range, the change in cloud point of **P5** looks like a vertical line, with dCP/dpH reaching 228 ^{o}C/pH.

Table 6: Cloud points (°C) of various copolymer solutions obtained on cooling as well as on heating (in parentheses).

pH	Cloud Points (°C)					
	P1	P2	P3	P4	P5	P6
2.00	—	57.5 (58.0)	50.6 (51.4)	—	—	—
2.50	—	55.8 (56.6)	49.0 (49.6)	—	—	—
3.00	43.3 (43.8)	52.5 (53.5)	46.2 (47.5)	16.5 (18.0)	—	—
3.50	—	45.3 (46.6)	26.4 (26.9)	18.3 (20.0)	—	—
4.00	—	29.0 (29.6)	—	23.6 (25.0)	—	—
4.50	—	11.5 (12.5)	—	48.0 (49.0)	15.2 (17.6)	10.0 (11.1)
4.75	—	—	—	69.0 (70.2)	71.9 (73.9)	71.1 (75.1)
7.00	41.9 (42.5)	—	—	—	—	—
10.00	41.0 (42.2)	—	—	—	—	—

— : not determined

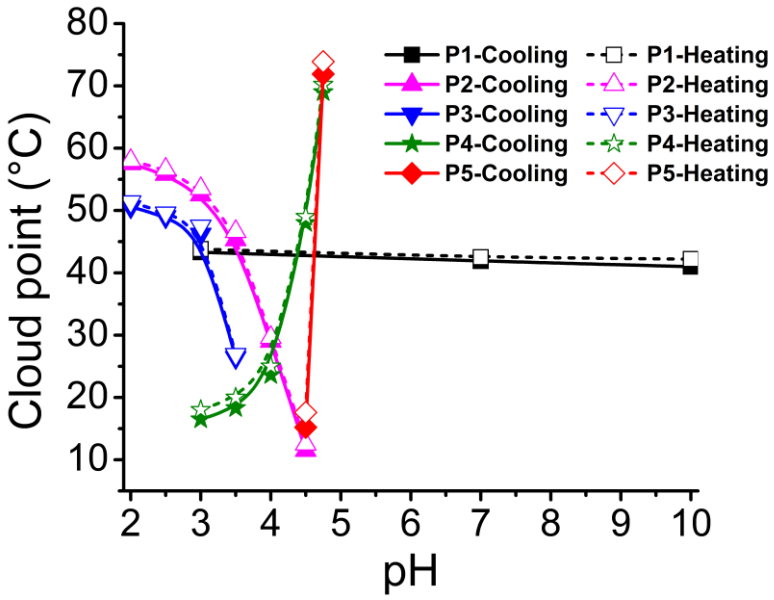

Figure 47. Change in cloud point as a function of solution pH for all random copolymers (samples 1-5). The seemingly vertical line for sample **P5** corresponds to a slope of 228 °C per unit pH.

The sample **P5** displays a stunning cloud point shift upon a small pH change, which implies that its water solubility switch could be ultrasensitive to pH. This indeed was confirmed by simple visual observation. Figure 48 shows photographs of the **P5** solution with slightly changing pH between 4.50 and 4.75 at 0.05 intervals. For all solutions, the photos were recorded after cooling the solution from 90 ^{o}C to room temperature (about 26 ^{o}C) under the same conditions except the solution pH. While the solution is still transparent at pH 4.60, it turns turbid at pH 4.65, meaning that the water solubility switching of **P5** actually occurs over a pH change as little as 0.05 unit! This observation implies that the solution at pH 4.60 still has UCST below room temperature but at pH 4.65 the UCST shifts to above room temperature. The significance of such ultrasensitive pH-induced UCST shift can be appreciated by comparing the apparent transparency change between two solutions with increasing pH difference: 4.60 with 4.65 (0.05 pH unit), 4.55 with 4.70 (0.15 pH unit) and 4.50 with 4.75 (0.25 pH unit). Clearly the difference resulting from the solubility switching is the largest between the solutions at pH 4.50 (totally transparent) and pH 4.75 (very opaque). This is because by increasing the pH difference, though still very small, the UCST gap becomes larger. In other words, at a given solution temperature (e.g. 37 ^{o}C), it is possible to switch the polymer from a thoroughly solubilized state (with UCST largely below 37 ^{o}C) to a well-dehydrated, insoluble state (with UCST much above 37 ^{o}C) using a slight pH change. This feature may be appealing for certain applications that require a straightforward solubility reversal upon a mild stimulus like a tiny pH change.

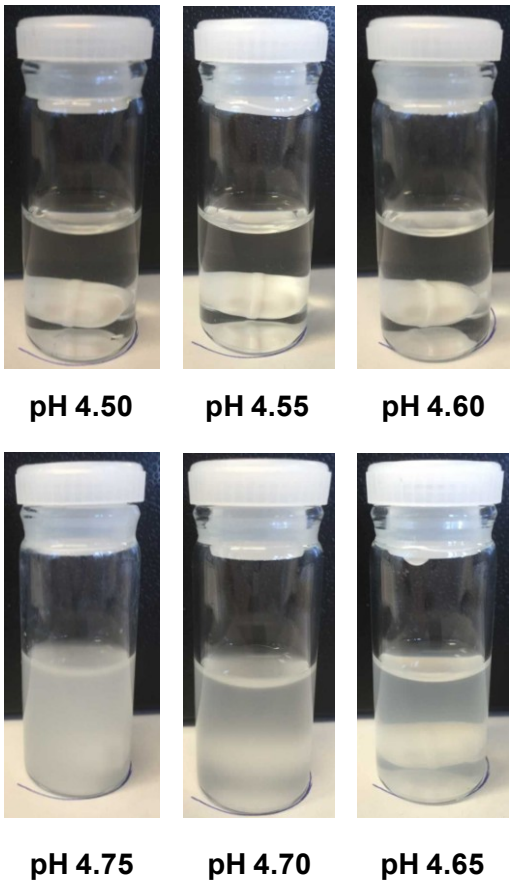

Figure 48. Photographs of the **P5** solution at room temperature with various pH from 4.50 to 4.75, showing the transition of the polymer from soluble to insoluble state over pH increase from pH 4.60 to 4.65.

Of course such large pH-induced UCST shift relies on the presence of ionizable groups in the polymer structure and, consequently, the UCST becomes sensitive to ions or ionic strength. But since the UCST swing is so large, even affected by the salt or electrolyte in solution, as long as the shift is large enough covering the solution temperature of interest (such as 37 ^{o}C), the water solubility switch is still possible. We tested this by measuring the cloud point of **P5** in three other, arbitrarily chosen, solutions differing in electrolyte or electrolyte concentration. Figure 49a shows the results of the cloud point shift of **P5** solutions upon pH change from 4.75 to 4.50: in the initial PBS (containing 137 mM NaCl,

2.7 mM KCl, 10 mM Na_2HPO_4 and 1.8 mM KH_2PO_4), in PBS with additional 350 mM NaCl added and in water with 75 mM and 150 mM $CaCl_2$ (divalent cation ions), respectively. It can be seen that as compared to PBS solution (Fig.46) the cloud point shift is reduced to some extent, indicating the effect of ions and ionic strength (Fig.49b). Nevertheless, the change remains important and in all cases the water solubility switch can still occur at 37 ^oC upon the 0.25 pH unit variation. It is interesting to note that when **P5** was dissolved in water (with only few added HCl or NaOH for adjusting pH), at pH 4.50 the polymer solution remain transparent in ice water, while at pH 4.75 it is still opaque above 90 ^oC, indicating >90 ^oC cloud point shift over the 0.25 unit change.

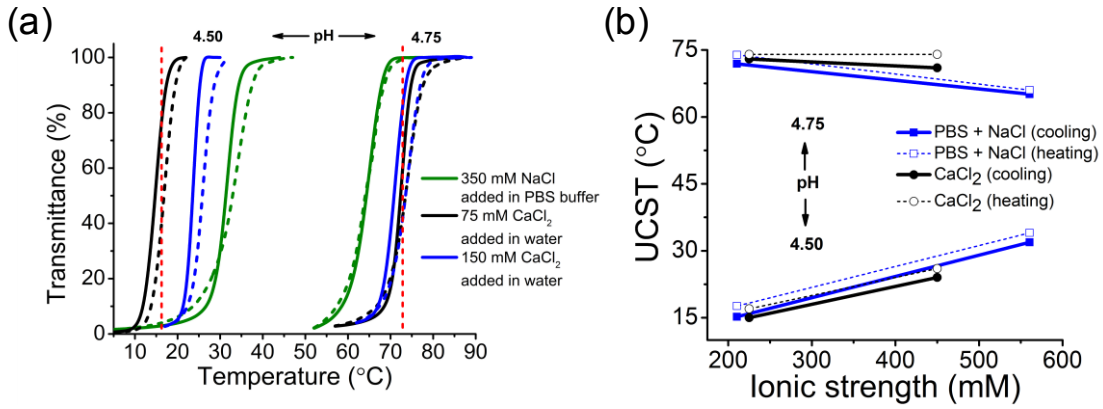

Figure 49. (a) Plots of solution transmittance vs. temperature for the **P5** solutions (polymer concentration: 5 mg/mL; heating and cooling rate: 1 ^oC/min; solid and dotted lines: cooling and heating runs respectively) and (b) Plots of the UCST change as a function of ionic strength (data was calculated from this Fig.a) at pH 4.75 and pH 4.50 in PBS with additional 350 mM NaCl added, in water with 75 mM $CaCl_2$ and in water with 150 mM $CaCl_2$. In this Fig.a, the two vertical red dotted lines indicate the cloud point positions of **P5** in PBS solution (from Figure 46b); and these transmittance curves were normalized to 100% for clarity.

3.3.2. Ultra-pH-sensitive Block Copolymer Micelle

To demonstrate a possible application, we used the sample **P5** as a macromolecular chain transfer agent to polymerize dimethylacrylamide (DMA) through RAFT, resulting in the sample **P6** (Table 5) that is a ABA-type triblock copolymer P(AAm-*co*-AN-*co*-4VP)-*b*-PDMA-*b*-P(AAm-*co*-AN-*co*-4VP). The two end blocks have the half molecular weight (or chain length) of **P5**, while the middle PDMA block is water soluble and insensitive to pH. The pH-induced cloud point shift of the **P6** solution under the same conditions was first investigated. The result in Figure 50 shows that the block copolymer behaves basically the same way as **P5**. Apparently, when the solution pH decreases from 4.75 to 4.50, the cloud point drop is even larger than **P5** (61 ^{o}C instead 57 ^{o}C). However, the transmittance change around the cloud point appears less abrupt than **P5**, which reflects the influence of the PDMA block. On cooling, when the P(AAm-*co*-AN-*co*-4VP) block undergoes the UCST type phase separation, the soluble PDMA block could reduce the propensity of chain aggregation, which may account for the less-sharp transmittance change. Actually, as the P(AAm-*co*-AN-*co*-4VP) block becomes insoluble in water, **P6** becomes an amphiphilic block copolymer and the formation of micellar aggregates would be expected. More interestingly, the huge cloud point shift means that the polymer micelle could be dissociated over a slight pH decrease.

It can be seen from Figure 50 that at 37 ^{o}C the P(AAm-*co*-AN-*co*-4VP) block in **P6** is midway between the cloud points at pH 4.75 and pH 4.50 (about 30 ^{o}C below or above), meaning that the micelle with the P(AAm-*co*-AN-*co*-4VP) core and PDMA corona may be very stable at pH 4.75 but totally dissolved at pH 4.50 because of the straightforward solubility reversal. This was confirmed by the DLS measurements carried out at 37 ^{o}C with **P6** in PBS solution. The results in Figure 51 show that stable micellar aggregates exist in the solution from pH 7.00 down to pH 4.75, with the average hydrodynamic diameter D_H around 90 nm. However, as pH is further decreased by 0.25 unit, to pH 4.50,

the micellar aggregates appear to be dissolved with the corresponding D_H dropped to around 10 nm.

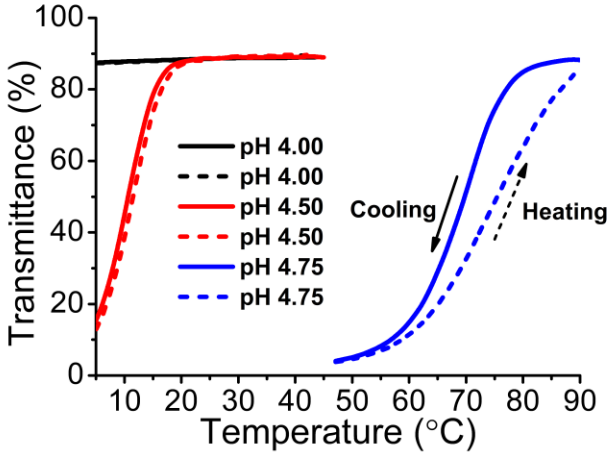

Figure 50. Plots of solution transmittance vs. temperature for the triblock copolymer P(AAm-*co*-AN-*co*-4VP)-*b*-PDMA-*b*-P(AAm-*co*-AN-*co*-4VP) in PBS solution at different pH values (polymer concentration: 5 mg/mL; heating and cooling rate: 1 ^{o}C/min).

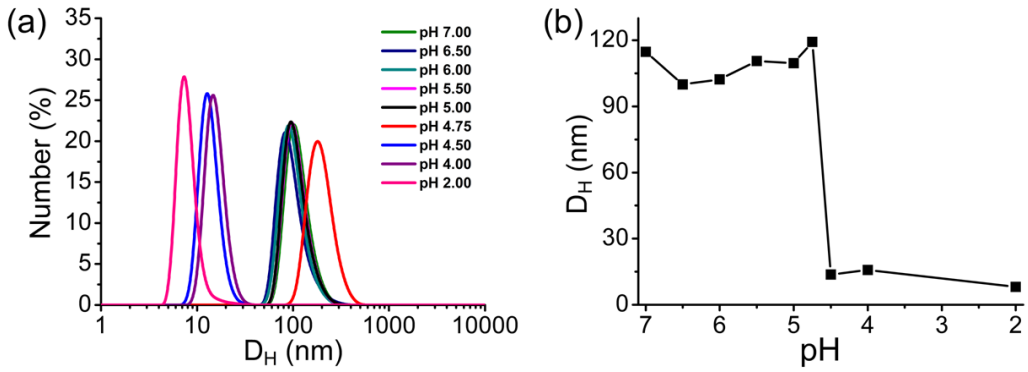

Figure 51. DLS results of the triblock copolymer P(AAm-*co*-AN-*co*-4VP)-*b*-PDMA-*b*-P(AAm-*co*-AN-*co*-4VP) in PBS solution: a) size distribution at different pH values, and b) plot of hydrodynamic diameter (D_H) vs. solution pH.

We then tested the loading of a model hydrophobic dye, Nile Red (NR), by the block copolymer micelle and its release upon pH change. For this experiment, the micelle could not be prepared by direct cooling of the aqueous solution below the UCST of the P(AAm-*co*-AN-*co*-4VP) block. Instead, **P6** and NR were dissolved in a common solvent DMSO before the solution was added into PBS solution followed by dialysis to remove DMSO (details in Experimental Section). The fluorescence emission spectra of NR in the micellar solution were recorded for the various solution pH (Fig.52a) and the emission maximum intensity was plotted vs. pH (Fig.52b). It is visible that indeed there is a drop of the fluorescence intensity with pH changing from 4.75 to 4.5, which implies an abrupt exposure of NR molecules to water in which they are not soluble and tend to aggregate (183,184). However, the fluorescence emission starts to decrease from pH 6. As seen in Figure 52c, TEM observations confirmed that the decrease in fluorescence of NR at higher pH was not caused by dissociation of the micelle, because stable micelles can still be observed by casting the NR-loaded micellar solution at pH 4.75 on a TEM grid. The dissociation of micelles occurred at pH 4.50, as the TEM image reveals large aggregates of polymer with precipitated NR. The fluorescence intensity of NR is sensitive to the polarity of the environment surrounding the dye molecules; the decrease over the pH range of 6.00-4.75 suggests an increasing dielectric constant inside the micelle even though the micellar structure remains intact. This hypothesis was further supported by additional fluorescence spectral analysis of pyrene-loaded micelles (Figure 53). It is possible that with decreasing pH from 6.00 to 4.75, while the P(AAm-*co*-AN-*co*-4VP) block remains insoluble (UCST>37 ^{o}C) and the micelle stable, an increase in dielectric constant could originate from an increasing hydration in the interior of the micelle. It is known that at T>LCST, the collapsed polymer chain forms globule that can still retain a significant amount of water (185).

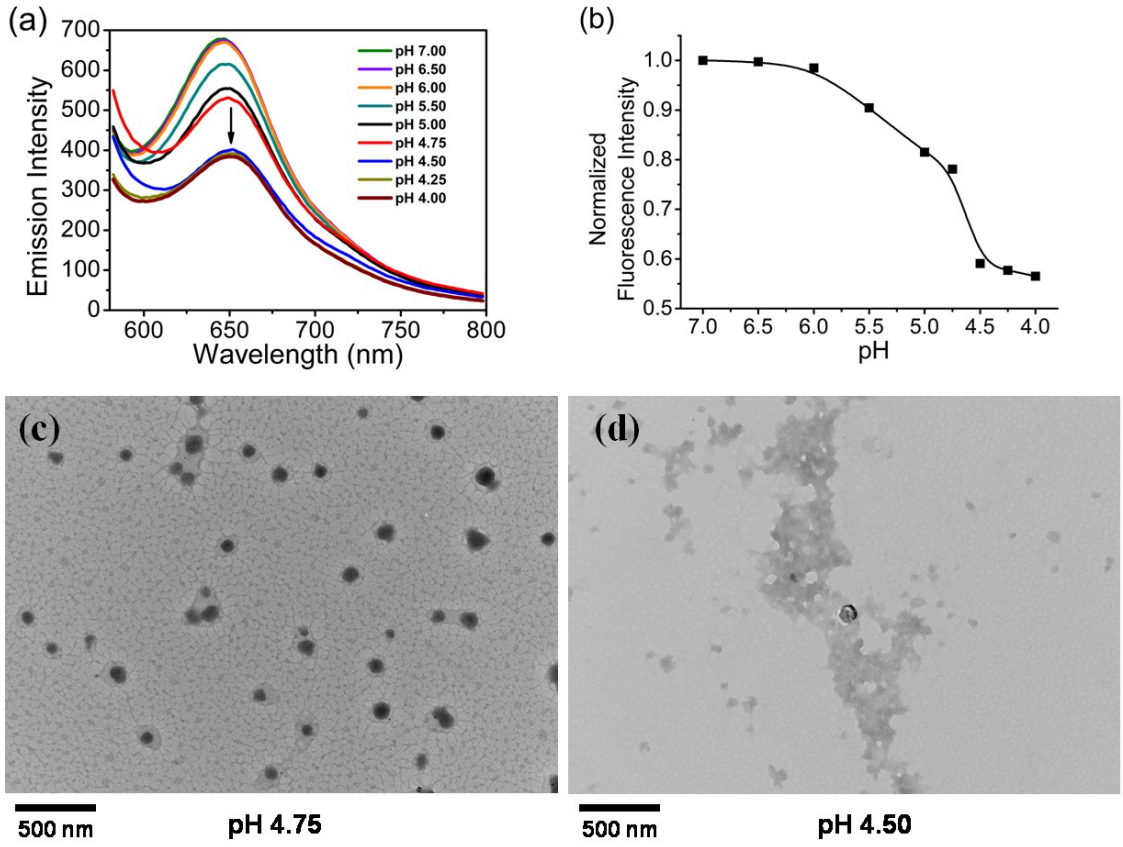

Figure 52. a) Fluorescence emission spectra of Nile Red-loaded micellar solution of P(AAm-*co*-AN-*co*-4VP)-*b*-PDMA-*b*-P(AAm-*co*-AN-*co*-4VP) recorded at various pH (λ_{ex}=540 nm); b) plot of normalized fluorescence intensity vs. solution pH; c) and d) TEM images obtained by casting the solution at pH 4.75 and 4.50 respectively.

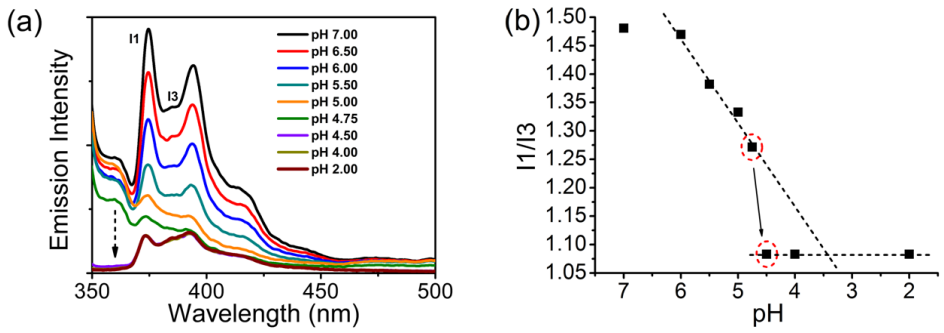

Figure 53. a) Fluorescence emission spectra of pyrene-loaded micellar solution of P(AAm-*co*-AN-*co*-4VP)-*b*-PDMA-*b*-P(AAm-*co*-AN-*co*-4VP) recorded at various pH ; b) variation of **I1**/**I3** in pyrene emission spectra as a function of solution pH.

Pyrene has negligible solubility in water, and thus very weak emission in the absence of **P6** (data not shown). When pyrene was encapsulated inside the micelle, it shows intense emission bands. Figure 53 shows the emission spectral change of the micellar solution from pH 7.00 to 2.00. The overall emission intensity reduces continuously upon pH decrease (Fig.53a). However, the most notable change occurs when pH changes from 4.75 to 4.50, especially for the apparent emission below 370 nm. The ratio of the emission intensities of the first (**I1**) and the third (**I3**) vibronic bands is plotted vs. pH (Fig.53b). It decreases gradually with decreasing pH before an abrupt drop upon pH change from 4.75 to 4.50, which implies change in dielectric constant of the environment surrounding pyrene molecules from hydrophobic to hydrophilic.

Such ultra-pH-sensitive block copolymer micelles may offer new possibilities for applications that can hardly be envisaged. For instance, in the case of pH-triggered cargo release, if one wants the loaded substance to be released in cell but only inside a compartment with the lowest pH, the micelle can be made to resist the cellular environment with highly varying pH or pH gradient, until it reaches the target compartment where it is dissolved over even a slight decrease in pH. In the present study,

using the block copolymer **P6**, this slight pH change that determines the micellar association-dissociation transition is from pH 4.75 to pH 4.50. Needless to say that depending on the actual application, with an appropriate choice of the weak acid or base comonomer, one can adjust the pH at which an ultrasensitive water solubility switch of the polymer occurs, which is the basis of possible applications.

3.4. Conclusions

We have used RAFT to synthesize P(AAm-*co*-AN-*co*-AAc) and P(AAm-*co*-AN-*co*-4VP) random copolymers with the purpose of exploiting the pH-induced shift of the UCST known for the uncharged P(AAm-*co*-AN) in order to achieve pH-controlled solubility switch in aqueous solution at room or body temperature (37 ^{o}C). By monitoring the change in the cloud point of the polymers in PBS solution, we found large shift upon small pH variation within the accessible temperature range of 5-90 ^{o}C, especially with 4VP as the pH-responsive trigger. For the sample **P5**, it showed a cloud point drop of 57 ^{o}C, from 72 ^{o}C to 15 ^{o}C, upon 0.25 pH unit decrease from 4.75 to 4.50; and its transition from soluble to insoluble state, or vice versa, could be visually observed upon pH change as little as 0.05 unit. This ultra-pH-sensitive UCST and the concomitant huge swing is likely to originate from a small solution enthalpy change associated with the phase separation in UCST polymers (18,148) and, therefore, might be common in other polymers of this kind. This is an attractive feature because it means that the water solubility of the polymer over a wide temperature range can be switched (or reversed) by a slight pH change in the solution. To demonstrate the possible applications, we then used **P5** as macromolecular chain transfer agent to polymerize dimethylacrylamide; the obtained triblock copolymer of P(AAm-*co*-AN-*co*-4VP)-*b*-PDMA-*b*-P(AAm-*co*-AN-*co*-4VP) retained the properties of **P5**. Consequently, the self-assembled micelle of the triblock copolymer in PBS solution at 37 ^{o}C could be stable upon pH decrease from 7.00 to until 4.75, because the UCST of

the P(AAm-*co*-AN-*co*-4VP) core remains largely above 37 ^{o}C. However, further pH decrease by 0.25 unit, to pH 4.50, could result in abrupt disassembly of the micelle because the UCST is dropped well below 37 ^{o}C. Our study revealed the potential of taking advantage of UCST polymers to develop polymers or their assemblies that are able to undergo abrupt solubility switch in aqueous solution in response to a small pH change, which may find new applications.

3.5. Statement of Contribution

This work was publicated on *Macromolecules*, 2016, 49 (4), pp 1424–1433 by Hu Zhang, Shengwei Guo, Weizheng Fan and Yue Zhao. This research work was conducted in the Université de Sherbrooke under the supervision of Prof. Zhao. Shengwei Guo proposed some useful suggestions and did part of the experiment of cloud point measurement with me. Weizheng Fan conducted the GPC measurement. I performed all the rest of experiments and characterizations reported in this manuscript.

CONCLUSIONS AND PERSPECTIVES

Our research conducted in this thesis made two important contributions to the field of thermosensitive polymers whose solubility in aqueous solution displays a critical phase transition temperature (LCST or UCST). Our first contribution is the demonstration of novel approaches for switching or reversing the polymer solubility at a constant solution temperature by means a pH variation in a very sensitive manner. Although the principle of such a solubility switch based on shifting the LCST (or UCST) through incorporation of pH-ionizable comonomer units (acid or base) in the polymer structure is known, the important fundamental question of how to amplify the solubility switch has not been addressed previously. When a polymer soluble in water turns insoluble, the polymer chain undergoes a transition from coiled (well hydrated) conformation to a collapsed (dehydrated) globule form before further agglomeration. However, the globule can still confine a significant amount of water and the actual dehydration degree is influenced by how far the solution temperature is distant from the LCST or UCST. For example, at room temperature (25 ^{o}C), a pH-induced shift of LCST (or UCST) between 15 ^{o}C and 35 ^{o}C or between -10 ^{o}C and 60 ^{o}C should both induce the solubility switch, but in the latter case the solubility reversal should be more straightforward between hydrated and dehydrated state, and the solubility switch (or phase separation) kinetics should be faster. This difference can have important implications in some applications.

To address this question, for LCST polymers (Chapter 1), we proposed the use of a comonomer bearing two acid groups, instead of one as is known, and experimentally confirmed the efficacy of the strategy for inducing large LCST shifts. The rationale in designing the comonomer is to have two acid groups of similar pKa with one linked to a rather hydrophobic moiety like phenyl. In this way, upon pH change around the pKa, the comonomer can switch between enhanced hydrophobic state with two protonated acids (at pH < pKa) and hydrophilic state with the two deprotonated acids (pH>pKa). With the

same number of comonomer units and pH variation, an increased hydrophobicity-hydrophilicity switch results in an increased LCST shift. This approach obviously is general and can be applied to or tested in many polymer designs in future studies. The comonomer design principle can also be extended to other systems. For instance, one can envisage the use of two bases of similar pKa to reverse the solubility switch upon pH increase (or decrease) as a result of reversed LCST shift. There is another interesting possibility worth exploitation. For most, if not all, pH-responsive polymers, the pH-induced property changes are observed mostly at pH around pKa, because the large part of protonation or deprotonation variation for either acid or base groups takes place in the close vicinity of pKa. In other words, generally only one pH-induced transition is possible. With our comonomer design principle, it is possible to have a comonomer bearing two acid or base groups of significantly different pKa. In such case, it is conceivable to produce two separate pH regions in which an abrupt change in the number of charged comonomer groups could be obtained. Consequently, large LCST shift may be observed in two different pH regions (or in a combined wide pH region).

While using pH-ionizable comonomers with UCST polymers (Chapter 3), the finding is quite stunning. Small pH change can induce a huge UCST shift. The extent of UCST change appears unprecedented, to the best of our knowledge. The likely explanation is the enthalpy of solution that can be very small for UCST polymers according to a report in the literature. Since the equilibrium phase transition temperature of the polymer solution is determined by the ratio of enthalpy of solution (or mixing) over entropy of solution ($\Delta H_m/\Delta S_m$), a small value of enthalpy of solution means that even a few more or less charged groups in the polymer, which affects the intermolecular interactions (polymer-polymer and polymer-water), could give rise to a relatively large variation of the enthalpy of solution and, thus, a large change in UCST. The finding is important because a small enthalpy of solution may be a general feature for UCST polymers, meaning that pH-induced large UCST shift could be obtained for many polymers giving

rise to ultra-pH-sensitivity. Moreover, the comonomer design developed for LCST polymers can be applied to UCST polymers to further enhance the ultrasensitive pH-controlled UCST. These possibilities need to be verified in future studies.

Our second contribution is the study described in Chapter 2. For the first time, using the controlled radical polymerization method of RAFT, we synthesized three diblock copolymers comprising the same H-bonding-based UCST block of P(AAm-*co*-AN), but differing in the other block (either hydrophobic or hydrophilic or a LCST polymer). We reported various UCST-dictated thermoresponsive behaviors of their self-assembled structures, which are straightforward, robust and can be observed in aqueous solutions containing ions, in contrast to the more-studied zwitterionic type of UCST polymers. This progress is a significant step forward for UCST polymers in itself. However, the most important is the point made by this study: much the same way as using a LCST polymer like PNIPAM, the UCST P(AAm-*co*-AN) can be introduced into controlled polymer architectures as exemplified by, but not limited to, block copolymers. In other words, our work demonstrated the great potential of exploring H-bonding-based, easily accessible UCST polymers of various structures or architectures (for example, dendrimers, brushes and hyperbranched polymers). Considering the extensive research and development on LCST polymers, which is still going strong, the so-called positive thermosensitivity of the UCST polymers may find advantages over the negative thermosensitivity of their LCST counterparts in certain applications. A growing interest in understanding UCST polymers and exploiting their applications can be expected in the years to come.

As we stated, until now, most studies were dedicated to LCST polymers. In contrast, UCST polymers were less investigated, especially on their applications. One example is using for bioseparation (96). Ureido-derivatized polymers, such as poly(allylurea) (PU) and poly(L-citrulline) derivatives, can display UCST behavior under physiological buffer conditions. They were examined to capture and separate particular proteins from a protein

mixture by cooling-induced phase separation as shown in Figure 54. The results demonstrated a selective and rapid capture of particular proteins from the protein mixtures, indicating a potential application of UCST polymers under biofriendly conditions.

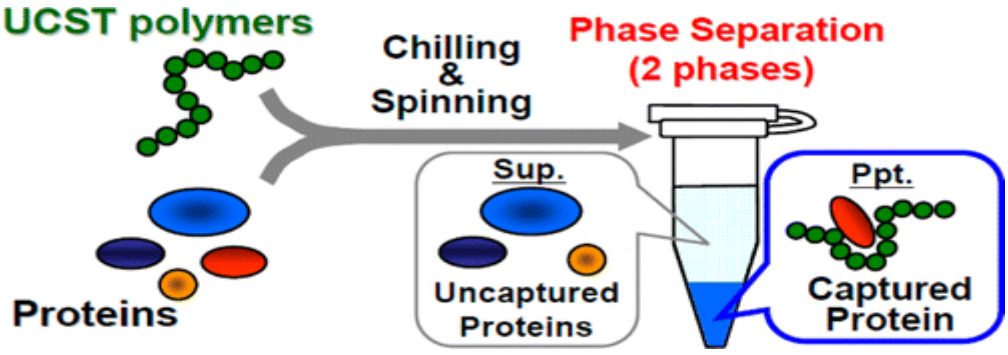

Figure 54. The scheme showing the rapid and selective separation of specific protein from the mixture by employing UCST polymer.

Although there were some examples of application of UCST polymers in literature, however, compared to LCST polymers, more efforts have to be done in this area. Here in perspective part of this thesis, we would like to briefly discuss few examples of the usage which has not been revealed. Some of these studies are on the way.

1. Near-Infrared Light-Triggered Gel to Sol Transition Based on Photothermal Effect

For the application of photoresponsive hydrogels in the biomedical field, the excitation wavelength has long been known as a challenging issue. Near-infrared (NIR) light (wavelengths roughly 700-1000 nm) is preferred because of its deeper tissue penetration and less detrimental effect on healthy cells as compared to ultraviolet (UV) light. Making NIR-responsive hydrogels, however, is not trivial, largely due to the lack of appropriate photochemical reactions (e.g. photocleavage) induced by one-photon absorption of NIR

light.(133, 186) In recent years some solutions to this problem have been proposed. For example, our group previously reported the loading of upconverting nanoparticles (UCNPs) in a UV-degradable hydrogel.(187) Upon NIR (980 nm) excitation, UCNPs emit UV light from the interior of the hydrogel that, in turn, is absorbed by the polymer, which activates a photocleavage reaction to cut the crosslinker segments and thus leads to the gel-sol transition. On the other hand, Kumacheva et al. showed that by loading gold nanorods (AuNRs) in a thermosensitive hydrogel having a lower critical solution temperature (LCST), NIR light could induce volume shrinkage of the hydrogel.(188-189) In this case, when the hydrogel, with the polymer at T<LCST, is exposed to NIR at a wavelength near the longitudinal surface plasmon resonance (SPR) of AuNRs, the light absorption generates heat released inside the hydrogel that can raise the temperature above LCST and thus results in the hydrogel volume shrinkage as the polymer becomes insoluble in water. These two examples present two general strategies and are representative of photochemical reaction- or photothermal effect-based NIR-responsive hydrogels.

However, to our knowledge, there is no report thus far on NIR light-sensitive hydrogels that can undergo the gel-sol transition under photothermal effect. Herein, we propose a proof-of-concept study to make the first case of this kind of hydrogel.

Figure 55 shows the hydrogel design. AuNRs are loaded in a hydrogel whose crosslinks are micelle cores constituted by a thermosensitive polymer displaying an upper critical solution temperature (UCST). The network structure is stable at T<UCST with the hydrophobic micelle cores, while upon NIR light exposure, heat released from AuNRs can raise the temperature above UCST and thus dissolve the micelle cores as the polymer becomes water-soluble. This gives rise to NIR induced gel-sol transition. Here, the positive thermosensitivity of UCST, opposite to LCST, is the key because LCST polymers cannot lead to the gel-sol transition in this manner. To test the design, we

synthesized an ABA-type triblock copolymer of P(AAm-*co*-AN)-*b*-PDMA-*b*-P(AAm-*co*-AN). As seen from its structure, the middle block is water soluble polydimethylacrylamide (PDMA) and the two end blocks are a random copolymer of acrylamide and acrylonitrile (P(AAm-*co*-AN)) whose UCST can easily be adjusted by varying the composition (93).

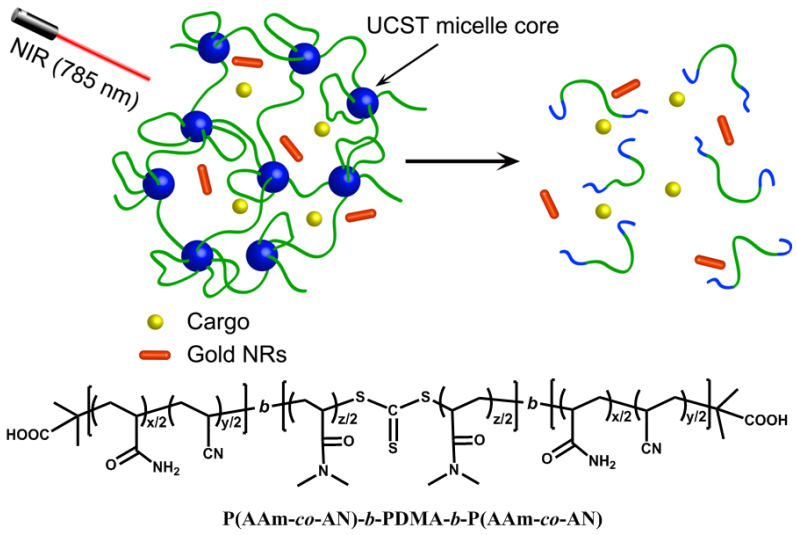

Figure 55. Upper: schematic Illustration of NIR-light-triggered UCST gel to sol process due to heating by encapsulated AuNRs. Lower: chemical structure of the UCST polymer forming the hydrogel.

Biomacromolecules can easily be loaded in the hybrid hydrogel. Fluorescein isothiocyanate conjugated bovine serum albumin (FITC-BSA) was dissolved in the triblock copolymer/AuNR solution at high temperature; the solution placed in a quartz cuvette was cooled to room temperature to form a piece of hydrogel at the bottom. As depicted in Figure 56a, after adding a certain amount of water into the cuvette, fluorescence emission spectrum of FITC-BSA could be recorded to monitor the release of the enzyme from the hydrogel exposed to the 785 nm laser from a side. Figure 56b plots the maximum fluorescence emission as a function of time, with the NIR irradiation times marked. The amount of protein remained basically unchanged until 5 min NIR irradiation

was applied (no spectral taking during the irradiation). Then, following each NIR irradiation, a jump of the amount of released protein was detected, while no significant release continued after the NIR exposure. The results indicate an NIR light induced release of FITC-BSA in an on-off fashion. In other words, during NIR irradiation, the gel-sol transition occurs and the reduced viscosity allows more protein to diffuse into the solution. However, once NIR is turned off, the fast cooling results in the reverse sol-gel transition that prevents further release of the protein from the hydrogel. A control test was carried out to confirm that the observed NIR-induced on-off release of the protein was originated from the AuNR-enabled photothermal effect. FITC-BSA was loaded in the hydrogel without AuNRs under otherwise the same conditions, and the loaded hydrogel was subjected to the same NIR irradiation sequence and times. As seen from the result also in Figure 56b, the repeated NIR irradiations resulted in no release. The release occurred only when the hydrogel was heated to 50 ^{o}C, above UCST of the P(AAm-co-AN) micelle core for the gel-sol transition.

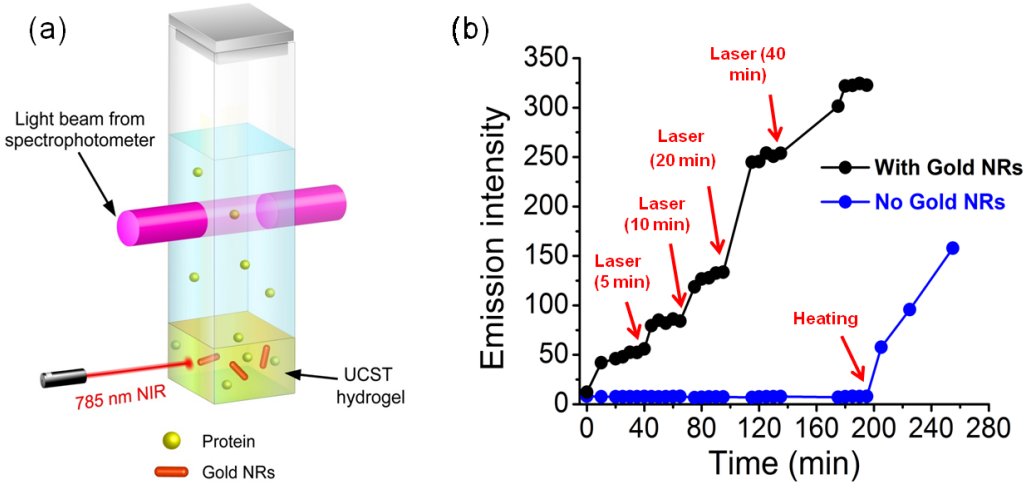

Figure 56. (a): Setup used to detect protein diffusing from the hydrogel into the aqueous solution after 785 nm laser irradiation. (b) Plots of the fluorescence emission intensity vs NIR irradiation time, showing a temporal control of the protein release by turning the NIR laser on and off.

This light-triggered Gel to Sol transition based on photothermal effect design is a unique feature of UCST polymer based on its positive thermosensitivity, which can't be achieved by LCST polymer having the opposite transition.

2. Ultra-light-sensitive UCST polymer

As pointed out earlier in the Introduction section, quite a number of external stimuli have been explored to design stimuli-responsive polymers, like, temperature, pH, light, ultrasound, carbon dioxide, and so on. A growing trend is to create the systems with multiple-responsive components, making it responsive to different stimuli. Among these multiple responsive polymers, thermo- and pH dual responsive polymers are the most studied systems. In the Chapter 1 and Chapter 3, we already studied the effect of pH on the thermoresponsive polymers (LCST/UCST). Especially in Chapter 3, pH has a large influence on the polymer's UCST. One sample exhibited a cloud point shifted over 50°C upon 0.25 pH units change, and its transition from soluble to insoluble state at room temperature can be visually observable over a pH change as little as 0.05 unit. This propriety of shape change in the polymers's solubility may be potentially used in drug delivery.

Actually, every external stimulus has its own distinct features as compared to other stimuli. Here, we take the stimulus, light, as an example. The most important advantages of using light in stimuli responsive polymers are that 1) remote activation is easily doable since laser light can travel a long distance; 2) spatially controlled activation is possible as the size-tunable light beam can be delivered to selected areas; 3) light-triggered processes can be halted and resumed "on-demand" by switching on/off the excitation light and 4) easy manipulation is expected thanks to the portable light-source devices.

Aiming to introduce these advantages of light into UCST polymers, the light responsive UCST polymers can be synthesized which the structure is shown in Figure 57. This block

copolymer, denoted as PEO-*b*-P(AAm-*co*-AN-*co*-ONB), contains a permanent hydrophilic block, poly(ethylene oxide)(PEO), and a UCST block (Poly(acrylamide-*co*-acrylonitrile)) with a little amount of light reposnive moieties (*o*-nitrobenzyl unit) . This UCST block of the polymer will forms the micelle core at T< UCST; light irradiation of the micellar solution could induce the cleavage of ONB groups. As a result, the UCST of the thermosensitive polymer decreases due to the conversion of hydrophobic ONB comonomer units onto hydrophilic methacrylic acid. Consequently, the block copolymer micelles can disassemble under light irradiation. The main difference between reported light responsive polymers and this proposed system is that only a very little amount of light responsive moieties is needed to switch the polymer from the insoluble state to soluble state at certain temperature (due to large UCST shift). The small portion of light responsive moieties means short responding time. This ultra-light-sensitive UCST will also base on small enthalpy change associated with the phase separation in the UCST polymers as explain in Chapter 2. The synthesized ultra-light-sensitive UCST polymers may be expected for using in drug delivery area, too (Fig.57).

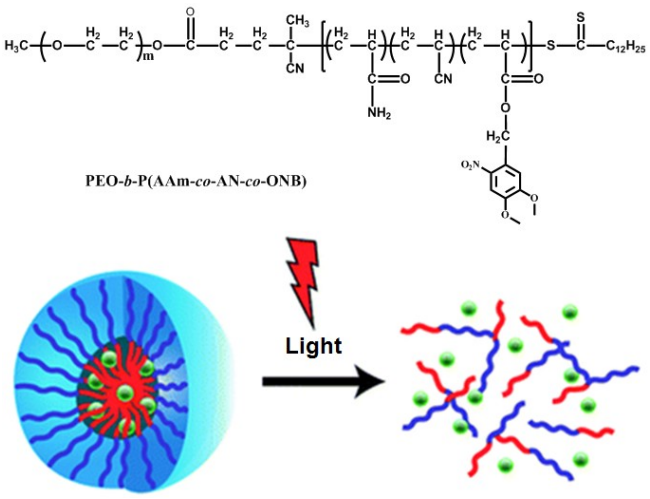

Figure 57. upper: the structure of light responsive UCST polymers; down: light triggered release of drugs from light responsive UCST polymers formed micelle.

BIBLIOGRAPHY

(1) Stuart, M. A. C.; Huck, W. T. S.; Genzer, J.; Müller, M.; Ober, C.; Stamm, M.; Sukhorukov, G. B.; Szleifer, I.; Tsukruk, V. V.; Urban, M.; Winnik, F.; Zauscher, S.; Luzinov, I.; Minko, S. Nat. Mater. 2010, 9 (2), 101–113.

(2) Mura, S.; Nicolas, J.; Couvreur, P. Nat. Mater. 2013, 12 (11), 991–1003.

(3) Jeong, B.; Gutowska, A. Trends Biotechnol. 2002, 20 (7), 305–311.

(4) Liu, F.; Urban, M. W. Prog. Polym. Sci. 2010, 35 (1–2), 3–23.

(5) Schmaljohann, D. Adv. Drug Deliv. Rev. 2006, 58 (15), 1655–1670.

(6) Alarcón, C. de las H.; Pennadam, S.; Alexander, C. Chem. Soc. Rev. 2005, 34 (3), 276–285.

(7) Mano, J. F. Adv. Eng. Mater. 2008, 10 (6), 515–527.

(8) Jochum, F. D.; Theato, P. Chem. Soc. Rev. 2013, 42 (17), 7468–7483.

(9) Meng, F.; Zhong, Z.; Feijen, J. Biomacromolecules 2009, 10 (2), 197–209.

(10) Hu, J.; Liu, S. Macromolecules 2010, 43 (20), 8315–8330.

(11) Roy, D.; Brooks, W. L. A.; Sumerlin, B. S. Chem. Soc. Rev. 2013, 42 (17), 7214–7243.

(12) Gandhi, A.; Paul, A.; Sen, S. O.; Sen, K. K. Asian J. Pharm. Sci. 2015, 10 (2), 99–107.

(13) Crespy, D.; Rossi, R. M. Polym. Int. 2007, 56 (12), 1461–1468.

(14) Pelton, R. Adv. Colloid Interface Sci. 2000, 85 (1), 1–33.

(15) Ward, M. A.; Georgiou, T. K. Polymers 2011, 3 (3), 1215–1242.

(16) Wei, H.; Cheng, S.-X.; Zhang, X.-Z.; Zhuo, R.-X. Prog. Polym. Sci. 2009, 34 (9), 893–910.

(17) Gibson, M. I.; O'Reilly, R. K. Chem. Soc. Rev. 2013, 42 (17), 7204–7213.

(18) Seuring, J.; Agarwal, S. Macromol. Rapid Commun. 2012, 33 (22), 1898–1920.

(19) Ebeling, B. Smart Nanohybrids of RAFT Polymers and Inorganic Particles; Springer, 2015.

(20) Wu, C.; Wang, X. Phys. Rev. Lett. 1998, 80 (18), 4092–4094.

(21) Van Durme, K.; Van Assche, G.; Van Mele, B. Macromolecules 2004, 37 (25), 9596–9605.

(22) Afroze, F.; Nies, E.; Berghmans, H. J. Mol. Struct. 2000, 554 (1), 55–68.

(23) Vshivkov, S. A.; Safronov, A. P. Macromol. Chem. Phys. 1997, 198 (10), 3015–3023.

(24) Lu, Y.; Zhou, K.; Ding, Y.; Zhang, G.; Wu, C. Phys. Chem. Chem. Phys. 2010, 12 (13), 3188–3194.

(25) Zhou, K.; Lu, Y.; Li, J.; Shen, L.; Zhang, G.; Xie, Z.; Wu, C. Macromolecules 2008, 41 (22), 8927–8931.

(26) Aseyev, V.; Tenhu, H.; Winnik, F. M. In Self Organized Nanostructures of Amphiphilic Block Copolymers II; Advances in Polymer Science; Springer Berlin Heidelberg, 2010; pp 29–89.

(27) Liu, R.; Fraylich, M.; Saunders, B. R. Colloid Polym. Sci. 2009, 287 (6), 627–643.

(28) Aoshima, S.; Kanaoka, S. In Wax Crystal Control · Nanocomposites · Stimuli-Responsive Polymers; Advances in Polymer Science;

Springer Berlin Heidelberg, 2007; pp 169–208.

(29) Aseyev, V. O.; Tenhu, H.; Winnik, F. M. In Conformation-Dependent Design of Sequences in Copolymers II; Advances in Polymer Science; Springer Berlin Heidelberg, 2006; pp 1–85.

(30) Dimitrov, I.; Trzebicka, B.; Müller, A. H. E.; Dworak, A.; Tsvetanov, C. B. Prog. Polym. Sci. 2007, 32 (11), 1275–1343.

(31) Wang, X.; Qiu, X.; Wu, C. Macromolecules 1998, 31 (9), 2972–2976.

(32) Maeda, Y.; Nakamura, T.; Ikeda, I. Macromolecules 2001, 34 (5), 1391–1399.

(33) Inomata, H.; Goto, S.; Saito, S. Macromolecules 1990, 23 (22), 4887–4888.

(34) Ito, D.; Kubota, K. Macromolecules 1997, 30 (25), 7828–7834.

(35) Ito, D.; Kubota, K. Polym. J. 1999, 31 (3), 254–257.

(36) Idziak, I.; Avoce, D.; Lessard, D.; Gravel, D.; Zhu, X. X. Macromolecules 1999, 32 (4), 1260–1263.

(37) Schild, H. G. Prog. Polym. Sci. 1992, 17 (2), 163–249.

(38) Hashimoto, C.; Nagamoto, A.; Maruyama, T.; Kariyama, N.; Irisa, Y.; Ikehata, A.; Ozaki, Y. Macromolecules 2013, 46 (3), 1041–1053.

(39) Panayiotou, M.; Freitag, R. Polymer 2005, 46 (3), 615–621.

(40) Gil, E. S.; Hudson, S. M. Prog. Polym. Sci. 2004, 29 (12), 1173–1222.

(41) Ishizone, T.; Seki, A.; Hagiwara, M.; Han, S.; Yokoyama, H.; Oyane, A.; Deffieux, A.; Carlotti, S. Macromolecules 2008, 41 (8), 2963–2967.

(42) Lutz, J.-F.; Akdemir, Ö.; Hoth, A. J. Am. Chem. Soc. 2006, 128 (40), 13046–13047.

(43) Lutz, J.-F. J. Polym. Sci. Part Polym. Chem. 2008, 46 (11), 3459–3470.

(44) Lutz, J.-F.; Hoth, A. Macromolecules 2006, 39 (2), 893–896.

(45) Lutz, J.-F.; Weichenhan, K.; Akdemir, Ö.; Hoth, A. Macromolecules 2007, 40 (7), 2503–2508.

(46) Lutz, J.-F. Adv. Mater. 2011, 23 (19), 2237–2243.

(47) Butun, V.; Armes, S. P.; Billingham, N. C. Polymer 2001, 42 (14), 5993–6008.

(48) Cho, S. H.; Jhon, M. S.; Yuk, S. H.; Lee, H. B. J. Polym. Sci. Part B Polym. Phys. 1997, 35 (4), 595–598.

(49) Fournier, D.; Hoogenboom, R.; Thijs, H. M. L.; Paulus, R. M.; Schubert, U. S. Macromolecules 2007, 40 (4), 915–920.

(50) Samal, S. K.; Dash, M.; Vlierberghe, S. V.; Kaplan, D. L.; Chiellini, E.; Blitterswijk, C. van; Moroni, L.; Dubruel, P. Chem. Soc. Rev. 2012, 41 (21), 7147–7194.

(51) Plamper, F. A.; Ruppel, M.; Schmalz, A.; Borisov, O.; Ballauff, M.; Müller, A. H. E. Macromolecules 2007, 40 (23), 8361–8366.

(52) Lee, A. S.; Bütün, V.; Vamvakaki, M.; Armes, S. P.; Pople, J. A.; Gast, A. P. Macromolecules 2002, 35 (22), 8540–8551.

(53) Weaver, J. V. M.; Armes, S. P.; Bütün, V. Chem. Commun. 2002, No. 18, 2122–2123.

(54) CRC Handbook of Chemistry and Physics, 96th Edition, 96 edition.; Haynes, W. M., Ed.; CRC Press, 2015.

(55) Costa, R. O. R.; Freitas, R. F. S. Polymer 2002, 43 (22), 5879–5885.

(56) Zhang, Q.; Hoogenboom, R. Prog. Polym. Sci. 2015, 48, 122–142.

(57) Konak, C.; Rathi, R. C.; Kopeckova, P.; Kopecek, J. Macromolecules 1994, 27

(8), 1992–1996.

(58) Lowe, A. B.; McCormick, C. L. Chem. Rev. 2002, 102 (11), 4177–4190.

(59) Mary, P.; Bendejacq, D. D.; Labeau, M.-P.; Dupuis, P. J. Phys. Chem. B 2007, 111 (27), 7767–7777.

(60) Schulz, D. N.; Peiffer, D. G.; Agarwal, P. K.; Larabee, J.; Kaladas, J. J.; Soni, L.; Handwerker, B.; Garner, R. T. Polymer 1986, 27 (11), 1734–1742.

(61) Huglin, M. B.; Radwan, M. A. Polym. Int. 1991, 26 (2), 97–104.

(62) Willcock, H.; Lu, A.; Hansell, C. F.; Chapman, E.; Collins, I. R.; O'Reilly, R. K. Polym. Chem. 2013, 5 (3), 1023–1030.

(63) Woodfield, P. A.; Zhu, Y.; Pei, Y.; Roth, P. J. Macromolecules 2014, 47 (2), 750–762.

(64) Tian, H.-Y.; Yan, J.-J.; Wang, D.; Gu, C.; You, Y.-Z.; Chen, X.-S. Macromol. Rapid Commun. 2011, 32 (8), 660–664.

(65) Shih, Y.-J.; Chang, Y. Langmuir 2010, 26 (22), 17286–17294.

(66) Maji, T.; Banerjee, S.; Biswas, Y.; Mandal, T. K. Macromolecules 2015, 48 (14), 4957–4966.

(67) Chang, Y.; Chen, W.-Y.; Yandi, W.; Shih, Y.-J.; Chu, W.-L.; Liu, Y.-L.; Chu, C.-W.; Ruaan, R.-C.; Higuchi, A. Biomacromolecules 2009, 10 (8), 2092–2100.

(68) Arotçaréna, M.; Heise, B.; Ishaya, S.; Laschewsky, A. J. Am. Chem. Soc. 2002, 124 (14), 3787–3793.

(69) Virtanen, J.; Arotçaréna, M.; Heise, B.; Ishaya, S.; Laschewsky, A.; Tenhu, H. Langmuir 2002, 18 (14), 5360–5365.

(70) Maeda, Y.; Mochiduki, H.; Ikeda, I. Macromol. Rapid Commun. 2004, 25 (14),

1330–1334.

(71) Chang, Y.; Yandi, W.; Chen, W.-Y.; Shih, Y.-J.; Yang, C.-C.; Chang, Y.; Ling, Q.-D.; Higuchi, A. Biomacromolecules 2010, 11 (4), 1101–1110.

(72) Yin, J.; Hu, J.; Zhang, G.; Liu, S. Langmuir 2014, 30 (9), 2551–2558.

(73) Ning, J.; Li, G.; Haraguchi, K. Macromolecules 2013, 46 (13), 5317–5328.

(74) Ning, J.; Li, G.; Haraguchi, K. Macromol. Chem. Phys. 2014, 215 (3), 235–244.

(75) Tian, M.; Wang, J.; Zhang, E.; Li, J.; Duan, C.; Yao, F. Langmuir 2013, 29 (25), 8076–8085.

(76) Azzaroni, O.; Brown, A. A.; Huck, W. T. S. Angew. Chem. Int. Ed. 2006, 45 (11), 1770–1774.

(77) Zhou, F.; Huck, W. T. S. Phys. Chem. Chem. Phys. 2006, 8 (33), 3815–3823.

(78) Pei, Y.; Travas-Sejdic, J.; Williams, D. E. Langmuir 2012, 28 (21), 8072–8083.

(79) Housni, A.; Zhao, Y. Langmuir 2010, 26 (15), 12933–12939.

(80) Buscall, R.; Corner, T. Eur. Polym. J. 1982, 18 (11), 967–974.

(81) Bokias, G.; Staikos, G.; Iliopoulos, I. Polymer 2000, 41 (20), 7399–7405.

(82) Fang, J.; Bian, F.; Shen, W. J. Appl. Polym. Sci. 2008, 110 (6), 3373–3378.

(83) Haas, H. C.; Schuler, N. W. J. Polym. Sci. [B] 1964, 2 (12), 1095–1096.

(84) Haas, H. C.; Moreau, R. D.; Schuler, N. W. J. Polym. Sci. Part -2 Polym. Phys. 1967, 5 (5), 915–927.

(85) Marstokk, O.; Nyström, B.; Roots, J. Macromolecules 1998, 31 (13), 4205–4212.

(86) Ostrovskii, D.; Jacobsson, P.; Nyström, B.; Marstokk, O.; Kopperud, H. B. M.

Macromolecules 1999, 32 (17), 5552–5560.

(87) Haas, H. C.; Chiklis, C. K.; Moreau, R. D. J. Polym. Sci. [A1] 1970, 8 (5), 1131–1145.

(88) Haas, H. C.; Manning, M. J.; Mach, M. H. J. Polym. Sci. [A1] 1970, 8 (7), 1725–1730.

(89) Glatzel, S.; Badi, N.; Päch, M.; Laschewsky, A.; Lutz, J.-F. Chem. Commun. 2010, 46 (25), 4517–4519.

(90) Seuring, J.; Agarwal, S. Macromol. Chem. Phys. 2010, 211 (19), 2109–2117.

(91) Seuring, J.; Bayer, F. M.; Huber, K.; Agarwal, S. Macromolecules 2012, 45 (1), 374–384.

(92) Liu, F.; Seuring, J.; Agarwal, S. J. Polym. Sci. Part Polym. Chem. 2012, 50 (23), 4920–4928.

(93) Seuring, J.; Agarwal, S. Macromolecules 2012, 45 (9), 3910–3918.

(94) Nagaoka, H.; Ohnishi, N.; Eguchi, M. Thermoresponsive polymer and production method thereof. US7847047 B2, December 7, 2010.

(95) Glatzel, S.; Laschewsky, A.; Lutz, J.-F. Macromolecules 2011, 44 (2), 413–415.

(96) Shimada, N.; Ino, H.; Maie, K.; Nakayama, M.; Kano, A.; Maruyama, A. Biomacromolecules 2011, 12 (10), 3418–3422.

(97) Shimada, N.; Nakayama, M.; Kano, A.; Maruyama, A. Biomacromolecules 2013, 14 (5), 1452–1457.

(98) Mishra, V.; Jung, S.-H.; Jeong, H. M.; Lee, H. Polym. Chem. 2014, 5 (7), 2411–2416.

(99) Fujihara, A.; Shimada, N.; Maruyama, A.; Ishihara, K.; Nakai, K.; Yusa, S. Soft

Matter 2015, 11 (26), 5204–5213.

(100) Meiswinkel, G.; Ritter, H. Macromol. Rapid Commun. 2013, 34 (12), 1026–1031.

(101) Schmidt, B. V. K. J.; Hetzer, M.; Ritter, H.; Barner-Kowollik, C. Macromol. Rapid Commun. 2013, 34 (16), 1306–1311.

(102) Käfer, F.; Liu, F.; Stahlschmidt, U.; Jérôme, V.; Freitag, R.; Karg, M.; Agarwal, S. Langmuir 2015, 31 (32), 8940–8946.

(103) Liu, F.; Jiang, S.; Ionov, L.; Agarwal, S. Polym. Chem. 2015, 6 (14), 2769–2776.

(104) Hou, L.; Wu, P. Soft Matter 2015, 11 (35), 7059–7065.

(105) Li, W.; Huang, L.; Ying, X.; Jian, Y.; Hong, Y.; Hu, F.; Du, Y. Angew. Chem. 2015, 127 (10), 3169–3174.

(106) Pineda-Contreras, B. A.; Liu, F.; Agarwal, S. J. Polym. Sci. Part Polym. Chem. 2014, 52 (13), 1878–1884.

(107) Bromberg, L. E.; Ron, E. S. Adv. Drug Deliv. Rev. 1998, 31 (3), 197–221.

(108) Guo, X.; Li, D.; Yang, G.; Shi, C.; Tang, Z.; Wang, J.; Zhou, S. ACS Appl. Mater. Interfaces 2014, 6 (11), 8549–8559.

(109) Schattling, P.; Jochum, F. D.; Theato, P. Polym. Chem. 2013, 5 (1), 25–36.

(110) Zhuang, J.; Gordon, M. R.; Ventura, J.; Li, L.; Thayumanavan, S. Chem. Soc. Rev. 2013, 42 (17), 7421–7435.

(111) Cheng, R.; Meng, F.; Deng, C.; Klok, H.-A.; Zhong, Z. Biomaterials 2013, 34 (14), 3647–3657.

(112) Gan, L. H.; Gan, Y. Y.; Deen, G. R. Macromolecules 2000, 33 (21), 7893–7897.

(113) González, N.; Elvira, C.; Román, J. S. Macromolecules 2005, 38 (22),

9298–9303.

(114) Jung, S.-H.; Song, H.-Y.; Lee, Y.; Jeong, H. M.; Lee, H. Macromolecules 2011, 44 (6), 1628–1634.

(115) Agarwal, S.; Zhang, Y.; Maji, S.; Greiner, A. Mater. Today 2012, 15 (9), 388–393.

(116) Hoffman, A. S. Adv. Drug Deliv. Rev. 2013, 65 (1), 10–16.

(117) Dong, L.; Hoffman, A. S. J. Controlled Release 1991, 15 (2), 141–152.

(118) Zhang, L.; Guo, R.; Yang, M.; Jiang, X.; Liu, B. Adv. Mater. 2007, 19 (19), 2988–2992.

(119) Chiang, W.-H.; Ho, V. T.; Huang, W.-C.; Huang, Y.-F.; Chern, C.-S.; Chiu, H.-C. Langmuir 2012, 28 (42), 15056–15064.

(120) Kyriakides, T. R.; Cheung, C. Y.; Murthy, N.; Bornstein, P.; Stayton, P. S.; Hoffman, A. S. J. Controlled Release 2002, 78 (1–3), 295–303.

(121) Gao, W.; Chan, J. M.; Farokhzad, O. C. Mol. Pharm. 2010, 7 (6), 1913–1920.

(122) Ge, Z.; Liu, S. Chem. Soc. Rev. 2013, 42 (17), 7289–7325.

(123) Kelley, E. G.; Albert, J. N. L.; Sullivan, M. O.; Thomas H. Epps, I. I. I. Chem. Soc. Rev. 2013, 42 (17), 7057–7071.

(124) Chen, G.; Hoffman, A. S. Nature 1995, 373 (6509), 49–52.

(125) Gao, X.; Cao, Y.; Song, X.; Zhang, Z.; Xiao, C.; He, C.; Chen, X. J. Mater. Chem. B 2013, 1 (41), 5578–5587.

(126) Bulmus, V.; Ding, Z.; Long, C. J.; Stayton, P. S.; Hoffman, A. S. Bioconjug. Chem. 2000, 11 (1), 78–83.

(127) Lin, X.; Tang, D.; Yu, Z.; Feng, Q. J. Mater. Chem. B 2014, 2 (6), 651–658.

(128) Chen, G.; Hoffman, A. S. Macromol. Rapid Commun. 1995, 16 (3), 175–182.

(129) Zeinali, E.; Haddadi-Asl, V.; Roghani-Mamaqani, H. RSC Adv. 2014, 4 (59), 31428–31442.

(130) Yin, X.; Hoffman, A. S.; Stayton, P. S. Biomacromolecules 2006, 7 (5), 1381–1385.

(131) Thavanesan, T.; Herbert, C.; Plamper, F. A. Langmuir 2014, 30 (19), 5609–5619.

(132) Zhao, Y. Macromolecules 2012, 45 (9), 3647–3657.

(133) Gohy, J.-F.; Zhao, Y. Chem. Soc. Rev. 2013, 42 (17), 7117–7129.

(134) Han, D.; Tong, X.; Boissière, O.; Zhao, Y. ACS Macro Lett 2011, 1 (1), 57–61.

(135) CSID: 238, http://www.chemspider.com/Chemical – Structure.238.html.

(136) CSID: 3951, http://www.chemspider.com/Chemical – Structure.3951.html.

(137) Heyda, J.; Soll, S.; Yuan, J.; Dzubiella, J. Macromolecules 2014, 47 (6), 2096–2102.

(138) Thang, S. H.; Chong, (Bill)Y. K.; Mayadunne, R. T. A.; Moad, G.; Rizzardo, E. Tetrahedron Lett. 1999, 40 (12), 2435–2438.

(139) Grenning, A. J.; Van Allen, C. K.; Maji, T.; Lang, S. B.; Tunge, J. A. J. Org. Chem. 2013, 78 (14), 7281–7287.

(140) Bergmann, A.; Reiser, O. Chem. – Eur. J. 2014, 20 (25), 7613–7615.

(141) Nakamura, K.; Nakajima, T.; Aoyama, T.; Okitsu, S.; Koyama, M. Tetrahedron 2014, 70 (43), 8097–8107.

(142) Bajpai, A. K.; Shukla, S. K.; Bhanu, S.; Kankane, S. Prog. Polym. Sci. 2008, 33 (11), 1088–1118.

(143) Kumar, A.; Srivastava, A.; Galaev, I. Y.; Mattiasson, B. Prog. Polym. Sci. 2007, 32 (10), 1205–1237.

(144) Xu, J.; Luo, S.; Shi, W.; Liu, S. Langmuir 2006, 22 (3), 989–997.

(145) Liu, F.; Seuring, J.; Agarwal, S. Polym. Chem. 2013, 4 (10), 3123–3131.

(146) Cummings, C.; Murata, H.; Koepsel, R.; Russell, A. J. Biomacromolecules 2014, 15 (3), 763–771.

(147) Chen, L.; Honma, Y.; Mizutani, T.; Liaw, D.-J.; Gong, J. P.; Osada, Y. Polymer 2000, 41 (1), 141–147.

(148) Seuring, J.; Agarwal, S. ACS Macro Lett. 2013, 2 (7), 597–600.

(149) Jia, X.; Chen, D.; Jiang, M. Chem. Commun. 2006, No. 16, 1736–1738.

(150) Mori, H.; Kato, I.; Saito, S.; Endo, T. Macromolecules 2010, 43 (3), 1289–1298.

(151) Shih, Y.-J.; Chang, Y.; Deratani, A.; Quemener, D. Biomacromolecules 2012, 13 (9), 2849–2858.

(152) Morimoto, N.; Muramatsu, K.; Wazawa, T.; Inoue, Y.; Suzuki, M. Macromol. Rapid Commun. 2014, 35 (1), 103–108.

(153) Yuan, W.; Zou, H.; Guo, W.; Wang, A.; Ren, J. J. Mater. Chem. 2012, 22 (47), 24783–24791.

(154) Aoki, T.; Kawashima, M.; Katono, H.; Sanui, K.; Ogata, N.; Okano, T.; Sakurai, Y. Macromolecules 1994, 27 (4), 947–952.

(155) Longenecker, R.; Mu, T.; Hanna, M.; Burke, N. A. D.; Stöver, H. D. H. Macromolecules 2011, 44 (22), 8962–8971.

(156) Sehlinger, A.; Kreye, O.; Meier, M. A. R. Macromolecules 2013, 46 (15), 6031–6037.

(157) Boustta, M.; Colombo, P.-E.; Lenglet, S.; Poujol, S.; Vert, M. J. Controlled Release 2014, 174, 1–6.

(158) Vasantha, V. A.; Jana, S.; Parthiban, A.; Vancso, J. G. Chem. Commun. 2013, 50 (1), 46–48.

(159) Thomas, D. B.; Convertine, A. J.; Myrick, L. J.; Scales, C. W.; Smith, A. E.; Lowe, A. B.; Vasilieva, Y. A.; Ayres, N.; McCormick, C. L. Macromolecules 2004, 37 (24), 8941–8950.

(160) Annaka, M. Colloids Surf. B Biointerfaces 2012, 99, 127–135.

(161) An, Q.; Qian, J.; Yu, L.; Luo, Y.; Liu, X. J. Polym. Sci. Part Polym. Chem. 2005, 43 (9), 1973–1977.

(162) He, J.; Tremblay, L.; Lacelle, S.; Zhao, Y. Polym. Chem. 2014, 5 (18), 5403–5411.

(163) Sato, T.; Tanaka, K.; Toyokura, A.; Mori, R.; Takahashi, R.; Terao, K.; Yusa, S. Macromolecules 2013, 46 (1), 226–235.

(164) Takahashi, R.; Sato, T.; Terao, K.; Qiu, X.-P.; Winnik, F. M. Macromolecules 2012, 45 (15), 6111–6119.

(165) Zhang, Q.; Hong, J.-D.; Hoogenboom, R. Polym. Chem. 2013, 4 (16), 4322–4325.

(166) Noh, M.; Mok, Y.; Nakayama, D.; Jang, S.; Lee, S.; Kim, T.; Lee, Y. Polymer 2013, 54 (20), 5338–5344.

(167) Wu, Y.; Wang, X.; Ling, Y.; Tang, H. RSC Adv. 2015, 5 (51), 40772–40778.

(168) Cao, X.; An, Z. Macromol. Rapid Commun. 2015, n/a – n/a.

(169) Arjunan Vasantha, V.; Junhui, C.; Ying, T. B.; Parthiban, A. Langmuir 2015, 31

(40), 11124–11134.

(170) Jiménez, Z. A.; Yoshida, R. Macromolecules 2015, 48 (13), 4599–4606.

(171) Liu, C.; Wang, S.; Zhou, H.; Gao, C.; Zhang, W. J. Polym. Sci. Part Polym. Chem. 2015, n/a – n/a.

(172) Deng, Y.; Xu, Y.; Wang, X.; Yuan, Q.; Ling, Y.; Tang, H. Macromol. Rapid Commun. 2015, n/a – n/a.

(173) Liu, F.; Agarwal, S. Macromol. Chem. Phys. 2015, 216 (4), 460–465.

(174) Meiswinkel, G.; Ritter, H. Macromol. Chem. Phys. 2013, 214 (24), 2835–2840.

(175) Cai, X.; Zhong, L.; Su, Y.; Lin, S.; He, X. Polym. Chem. 2015, 6 (20), 3875–3884.

(176) Zhu, Y.; Lowe, A. B.; Roth, P. J. Polymer 2014, 55 (17), 4425–4431.

(177) Huang, G.; Li, H.; Feng, S.-T.; Li, X.; Tong, G.; Liu, J.; Quan, C.; Jiang, Q.; Zhang, C.; Li, Z. Macromol. Chem. Phys. 2015, 216 (9), 1014–1023.

(178) Das, A.; Ghosh, S. Angew. Chem. Int. Ed. 2014, 53 (4), 1092–1097.

(179) Zhang, H.; Tong, X.; Zhao, Y. Langmuir 2014, 30 (38), 11433–11441.

(180) Zhang, H.; Marmin, T.; Cuierrier, É.; Soldera, A.; Dory, Y.; Zhao, Y. Polym. Chem. 2015, 6 (37), 6644–6650.

(181) Chen, X.; Sun, H.; Xu, J.; Han, X.; Liu, H.; Hu, Y. RSC Adv. 2015, 5 (105), 86584–86592.

(182) Lai, J. T.; Filla, D.; Shea, R. Macromolecules 2002, 35 (18), 6754–6756.

(183) Han, D.; Tong, X.; Zhao, Y. Langmuir 2012, 28 (5), 2327–2331.

(184) Han, D.; Tong, X.; Zhao, Y. Macromolecules 2011, 44 (3), 437–439.

(185) Pelton, R. J. Colloid Interface Sci. 2010, 348 (2), 673–674.

(186) Fomina, N.; McFearin, C.; Sermsakdi, M.; Edigin, O.; Almutairi, A. *J. Am. Chem. Soc.* 2010, *132* (28), 9540–9542.

(187) Yan, B.; Boyer, J.-C.; Habault, D.; Branda, N. R.; Zhao, Y. *J. Am. Chem. Soc.* 2012, *134* (40), 16558–16561.

(188) Gorelikov, I.; Field, L. M.; Kumacheva, E. J. Am. Chem. Soc. 2004, 126 (49), 15938–15939.

(189) Das, M.; Sanson, N.; Fava, D.; Kumacheva, E. Langmuir 2007, 23 (1), 196–201.